NASA CONTRACTOR REPORT

NASA CR-1572

A STUDY OF PULSE PROPAGATION OF ELECTROMAGNETIC SIGNALS THROUGH THE SOLAR CORONA

by C. M. Knop, Y. Shiau, and V. Gylys

Prepared by
CONSULTANTS IN ELECTRODYNAMICS
Oak Park, Ill.
for Langley Research Center

NATIONAL AERONAUTICS AND SPACE ADMINISTRATION • WASHINGTON, D. C. • JULY 1970

NASA CR-1572

A STUDY OF PULSE PROPAGATION OF ELECTROMAGNETIC SIGNALS THROUGH THE SOLAR CORONA

By C. M. Knop, Y. Shiau, and V. Gylys

Prepared under Contract No. NAS 1-9142 by
CONSULTANTS IN ELECTRODYNAMICS
Oak Park, Ill.

for Langley Research Center

NATIONAL AERONAUTICS AND SPACE ADMINISTRATION

For sale by the Clearinghouse for Federal Scientific and Technical Information
Springfield, Virginia 22151 – CFSTI price $3.00

TABLE OF CONTENTS

		Page
	SUMMARY	1
I.	INTRODUCTION	5
II.	SOLAR CORONA CHARACTERIZATION	9
III.	PROPAGATION MODEL	9
	a. Propagation Path	9
	b. W.K.B. Solution for $\bar{\Psi}$	15
	c. Solution for $\Psi(L,t)$ for a Stepped Carrier at Transmitter	17
	1. Formulation	17
	2. Discussion of Stationary Phase	21
	3. Convolution Solution	24
	4. Rise Time	31
	5. Distortion Parameter	33
IV.	CORRELATION RECEIVER - MEASUREMENT OF $\bar{n}(\rho)$	35
	a. Transmitted Code-Correlation Function	35
	b. Received Code-Correlation Function	37
	c. Plasma Diagnostics with Single Carrier	43
	d. Plasma Diagnostics with Two (or More) Carriers	45
V.	OBTAINMENT OF n(r) VARIATION FROM KNOWLEDGE OF $\bar{n}(\rho)$	45
VI.	EXAMPLE FOR DIAGNOSTICS USING V.H.F. CARRIERS	48
VII.	EFFECTS OF NOISE ON MEASUREMENT ACCURACY	55
	a. R.M.S. Error in Location Time of Correlation Peak -- Heuristic Derivation	55

TABLE OF CONTENTS (Continued)

		Page
	b. R.M.S. Error in Integrated Electron Density Measurement	61
	c. Determination of Output Signal to Noise Ratio	65
	1. Received Signal Energy, E_{IN}	68
	d. Selection of Receiver Front End Bandwidth	74
	e. Effect of Antenna and Transmission Line, Etc. Bandwidths	75
VIII.	CONCLUSIONS AND RECOMMENDATIONS	76

APPENDICES

I.	SOLUTION TO WAVE EQUATION IN SLIGHTLY NON-HOMOGENEOUS SOLAR CORONA	79
II.	OUTPUT CONTRIBUTION AT LOWER FREQUENCIES	85
III.	A CONCISE REVIEW OF THE PROPAGATION OF A STEPPED CARRIER WAVE THROUGH A HOMOGENEOUS PLASMA	87
IV.	PROOF OF $\left\|t - t_g\right\| < < t_o\overline{P^2}$	93
V.	ALTERNATE DERIVATION OF RISE TIME	95
VI.	SIMPLIFICATION OF $\Psi(L,t)$ EXPRESSION	97
VII.	CORRELATION RECEIVER OUTPUT	101
VIII.	PROGRAMMING OF CORRELATION FUNCTION	111
IX.	THE TRIPLE FOLDED BARKER CODE	119
X.	PROOF THAT RADIAL AND OFFSET ELECTRON DENSITIES ARE ABEL TRANSFORM PAIRS	125

TABLE OF CONTENTS (Continued)

APPENDICES (Continued)

		Page
XI.	DETERMINATION OF THE k FACTOR	131
XII.	DISCUSSION OF RECEIVER DESIGN	133
XIII.	EFFECT OF IONOSPHERE ON SOLAR PROBE EXPERIMENT	143
XIV.	EFFECTS OF REFRACTION OF SOLAR CORONA -- GEOMETRICAL OPTICS SOLUTION	149
	a. Introduction	149
	b. Ray-Path Equation	149
	c. Effects of Refraction Due to Refractive Index $n(r)$ -- Comparison with Vacuum Case $n(r) = 1$	152
	d. Conclusions	157
XV.	WAVEGUIDE SIMULATION OF THE SOLAR CORONA	159
	a. Basis of Simulation	159
	b. Example of Solar Corona Simulation by Waveguide	164
XVI.	COMMUNICATION BANDWIDTH AT S BAND	169
XVII.	DUAL FREQUENCY EXPERIMENT AT S AND X BAND	173
XVIII.	PLASMA DIAGNOSTICS VIA A.M. OR N.B.F.M.	181
	a. Amplitude Modulation (A.M.)	181
	b. Special Case of Low Modulation Index	184
	c. Narrow Band Frequency Modulation (N.B.F.M.)	185
	d. Conclusion	188

TABLE OF CONTENTS (Continued)

	Page
LIST OF MAJOR SYMBOLS	191
REFERENCES	195

LIST OF FIGURES

Fig.		Page
1	Plasma, Collision, and Cyclotron Frequency in Solar Environment from Various Models	10
2	Geometry of Propagation Path through Solar Corona	13
3	Dependence of Stationary Phase Frequency on Time	22
4a	Universal Curve for the Amplitude of the Main Signal	29
4b	Universal Curve for Phase of the Main Signal	30
5	Build Up of Pulse of Input Duration T	34
6	The 127 Bit Pseudo Random Code	36
7	Auto-Correlation Function of 127 Bit Pseudo Random Code	38
8	Correlation Receiver	41
9	Correlation Receiver Output Response - Computed	44
10	Motion of Solar Probe Satellite Relative to the Earth	49
11	Dependence of Single Frequency Rise Time, Delay Time, Distortion Parameter, and Dual Frequency Differential Delay Time on Trajectory	53
12	Effect of Noise on Location of Peak Correlation Output	56
13	Dependence of the Factor k on the Distortion Parameter	59
14	R.M.S. Error in Correlation Peak Location Time	62

LIST OF FIGURES (Continued)

Fig.		Page
15	Square of Percent Error in Measurement of Integrated Columnar Electron Density for Dual Frequency (70 and 80 mHz.) Experiment	67
16a	Noise Temperature at Medium and High Frequencies (E. C. Hayden)	71
16b	Noise Temperature at Microwave Frequencies (Pierce-Kompfner, After D. C. Hugg)	71
17	Antenna Noise Temperature	72
18	Typical Front End Receiver Amplifier Noise Temperature	73
IX-1	Auto-Correlation Function of Triple Folded Barker Code	121
XII-1	Rise Time and Effective Bandwidth Dependence on Distortion Parameter	135
XIII-1	Typical Ionosphere Electron Profiles	144
XIII-2	Sketch of Plasma Frequency Variation in Solar Corona Including Ionosphere	145
XIV-1	Ray Path Geometry for Solar Probe Problem	151
XIV-2	Computed Curves for Ray Path Parameter b	153
XV-1	X Band Waveguide Length Required to Simulate V.H.F. Solar Experiment	166
XVI-1	Usable Bandwidth through Solar Corona at S Band Carrier	171

LIST OF TABLES

Table		Page
I	Solar Corona Parameters Dependent upon Distance from the Sun	11
II	Tabulations of T_d, t_R, and β for Single Carrier Frequency (f_o = 75 mHz) and ΔT for Dual Carrier Frequency (f_o = 70 and 80 mHz)	51
III	The Factor k for Correlation Output Curves	58
IV	Measurement Error in $\bar{n}$	66
V	Computations of Input Energy Levels	69
VIII-1	Auto-Correlation Coefficients (a_k and b_k), and Auto-Correlation Function, r_k, for N = 127 Pseudo Random Code	115
IX-1	$y(\tau)$ Computations for β = 2 for the Triple Folded Barker Code	122
XI-1	Tabulations of k Versus β	132
XII-1	Rise Time and Effective Bandwidth Computations	136
XII-2	Computations of Input Signal to Noise Power Ratio, $(S_o/N_o)_{in}$	140
XIV-1	Ray Starting Angles (ϕ_s and ϕ_{sv}) Calculations	156
XVII-1	ΔT for S-X Band Experiment	179
XVIII-1	Summary of Plasma Diagnostics Via A.M. or N.B.F.M.	190

A STUDY OF PULSE PROPAGATION OF ELECTROMAGNETIC SIGNALS THROUGH THE SOLAR CORONA

By C. M. Knop, Y. Shiau, and V. Gylys
Consultants in Electrodynamics
Oak Park, Illinois

SUMMARY

This report reviews the basis of a small solar probe propagation experiment to measure the radial variation of electron density in the Solar Corona. Although a concise review of the entire scheme is given, emphasis is placed on a rigorous formulation of the dispersion undergone by a stepped carrier wave and a coded group of such waves.

It is shown that the electron density can be determined by use of a cross-correlation receiver, either to measure the shape of the correlation response at a single carrier frequency (in the V.H.F. range or higher) or, alternatively, by using several coded carriers at sufficient separation times, and measuring the time difference between the peaks of the corresponding correlation responses. It is shown that the received correlation functions, $y(\tau)$, are characterized by a single solar distortion parameter, β, which is the ratio of the rise time of the envelope of a single stepped carrier to the $\sqrt{2}$ times the bit length. For the subject V.H.F. experiment, β has a range from approximately

$0 \leq \beta \leq 2$. The correlation curves for this range are computed and given.

An example experiment using V.H.F. frequencies is given for a pseudo random code with a typical satellite trajectory.

The effects of noise on the accuracy with which the measured correlation curves for the dual frequency experiment can be used to deduce the integrated electron density, $\bar{n}$, of the solar corona are then determined. It is shown, using a formulation involving the peak value of the output correlation function and its second derivative, that if the correlation output signal to noise power ratio is greater than approximately 10 Db., the percentage R.M.S. error made in measuring $\bar{n}$ is less than 5.0 percent, for $\beta \gtrsim 0.08$. The large signal to noise power ratio required of 10 Db. or more can be realized by a properly designed correlation receiver since this ratio is under the upper bound of twice the input energy signal to noise ratio which is shown to be at least 13 Db.

It is concluded that the small solar probe V.H.F. experiment is conceptually valid and can be used to measure the solar corona electron density with a small error. However, the experiment requires state of the art engineering efforts to realize the 50 Db. gain receiving antenna and (to a lesser degree) the correlation receiver.

In addition to the above review of the V.H.F. experiment consideration is also given to: effect of finite antenna and transmission line, etc., bandwidth; effects of the use of alternate (Triple Folded Barker) codes; discussion of receiver design; effect of the ionosphere; effects of refraction; waveguide simulation of the solar corona; communication bandwidth of the solar corona at S-Band; performance of the dual frequency experiment at S and X Band; and basis of diagnostics of the corona using continuous amplitude or narrow band frequency modulation. These findings should all be considered in the determination of possible alternate propagation experiments designed to deduce the solar corona electron density.

I. INTRODUCTION

The main purpose of this report is to concisely and critically review a propagation method [1, 2, 3]* designed to measure the radial point by point electron density variation, n(r), of the solar corona. The method consists of sending pulsed carrier waves from a small satellite in a prescribed trajectory about the sun and receiving these pulses on the earth. By adopting contemporary models of the solar corona and using a sufficiently high carrier frequency (V.H.F. or above) it is shown that the nonhomogeneous solar corona can be represented by an equivalent homogeneous plasma and that the received pulses can then be entirely described by the main signal regime of the response of a homogeneous long path plasma to a stepped carrier. Universal curves describing the envelope build up (with its pertinent rise time, t_R) and the phase modulation which a single stepped carrier undergoes are reviewed.

Although it is possible in principle to determine the integrated columnar electron density, $\bar{n}(\rho)$, of the solar path by measuring the rise time, t_R , to combat the noise levels, a cross-correlation scheme is described. In this scheme a series of N phase shift keyed (phase of either 0^o or 180^o in some prescribed pseudo random fashion) carriers, i.e. bits, each of duration, T , are transmitted. The pseudo

* The numeral in brackets, [ ] , denotes reference number.

randomness is chosen such that the auto-correlation function of the envelope of this series has a well-defined sharp peak. It is then shown that the shape of the received normalized cross correlation function, $y(\tau)$, is a distorted version of that transmitted due to the dispersion of the plasma and is completely characterized by a single distortion parameter, $\beta \equiv \frac{t_R}{T\sqrt{2}}$, the ratio of the rise time to the $\sqrt{2}$ times the bit length. Thus the parameter, β, uniquely characterizes the solar propagation path.

For a pseudo random code having $N = 127$, computed curves of $y(\tau)$ versus β are given for values of $0 \leq \beta \leq 2$. These curves reveal that serious distortion of the correlation function begins to occur for β near unity since then the rise time equals the $\sqrt{2}$ bit time and a single pulse loses its identity. Hence, by measuring the correlation function, as can be done with a correlation receiver, as described, one can measure β, and hence determine $\bar{n}$ through the relation

$$\bar{n}(\rho) = 2c\beta^2 f_o^3 \frac{T^2}{81} .$$

Alternatively one can transmit another series of pulses at a time T_s later and at a different carrier frequency after the first series has completely decayed. It is shown that the center of the correlation functions (which are all peaks for the values of β considered) are separated in time by ΔT,

where ΔT is the differential main signal or group delay time, $\Delta T = \frac{81\,\bar{n}}{2f_{o_1}^2 c}\left[1 - \left(\frac{f_{o_1}^2}{f_{o_2}^2}\right)\right]$, with f_{o_1} and f_{o_2} being the two carrier frequencies.

Once the quantity $\bar{n}(\rho)$ is determined from measurement, the method of Harrington involving use of an Abelian transformation is employed to obtain the actual radial distribution of the solar corona electron density, $n(r)$.

The report up to this point (with the exception of specifying the pseudo random code) is completely general in that it is valid for any carrier of V.H.F. range or above. However, as a specific example, use of carriers at 70, 75, and 80 mHz are considered with an assumed $1/r^2$ dependence in electron density, and a plot of the calculated β versus satellite location is given. These calculations reveal that β can vary between near zero to nearly two as the satellite is in the range between inferior and superior conjunction. As such, the cross-correlation functions previously computed can be used for this case.

A curve of ΔT versus satellite location is given for the 70 and 80 mHz combination.

After reviewing the Albelian transformation relationship between $\bar{n}(\rho)$ and $n(r)$, the effects of noise on the accuracy with which ΔT can be measured and $\bar{n}$ determined

are determined using a formulation involving the peak value of the output correlation function and its second derivative and the computed $y(\tau)$ curves. A curve of the product of percent R.M.S. error in $\bar{n}$ times the output signal to noise power ratio, $\left(\frac{S_o}{N_o}\right)_{out}$, versus the distortion parameter, β, is given, and reveals that for $\left(\frac{S_o}{N_o}\right)_{out} \gtrsim 10$ that the error in $\bar{n}$ is less than 5% for $\beta \gtrsim 0.08$.

Thus the validity of the basis of the dual frequency experiment is established. The report also covers (primarily in the Appendices) some engineering type considerations regarding the receiver design, the effects of finite antenna and transmission line cable, etc., bandwidth, the effect of the ionosphere, the effects of the use of an alternate pseudo random code (Triple Folded Barker), the effect of refraction, the desirability of waveguide simulation of the solar corona to experimentally establish the validity of the experiment, the communication bandwidth of the solar corona at S-Band, the performance of the dual frequency experiment at S and X Band, and the basis of diagnostics of the corona using continuous A.M. or N.B.F.M. modulation. These points are given to assist in further assessment of any solar propagation experiment.

II. SOLAR CORONA CHARACTERIZATION

Contemporary models of the solar corona plasma frequency, f_p , distribution all assume spherical symmetry about the sun with only a radial variation outward from the sun. Various models [4, 5, 6, 7, 8] give the $f_p(r)$, ($r = R/R_o$ is the radial distance from the sun normalized with respect to the radius of the sun) distributions shown in Fig. 1. The most comprehensive model known to this writer is that given by Hruby, et al [4] , as summarized in Table I. From this table it is seen that both the collision frequency, ν , and the gyro-magnetic frequencies in the radial and circumferential directions (i.e. $f_{B_r} = \frac{eB_r}{2\pi m}$, $f_{B_\phi} = \frac{eB_\phi}{2\pi m}$ as also plotted in Fig. 1) are negligible compared to a V.H.F. or higher frequency.

Thus, in the absence of solar flares or other sporadic solar phenomenon, the solar corona appears to a V.H.F. or higher carrier frequency as a cold, collisionless, isotropic, plasma with a radially decaying plasma frequency.

III. PROPAGATION MODEL

a. Propagation Path

Consider then a transmitting source located such that its perpendicular distance (or offset distance) from the center of the sun is $R_\perp$, as depicted in Fig. 2. If we denote

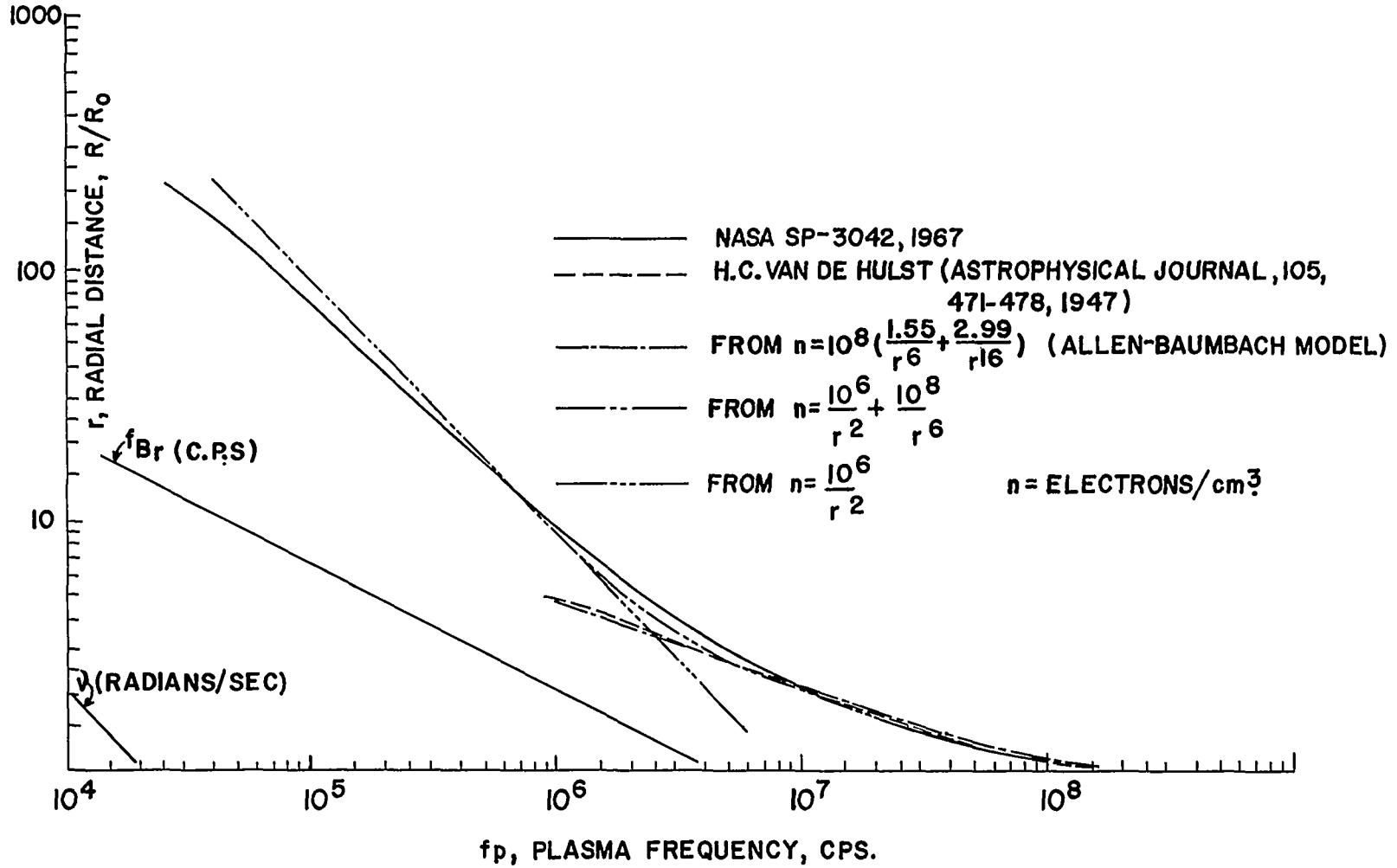

FIG.1. PLASMA, COLLISION, AND CYCLOTRON FREQUENCY IN SOLAR ENVIRONMENT FROM VARIOUS MODELS.

TABLE I. SOLAR CORONA PARAMETERS DEPENDENT UPON DISTANCE FROM THE SUN. [4]

r	N	T	V	f_p	ν	B_r	B_ϕ	h_d
1.10	1.176E 14	9.156E 05	1.074E 03	9.736E 07	1.463E 01	1.347E-04	6.893E-07	6.090E-03
1.20	4.677E 13	1.318E 06	2.268E 03	6.140E 07	3.535E 00	1.132E-04	6.318E-07	1.158E-02
1.30	2.353E 13	1.430E 06	3.842E 03	4.355E 07	1.606E 00	9.645E-05	5.832E-07	1.701E-02
1.40	1.475E 13	1.430E 06	5.285E 03	3.448E 07	1.018E 00	8.316E-05	5.416E-07	2.149E-02
1.50	9.533E 12	1.430E 06	7.123E 03	2.772E 07	6.641E-01	7.244E-05	5.055E-07	2.673E-02
1.60	6.252E 12	1.430E 06	9.546E 03	2.245E 07	4.396E-01	6.367E-05	4.739E-07	3.301E-02
1.80	3.156E 12	1.415E 06	1.494E 04	1.595E 07	2.287E-01	5.031E-05	4.212E-07	4.621E-02
2.00	2.006E 12	1.378E 06	1.904E 04	1.271E 07	1.525E-01	4.075E-05	3.791E-07	5.720E-02
2.20	1.275E 12	1.342E 06	2.476E 04	1.014E 07	1.016E-01	3.368E-05	3.446E-07	7.081E-02
2.40	8.102E 11	1.307E 06	3.274E 04	8.081E 06	6.774E-02	2.830E-05	3.159E-07	8.765E-02
2.60	5.975E 11	1.246E 06	3.782E 04	6.939E 06	5.386E-02	2.411E-05	2.916E-07	9.966E-02
2.80	4.573E 11	1.181E 06	4.261E 04	6.071E 06	4.475E-02	2.079E-05	2.708E-07	1.109E-01
3.00	3.500E 11	1.120E 06	4.850E 04	5.311E 06	3.718E-02	1.811E-05	2.527E-07	1.235E-01
3.30	2.552E 11	1.043E 06	5.497E 04	4.535E 06	3.024E-02	1.497E-05	2.298E-07	1.395E-01
3.60	1.860E 11	9.706E 05	6.336E 04	3.872E 06	2.460E-02	1.258E-05	2.106E-07	1.576E-01
4.00	1.280E 11	8.850E 05	7.459E 04	3.212E 06	1.948E-02	1.019E-05	1.896E-07	1.815E-01
4.50	9.327E 10	8.185E 05	8.088E 04	2.742E 06	1.599E-02	8.049E-06	1.685E-07	2.044E-01
5.00	6.796E 10	7.569E 05	8.991E 04	2.340E 06	1.312E-02	6.520E-06	1.516E-07	2.303E-01
5.50	5.055E 10	7.002E 05	9.990E 04	2.018E 06	1.098E-02	5.388E-06	1.379E-07	2.569E-01
6.00	3.900E 10	6.480E 05	1.088E 05	1.773E 06	9.522E-03	4.528E-06	1.264E-07	2.813E-01
6.50	3.224E 10	6.161E 05	1.122E 05	1.612E 06	8.497E-03	3.858E-06	1.166E-07	3.017E-01
7.00	2.665E 10	5.858E 05	1.170E 05	1.465E 06	7.582E-03	3.327E-06	1.083E-07	3.236E-01
7.50	2.203E 10	5.569E 05	1.233E 05	1.332E 06	6.765E-03	2.898E-06	1.011E-07	3.470E-01
8.00	1.821E 10	5.295E 05	1.311E 05	1.211E 06	6.037E-03	2.547E-06	9.478E-08	3.722E-01
9.00	1.356E 10	4.877E 05	1.390E 05	1.046E 06	5.094E-03	2.012E-06	8.424E-08	4.138E-01
10.00	1.030E 10	4.510E 05	1.483E 05	9.111E 05	4.353E-03	1.630E-06	7.582E-08	4.567E-01
11.00	8.613E 09	4.280E 05	1.466E 05	8.332E 05	3.939E-03	1.347E-06	6.893E-08	4.865E-01
12.00	7.202E 09	4.062E 05	1.473E 05	7.619E 05	3.564E-03	1.132E-06	6.318E-08	5.183E-01
13.00	6.022E 09	3.855E 05	1.501E 05	6.967E 05	3.225E-03	9.645E-07	5.832E-08	5.522E-01
14.00	5.036E 09	3.658E 05	1.548E 05	6.371E 05	2.918E-03	8.316E-07	5.416E-08	5.883E-01
15.00	4.211E 09	3.472E 05	1.612E 05	5.826E 05	2.641E-03	7.244E-07	5.055E-08	6.267E-01
16.00	3.600E 09	3.160E 05	1.658E 05	5.387E 05	2.593E-03	6.367E-07	4.739E-08	6.466E-01
18.00	2.868E 09	2.870E 05	1.644E 05	4.808E 05	2.384E-03	5.031E-07	4.212E-08	6.904E-01
20.00	2.285E 09	2.607E 05	1.672E 05	4.291E 05	2.191E-03	4.075E-07	3.791E-08	7.372E-01
22.00	1.820E 09	2.367E 05	1.734E 05	3.830E 05	2.014E-03	3.368E-07	3.446E-08	7.871E-01
24.00	1.501E 09	2.229E 05	1.767E 05	3.478E 05	1.818E-03	2.830E-07	3.159E-08	8.411E-01
26.00	1.256E 09	2.132E 05	1.799E 05	3.182E 05	1.629E-03	2.411E-07	2.916E-08	8.991E-01
28.00	1.051E 09	2.039E 05	1.853E 05	2.911E 05	1.459E-03	2.079E-07	2.708E-08	9.611E-01
30.00	8.800E 08	1.950E 05	1.929E 05	2.663E 05	1.307E-03	1.811E-07	2.527E-08	1.027E 00
33.00	7.220E 08	1.820E 05	1.943E 05	2.412E 05	1.188E-03	1.497E-07	2.298E-08	1.096E 00

TABLE I. SOLAR CORONA PARAMETERS DEPENDENT UPON DISTANCE FROM THE SUN. [4]
(CONTINUED)

r	N	T	V	f_p	ν	B_r	B_ϕ	h_d
36.00	5.924E 08	1.699E 05	1.990E 05	2.185E 05	1.081E-03	1.258E-07	2.106E-08	1.169E 00
40.00	4.550E 08	1.550E 05	2.098E 05	1.915E 05	9.527E-04	1.019E-07	1.896E-08	1.274E 00
45.00	3.537E 08	1.420E 05	2.133E 05	1.688E 05	8.449E-04	8.249E-08	1.685E-08	1.383E 00
50.00	2.750E 08	1.300E 05	2.222E 05	1.489E 05	7.493E-04	6.520E-08	1.516E-08	1.501E 00
55.00	2.225E 08	1.217E 05	2.270E 05	1.339E 05	6.692E-04	5.388E-08	1.379E-08	1.614E 00
60.00	1.800E 08	1.140E 05	2.358E 05	1.204E 05	5.976E-04	4.528E-08	1.264E-08	1.737E 00
65.00	1.530E 08	1.078E 05	2.363E 05	1.111E 05	5.527E-04	3.858E-08	1.166E-08	1.831E 00
70.00	1.301E 08	1.019E 05	2.397E 05	1.024E 05	5.112E-04	3.327E-08	1.083E-08	1.931E 00
75.00	1.106E 08	9.627E 04	2.456E 05	9.440E 04	4.729E-04	2.898E-08	1.011E-08	2.036E 00
80.00	9.400E 07	9.100E 04	2.539E 05	8.704E 04	4.374E-04	2.547E-08	9.478E-09	2.147E 00
90.00	7.320E 07	8.316E 04	2.577E 05	7.681E 04	3.897E-04	2.012E-08	8.424E-09	2.326E 00
100.00	5.700E 07	7.600E 04	2.680E 05	6.778E 04	3.472E-04	1.630E-08	7.582E-09	2.520E 00
110.00	4.733E 07	7.150E 04	2.668E 05	6.176E 04	3.160E-04	1.347E-08	6.893E-09	2.682E 00
120.00	3.930E 07	6.726E 04	2.699E 05	5.628E 04	2.875E-04	1.132E-08	6.318E-09	2.855E 00
130.00	3.263E 07	6.328E 04	2.770E 05	5.128E 04	2.617E-04	9.645E-09	5.832E-09	3.039E 00
140.00	2.710E 07	5.953E 04	2.876E 05	4.673E 04	2.382E-04	8.316E-09	5.416E-09	3.235E 00
150.00	2.250E 07	5.600E 04	3.018E 05	4.258E 04	2.167E-04	7.244E-09	5.055E-09	3.443E 00
160.00	1.913E 07	5.360E 04	3.119E 05	3.927E 04	1.969E-04	6.367E-09	4.739E-09	3.653E 00
180.00	1.383E 07	4.911E 04	3.409E 05	3.339E 04	1.625E-04	5.031E-09	4.212E-09	4.113E 00
200.00	1.000E 07	4.500E 04	3.819E 05	2.839E 04	1.342E-04	4.075E-09	3.791E-09	4.630E 00
215.00	7.922E 06	4.277E 04	4.172E 05	2.527E 04	1.149E-04	3.526E-09	3.527E-09	5.071E 00

$r = R/R_o$ = NORMALIZED RADIAL DISTANCE FROM CENTER OF SUN.

N = NUMBER DENSITY OF ELECTRONS, #/METER^3.

T = ELECTRON TEMPERATURE, DEGREES KELVIN.

V = SOLAR WIND VELOCITY, METERS/SEC.

f_p = PLASMA (ELECTRON) FREQUENCY, CYCLES/SEC.

ν = COLLISION FREQUENCY, RADIANS/SEC.

B_r = RADIAL COMPONENT OF MAGNETIC FIELD, WEBERS/METER^2.

B_ϕ = CIRCUMFERENTIAL COMPONENT OF MAGNETIC FIELD, WEBERS/METER^2.

h_d = DEBYE LENGTH = $\left[(\epsilon_v kT)/N_e^2\right]^{\frac{1}{2}}$, METERS.

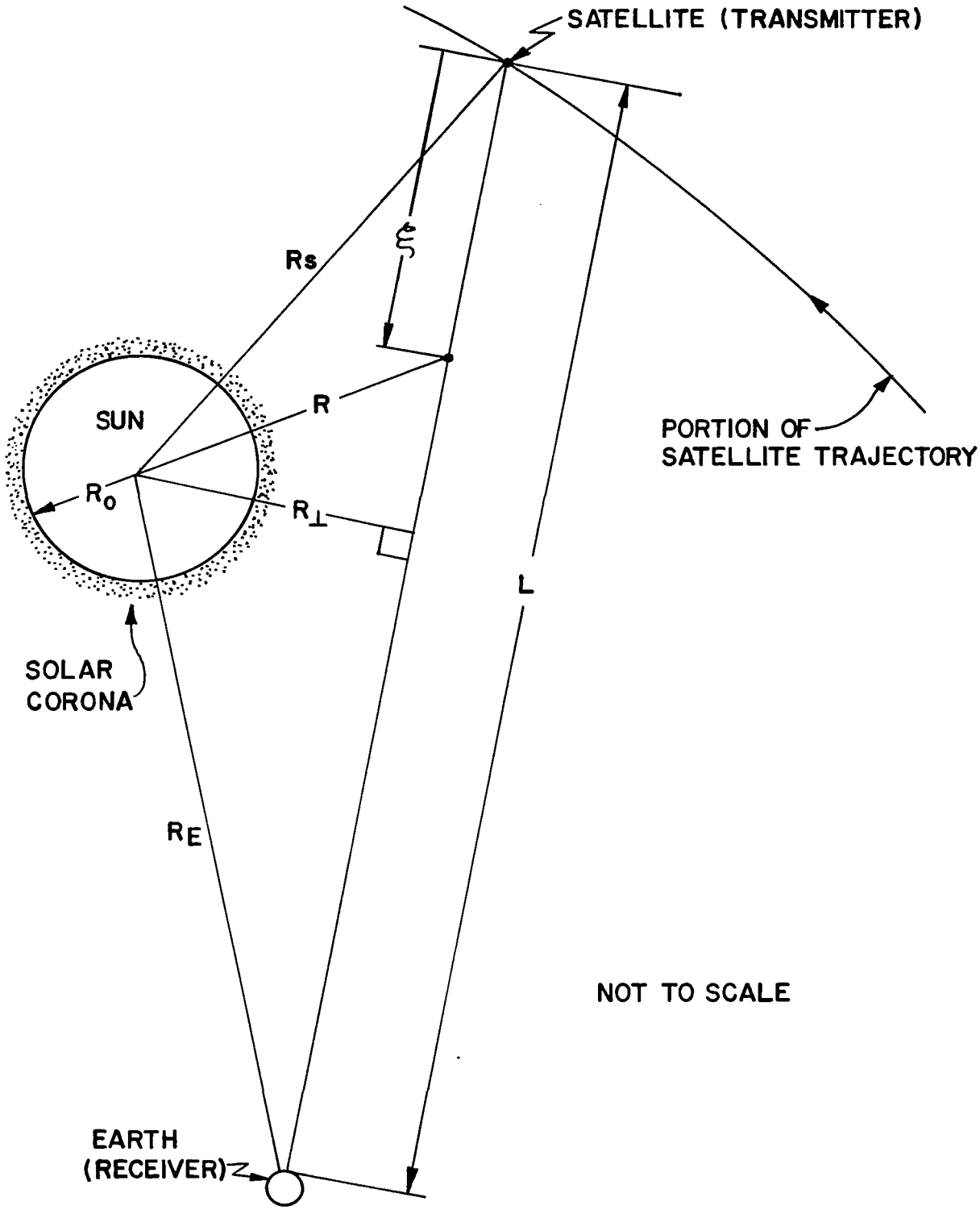

FIG.2. GEOMETRY OF PROPAGATION PATH THROUGH SOLAR CORONA.

by $\Psi(\xi,t)$ any component of the electric or magnetic field propagating along the assumed path, as shown in Fig. 2, it follows from Maxwell's equations that the Fourier Transform of $\Psi(\xi,t)$, denoted by $\bar{\Psi}(\xi,\omega)$ obeys the scalar wave equation

$$\nabla^2\bar{\Psi}(\xi,\omega)+\beta_p^2(\xi,\omega)\bar{\Psi}(\xi,\omega) = 0 \tag{1}$$

where β_p is the phase factor

$$\beta_p^2 = \frac{\omega^2}{c^2}\epsilon_r(\xi,\omega) \tag{2}$$

and ϵ_r is the equivalent relative dielectric constant of the solar corona

$$\epsilon_r = 1 - \frac{\omega_p^2(\xi)}{\omega^2} \tag{3}$$

Here ω_p is assumed to be a function of r only.

The received signal at the earth's location ($\xi = L$) is then given by the Fourier inversion:

$$\Psi(L,t) = \int_{-\infty}^{\infty} \bar{\Psi}(L,\omega)e^{j\omega t}\,d\omega \tag{4}$$

Here we will first solve (1) for $\bar{\Psi}$ then solve (4) for Ψ.

b. W.K.B. Solution for $\bar{\Psi}$

For the solar corona, it can be shown (Appendix I) that the rate of change of ϵ_r is very, very small with respect to a wavelength displacement along the assumed propagation path, for all frequencies much greater than the maximum angular plasma frequency, $\omega_{p_{max}}$, encountered along the path, i.e.

$$\left| \frac{\frac{d\epsilon_r}{d\left(\frac{\xi}{\lambda}\right)}}{4\pi\epsilon_r} \right| << 1 \quad \text{for} \quad |\omega| \gtrsim \omega_m \equiv 3\omega_{p_{max}} \tag{5}$$

where $\lambda = \frac{\lambda_v}{\sqrt{\epsilon_r}}$, $\lambda_v = 2\pi\frac{c}{\omega}$ = free space wavelength at frequency $\omega = 2\pi f$.

This condition is sufficient to allow us to write for $\bar{\Psi}$ the W.K.B. type solution, over this high frequency region, of

$$\bar{\Psi}(\xi,\omega) = \bar{\Psi}_o \, e^{-j\int_0^L \beta_p(\xi)d\xi} \quad \text{for} \; |\omega| \gtrsim \omega_m \tag{6}$$

where $\bar{\Psi}(\xi,\omega)$ for $\omega \leq \omega_m$ is still unknown, and where $\bar{\Psi}_o$ is the Fourier Transform of the transmitter field (assumed known), i.e.

$$\bar{\Psi}_o = \frac{1}{2\pi} \int_{-\infty}^{\infty} \Psi(0,t) e^{-j\omega t} \, dt \tag{7}$$

Now

$$\int_0^L \beta_p(\xi) d\xi = \frac{\omega}{c} \int_0^L \sqrt{1 - \frac{\omega_{p(\xi)}^2}{\omega^2}} \, d\xi \tag{8}$$

but for $|\omega| \geq \omega_m$ we can write

$$\sqrt{1 - \frac{\omega_p^2(\xi)}{\omega^2}} \approx 1 - \frac{1}{2} \frac{\omega_p^2(\xi)}{\omega^2} \tag{9}$$

and, therefore,

$$\int_0^L \beta_p(\xi) d\xi = \frac{\omega L}{c} \left[1 - \frac{\overline{\omega_p^2}}{2\omega^2} \right] \tag{10}$$

where

$$\overline{\omega_p^2} \equiv \frac{1}{L} \int_0^L \omega_p^2(\xi) d\xi \tag{11}$$

i.e., $\overline{\omega_p^2}$ is an average squared plasma frequency for the given propagation path. Thus

$$\bar{\Psi}(L,\omega) = \begin{cases} \bar{\Psi}_o \, e^{-j\frac{\omega L}{c}\left[1 - \frac{1}{2}\frac{\overline{\omega_p^2}}{\omega^2}\right]} & |\omega| \gtrsim \omega_m \\ \bar{\Psi}(L,\omega) \quad \text{(still unknown)} & |\omega| \lesssim \omega_m \end{cases} \tag{12}$$

This completes the solution for $\bar{\Psi}$ as far as we require, as will be seen.

c. Solution for $\Psi(L,t)$ for a Stepped Carrier at Transmitter

1. Formulation

From (12) we see that for all frequencies, $|\omega| \gtrsim \omega_m$, the solar corona has been reduced to that of an equivalent homogeneous plasma with plasma frequency $\bar{\omega}_p$. Now, from (4), we can then write

$$\Psi(L,t) = \Psi_{HI} + \Psi_{LOW} \tag{13}$$

where Ψ_{HI} is due to the high frequency components ($|\omega| \gtrsim \omega_m$) and Ψ_{LOW} due to the low frequency components ($|\omega| \lesssim \omega_m$), i.e.

$$\Psi_{HI} = \int_{-\infty}^{-\omega_m} + \int_{\omega_m}^{\infty} \bar{\Psi}_o \, e^{-j\frac{\omega L}{c}\left[1 - \frac{1}{2}\frac{\overline{\omega_p^2}}{\omega^2}\right]} e^{j\omega t} \, d\omega \tag{14}$$

$$\Psi_{LOW} = \int_{-\omega_m}^{\omega_m} \bar{\Psi}(L,\omega) e^{j\omega t} \, d\omega \tag{15}$$

By adding and subtracting the contribution from $-\omega_m$ to ω_m in Ψ_{HI}, we can write

$$\Psi(L,t) = \int_{-\infty}^{\infty} \bar{\Psi}_o \, e^{j\Phi(\omega)} \, d\omega + \Delta\Psi(L,t) \tag{16}$$

where

$$\Phi(\omega) = \omega t - \frac{\omega L}{c}\left[1 - \frac{1}{2}\frac{\overline{\omega_p^2}}{\omega^2}\right] \tag{17}$$

$$\Delta\Psi(L,t) = \int_{-\omega_m}^{\omega_m} \left[\bar{\Psi}(L,\omega) e^{j\omega t} - \bar{\Psi}_o e^{j\Phi(\omega)}\right] d\omega \tag{18}$$

Suppose now a stepped carrier wave is turned on at the satellite at time $t = 0$, i.e.,

$$\Psi(0,t) = 1(t) \sin \omega_o t \tag{19}$$

with

$$1(t) = \begin{cases} 1 & t > 0 \\ 0 & t < 0 \end{cases} \tag{20}$$

This has a frequency spectrum which is peaked at $\omega = \omega_o$, and since $\omega_o >> \omega_m$, we can anticipate (as is shown in Appendix II) that $\Delta\Psi(L,t)$ will be a negligible contribution to $\Psi(L,t)$. Thus, from (16)

$$\Psi(L,t) \approx \int_{-\infty}^{\infty} \bar{\Psi}_o \, e^{j\Phi(\omega)} \, d\omega \tag{21}$$

The quickest way to evaluate (21) is by the method of convolution over the time domain [9]. Thus, let $h(t)$ be the response of the system to a delta function input,

$$h(t) = \frac{1}{2\pi} \int_{-\infty}^{\infty} e^{j\Phi(\omega)} \, d\omega \tag{22}$$

then the output, $\Psi(L,t)$, for the input $\Psi(0,t)$, is [10]

$$\Psi(L,t) = \int_{-\infty}^{\infty} h(\tau) \, \Psi(0,t-\tau) \, d\tau \tag{23}$$

We first determine $h(\tau)$. To this end we expand $\Phi(\omega)$ in a Taylor series about ω_o, viz.

$$\Phi(\omega) = \Phi(\omega_o) + \Phi'(\omega_o)(\omega-\omega_o) + \Phi''(\omega_o) \frac{(\omega-\omega_o)^2}{2} + \text{h.t.} \tag{24}$$

where the prime denotes differentiation with respect to ω, and we drop the higher order, h.t. , terms which is valid if

$$\left|\Phi'''(\omega_o)\,\frac{(\omega-\omega_o)^3}{6}\right| << \left|\frac{\Phi''(\omega_o)(\omega-\omega_o)^2}{2}\right| \tag{25}$$

i.e., if

$$\left|(\omega-\omega_o)\right| << 3\left|\frac{\Phi''(\omega_o)}{\Phi'''(\omega_o)}\right| \quad . \tag{26}$$

Now, here

$$\Phi(\omega_o) = \omega_o t - t_o\left(\omega_o - \tfrac{1}{2}\frac{\overline{\omega_p^2}}{\omega_o}\right) \tag{27}$$

$$\Phi'(\omega_o) = t - t_o\left(1 + \tfrac{1}{2}\frac{\overline{\omega_p^2}}{\omega_o^2}\right) \tag{28}$$

$$\Phi''(\omega_o) = +\,t_o\left(\frac{\overline{\omega_p^2}}{\omega_o^3}\right) \tag{29}$$

$$\Phi'''(\omega_o) = -\,\frac{3\overline{\omega_p^2}}{\omega_o^4}\,t_o \tag{30}$$

Thus, from (26), (24) is valid if

$$\left|\frac{\omega}{\omega_o} - 1\right| << 1 \tag{31}$$

2. Discussion of Stationary Phase

At this point we ask ourselves what the significance of this inequality in the frequency domain is as far as response in the time domain is concerned. This question is answered by recognizing that at any given instant of time the output comes mainly from those frequencies, ω_s, which are in phase with one another (i.e., that group of frequencies having a stationary phase). The stationary phase frequencies contribute as $\frac{1}{\sqrt{L}}$, whereas the others contribute as $\frac{1}{L}$, as shown in Appendix III. The phase is stationary for $\Phi'(\omega) = \partial_\omega \Phi = 0$, which from (17) is

$$\Phi'(\omega)\Big|_{\omega=\omega_s} = 0 = t - t_o\left(1 + \frac{\overline{\omega_p^2}}{\omega_s^2}\right) \tag{32}$$

i.e., at the instant t the stationary phase frequencies are

$$\omega_s = \pm \frac{1}{\sqrt{2}} \frac{\overline{\omega_p}}{\sqrt{\frac{t}{t_o} - 1}} \tag{33}$$

A normalized plot of (33) is shown in Fig. 3, and discloses that at the initial arrival of the signal (i.e., at $t = t_o$) the infinite frequencies come in; and as t becomes indefinitely large, ω_s approaches $\overline{\omega_p}$. Furthermore, at the group

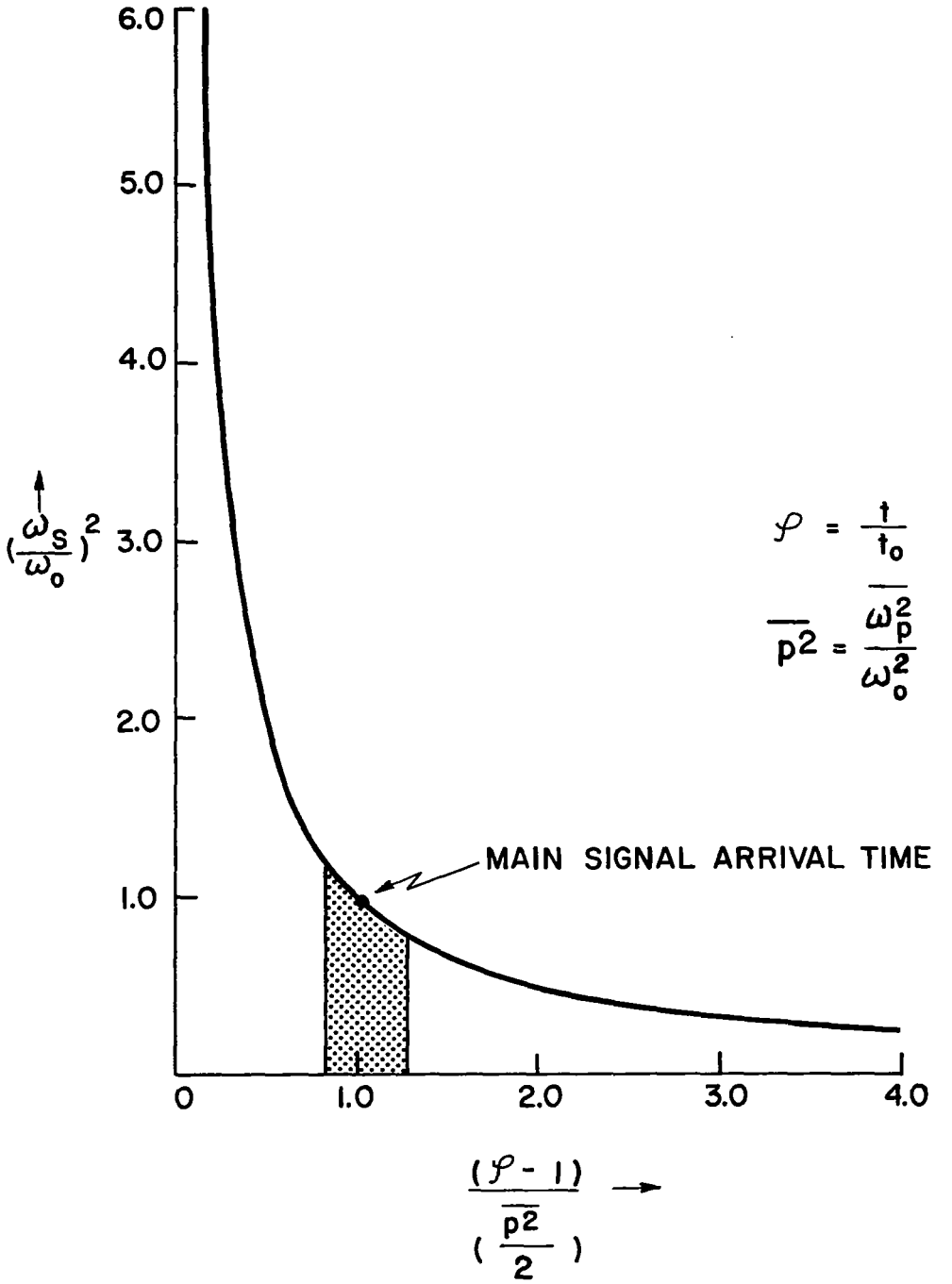

FIG.3. DEPENDENCE OF STATIONARY PHASE FREQUENCY ON TIME.

velocity time, $t_g = \frac{L}{v_g}$, where $v_g = \left.\frac{1}{\frac{d\beta_p}{d\omega}}\right|_{\omega=\omega_o}$, the significant frequencies are those at and near the carrier ω_o. This is seen as follows here: $\beta = \frac{\omega}{c}\left(1 - \frac{1}{2}\frac{\overline{\omega_p^2}}{\omega^2}\right)$, therefore,

$$v_g = \frac{c}{1 + \frac{1}{2}\frac{\overline{\omega_p^2}}{\omega_o^2}} \tag{34}$$

hence

$$t_g = \frac{L}{v_g} = t_o\left(1 + \frac{1}{2}\frac{\overline{\omega_p^2}}{\omega_o^2}\right) \tag{35}$$

Hence, from (33) the frequency which contributes most significantly is $\pm\omega_o$. Thus, the inequality (31) can be re-expressed in the time domain, using (33) and (35), as (see Appendix IV)

$$|t - t_g| << t_o\overline{P^2} \tag{36}$$

where $\overline{P^2} = \frac{\overline{\omega_p^2}}{\omega_o^2}$. Thus when we obtain $h(t)$ from (22) and then $\Psi(L,t)$ from (23), the solution so obtained will only be valid for regions of time about the time t_g satisfying (36).

Thus, the solution obtained will have a frequency spectrum given by (31), representing the time region of (36). If, for example, $\left|\frac{t - t_g}{t_o}\right| \leq \frac{1}{10} P^2$, then $(\omega/\omega_o)^2 = 1 \pm 0.20$, as shown shaded in Fig. 3.

3. Convolution Solution

Inserting (24) into (22) gives (after changing variables from $\omega - \omega_o$ to ω' and then dropping the primes)

$$h(t) = \frac{e^{j\Phi(\omega_o)}}{2\pi} f(t - t_g) \tag{37}$$

where

$$f(t) = \int_{-\infty}^{\infty} e^{j\frac{\Phi''(\omega_o)\omega^2}{2}} e^{j\omega t} d\omega \tag{38}$$

The result (38) is recognized as the Fourier transform of a Gaussian which is itself a Gaussian (obtained by completing the square and using the complete Fresnel integral $\int_{-\infty}^{\infty} e^{jax^2} dx = \sqrt{\frac{\pi j}{a}}$), thus

$$f(t) = \sqrt{\frac{2\pi}{\Phi''(\omega_o)}} e^{-j\frac{t^2}{2\Phi''(\omega_o)}} e^{j\frac{\pi}{4}} \tag{39}$$

Thus, (37) gives

$$h(t) = \frac{e^{j\Phi(\omega_o)}}{2\pi}\sqrt{\frac{2\pi}{\Phi''(\omega_o)}}\; e^{j\frac{\pi}{4}}\; e^{-j\frac{(t - t_g)^2}{2\Phi''(\omega_o)}} \qquad (40)$$

Substituting this result into (23) with

$$\Psi(0,t-\tau) = 1(t-\tau)\sin\omega_o(t-\tau)$$

$$= I_m\, 1(t-\tau)\, e^{j\omega_o(t-\tau)} \qquad (41)$$

where I_m denotes imaginary part and realizing the imaginary part of (23) should then be taken, gives

$$\Psi(L,t) = I_m\sqrt{\frac{j\pi}{BL}}\,\frac{e^{j\Phi(\omega_o)}}{2\pi}\int_{-\infty}^{t} e^{-j\frac{(\tau - t_g)^2}{4BL}}\, d\tau \qquad (42)$$

Above the symbol $B = +\dfrac{\Phi''(\omega_o)}{2L}$ has been introduced for brevity.

Letting $x^2 = j\dfrac{(\tau - t_g)^2}{4BL}$, and using the definitions of the complimentary erf Z and erfc Z functions, i.e.

$$\text{erfc } Z \equiv \frac{2}{\sqrt{\pi}}\int_{Z}^{\infty} e^{-x^2}\, dx = 1 - \text{erf } Z \qquad (43)$$

then gives [9] ,

$$\Psi(L,t) = I_m\left\{\tfrac{1}{2}\, e^{j\Phi(\omega_o)}\ \text{erfc}\ Z_o\right\} \tag{44}$$

where

$$Z_o = -\frac{(t - t_g)(1 + j)}{2\sqrt{2BL}} \tag{45}$$

Extracting the imaginary part and simplifying in terms of Fresnel integrals, using the identity [11], (p. 301 7.3.22),

$$\frac{(1 + j)}{2}\ \text{erf}\left[\frac{\sqrt{\pi}}{2}\ (1 - j)\ X\right] = C(X) + jS(X) \tag{46}$$

and the facts that the conjugate of an erf function is the erf function of the conjugate, and that both the C(X) and S(X) functions are odd, enables one to write (44) in the form of Haskell-Case result [12]

$$\Psi(L,t) = B(t)\ \sin\left[\Phi(\omega_o) + \theta_o(t)\right] \tag{47}$$

where

$$B(t) = \frac{1}{\sqrt{2}}\ \sqrt{\left[C(v) + \tfrac{1}{2}\right]^2 + \left[S(v) + \tfrac{1}{2}\right]^2} \tag{48}$$

$$\theta(t) = \arctan\left[\frac{C(v) - S(v)}{1 + C(v) + S(v)}\right] \tag{49}$$

with

$$v = \frac{t - t_g}{\sqrt{\pi \Phi''(\omega_o)}} = \frac{1}{\bar{P}}\sqrt{\frac{\eta}{\pi}}\left(\frac{t - t_g}{t_o}\right) \tag{50}$$

where $\bar{P} = \sqrt{\overline{P^2}}$, $\eta = \omega_o t_o$, $C(v) = \int_0^v \cos\frac{\pi}{2}x^2\,dx$,

$S(v) = \int_0^v \sin\frac{\pi}{2}x^2\,dx$.

It remains to determine the time range of validity of the solution (47). This is obtained from (36), which expressed in terms of the normalization parameter v can be written as

$$|v| << \bar{P}\sqrt{\frac{\eta}{\pi}} \tag{51}$$

For the solar corona-earth path at V.H.F. carriers, (as we will see shortly, p. 161) $\left(\bar{P}\sqrt{\frac{\eta}{\pi}}\right)_{max} \gtrsim 200$. Hence (47) will be valid for $|v| \lesssim 20$.

A universal plot [12] of the envelope $B(v)$ is shown in Fig. 4a, and the phase, $\theta(v)$, in Fig. 4b. It is noted that $v = 0$ corresponds to the time $t = t_g$, and that for $v = -20$, the amplitude is essentially zero, similarly to the right for $v = +20$ the amplitude is essentially unity. This means that the Sommerfeld, Anterior Transient, and Posterior Transient portions of the response of this extremely long, slightly dispersive, homogeneous plasma to a stepped carrier (these portions are lucidly derived in the excellent paper by Haskell and Case [12] and are also independently and concisely derived in Appendix III of this report) are of insignificant magnitude and, as such, the main signal (also called the group velocity signal, or quasi-monochromatic solution) as given by (47) can actually be used to describe the signal over the entire time region from $-\infty \leq t \leq \infty$. (It is to be stressed that this is not true in general, since the signal arrives at time, t_o, but due to the long path length and small $\overline{\omega}_p$, the signal here is essentially zero until just before the time t_g, whereafter it builds up very quickly to the steady state.) This is indeed a fortuitous result since a series of stepped carriers will be used and the relative mathematical simplicity of (47) is advantageous, as will be seen.

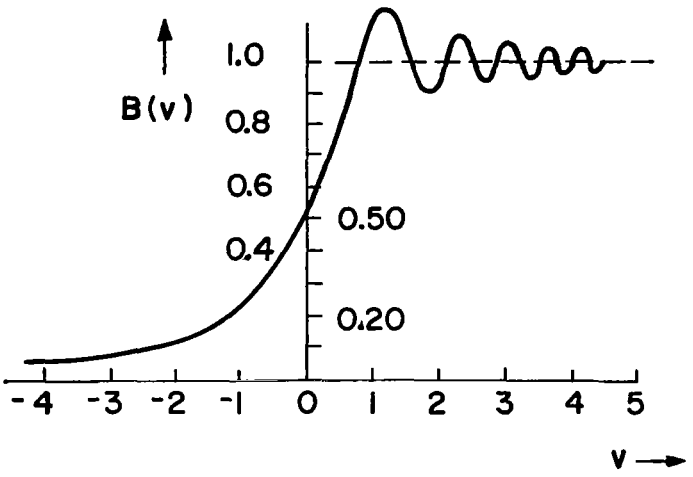

FIG. 4a. UNIVERSAL CURVE FOR THE AMPLITUDE OF THE MAIN SIGNAL.

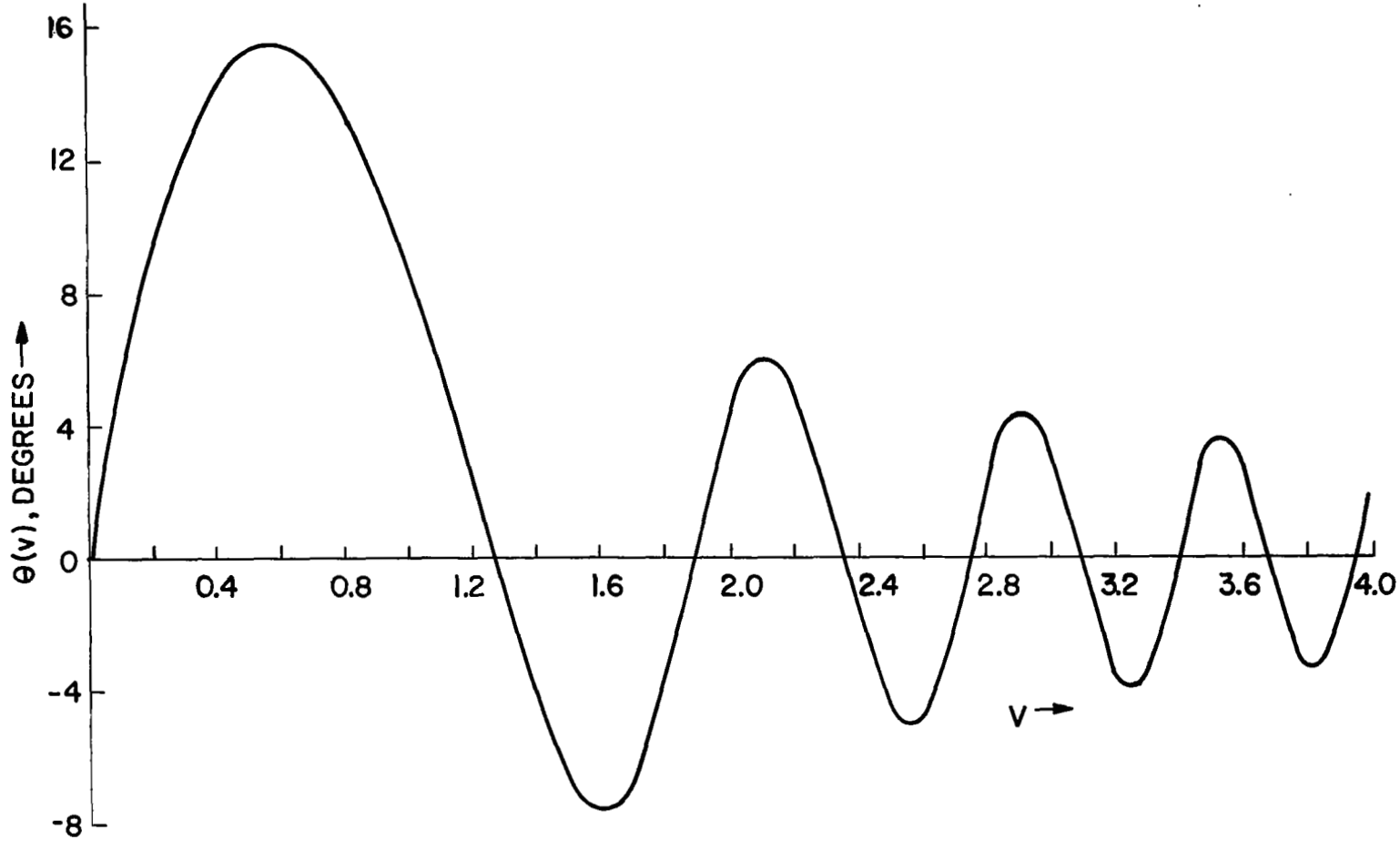

FIG. 4b. UNIVSAL CURVE FOR PHASE OF THE MAIN SIGNAL.

4. Rise Time

From Fig. 4a, it is noted that the envelope builds up from a small value to near unity in a small increment about $v = 0$. Following Hodara [13] let us arrive at a quantitative measure of this rise time by recognizing that time is the derivative of phase with respect to frequency, i.e., let

$$t_R \equiv \Phi'\left(\omega_o + \frac{\Delta\omega}{2}\right) - \Phi'\left(\omega_o - \frac{\Delta\omega}{2}\right) \tag{52}$$

where we realize $\Phi'\left(\omega_o - \frac{\Delta\omega}{2}\right) < \Phi'\left(\omega_o + \frac{\Delta\omega}{2}\right)$ as seen from (29). Using

$$\Phi'\left(\omega_o \pm \frac{\Delta\omega}{2}\right) \approx \Phi'(\omega_o) \pm \frac{\Delta\omega}{2}\,\Phi''(\omega_o) \tag{53}$$

gives, since $\Delta\omega = 2\pi\Delta f$, and $t_R = \frac{1}{\Delta f}$, (using (29))

$$t_R = \sqrt{2\pi\Phi''(\omega_o)} = \sqrt{\frac{t_o\overline{P^2}}{f_o}} \tag{54}$$

which can be expressed in terms of the differential delay time, T_d, defined as the time between the initial arrival of the signal, t_o, and the group arrival time, t_g, i.e.

$$T_d \equiv t_g - t_o \tag{55}$$

which, from (35), becomes

$$T_d = \tfrac{1}{2} t_o \overline{P^2} = \frac{81}{2cf_o^2} \bar{n}(\rho) \tag{56}$$

where $\bar{n}(\rho)$ is the integrated columnar electron density

$$\bar{n}(\rho) = \int_0^L n(\xi)\, d\xi \tag{57}$$

Hence*

$$t_R = \sqrt{\frac{2T_d}{f_o}} \quad . \tag{58}$$

If we now evaluate the corresponding value of v at $t = t_g \pm (t_R/2)$, we see from (50) that in this rise time period v varies over $\pm v_R$, where

$$v_R = \sqrt{\frac{\eta}{\pi}} \frac{t_R}{\bar{P} t_o} = \frac{1}{\sqrt{2}} \tag{59}$$

Hence from Fig. 4a, we see that in the time increment $t_g - \frac{t_R}{2}$ to $t_g + \frac{t_R}{2}$, the envelope rises from approximately 0.25 to 0.90. This is similar to other definitions of rise time [14].

* For an alternate derivation of t_R, see Appendix V.

5. Distortion Parameter

Suppose now a single pulse of duration T is released at the transmitter, i.e.

$$\Psi_p(0,t) = \left[1(t) - 1(t - T)\right] \sin \omega_o t \qquad (60)$$

which is seen to be the superposition of two stepped carriers of opposite signs separated in time by T. From (47) we can immediately write the output pulse as

$$\Psi_p(L,t) = \Psi(L,t) - \Psi(L,t - T) \qquad (61)$$

A rough sketch of the resulting pulse obtained by superposition, (61), is shown in Fig. 5. It is immediately seen that if the pulse duration T is so small that the second stepped carrier comes in before the first has built up (i.e., if $T < t_R$), serious distortion will begin to occur. This suggests defining a distortion parameter, β, as some ratio of rise time to bit (pulse duration) time. For convenience, we define (since the quantity $t_R/\sqrt{2}$ appears in the development),

$$\beta \equiv \frac{t_R}{T\sqrt{2}} \qquad (62)$$

Hence we will expect serious pulse distortion to start to occur for β near unity or greater.

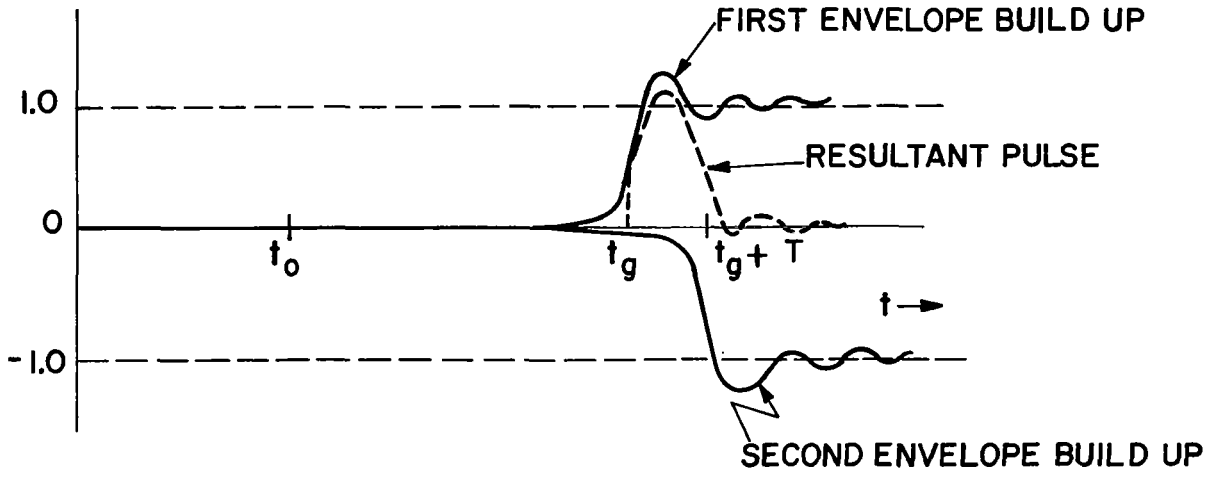

FIG. 5. BUILD UP OF PULSE OF INPUT DURATION T.

IV. CORRELATION RECEIVER - MEASUREMENT OF $\bar{n}(\rho)$

a. Transmitted Code-Correlation Function

Suppose now a series of pulses of constant frequency, ω_o, and of fixed duration, T , are turned on and off with either 0^o or 180^o phase (phase shift keyed). Further, let there be a total of N such pulses with any n^{th} pulse turned on to obey the following rule: (here a +1 denotes the phase is 0^o , and a -1 is 180^o)

$$\left.\begin{array}{ll} X(n) = +1 & 1 \leq n \leq 7 \\ X(n) = X(n-7) \oplus X(n-1) & 8 \leq n \leq N \\ X(n) = 0 & \begin{cases} n \leq 0 \\ n \geq 127 \end{cases} \end{array}\right\} \qquad (63)$$

where the $\oplus$ operator is defined by

$$\left.\begin{array}{lll} 1 \oplus 1 = -1 & & -1 \oplus +1 = +1 \\ & \text{and} & \\ -1 \oplus -1 = -1 & & 1 \oplus -1 = +1 \end{array}\right\} \qquad (64)$$

If we let $N = 127$, the resulting pulse train looks like Fig. 6, where only the amplitudes (a negative 1 amplitude denotes 180^o phase, a plus 1 amplitude 0^o phase) are shown.

Thus, this pulse train or code can be written as:

$$\Psi(0,t) = m(t) \sin \omega_o t = I_m \left[m(t) \; e^{j\omega_o t} \right] \qquad (65)$$

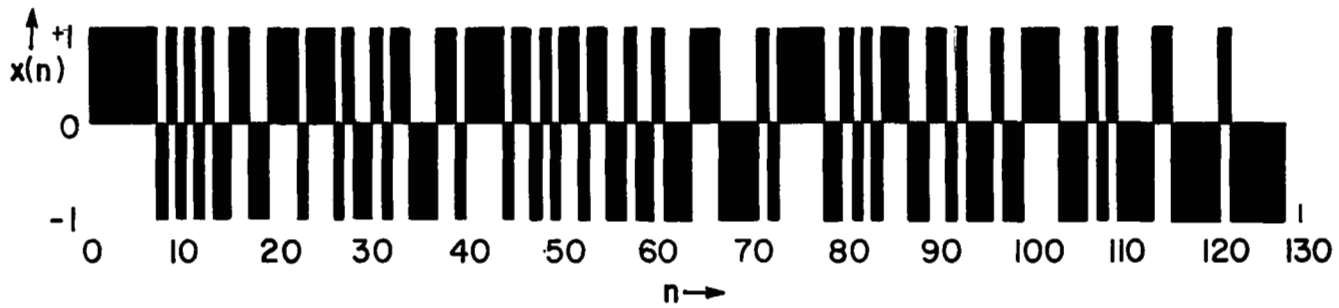

FIG. 6. THE 127 BIT PSEUDO RANDOM CODE.

where I_m denotes imaginary part, and

$$m(t) = \sum_{n=1}^{N=127} X(n) \left[1(t) - 1(t - nT)\right] \quad . \tag{66}$$

If we now compute the auto-correlation function, $r(x)$, of this transmitted code, defined as

$$r(x) = \int_{-\infty}^{\infty} m(w - x)\, m(w)\, dw \tag{67}$$

where x and w are times normalized with respect to the bit length, T, one obtains

$$r(x) = \sum_{n=1}^{n=127 - x} X(n)\, X(n + x) \tag{68}$$

The result $r(x)$ is plotted in Fig. 7, and is seen to have a peak of $N = 127$, 2 bits wide, and a maximum side lobe of 9. This particular code is an example of a pseudo random code having a well-defined sharp peak.

b. Received Code-Correlation Function

When the signal (65) is propagated through the solar corona along a typical path as depicted in Fig. 2, it arrives in the form of a superposition of (47), namely

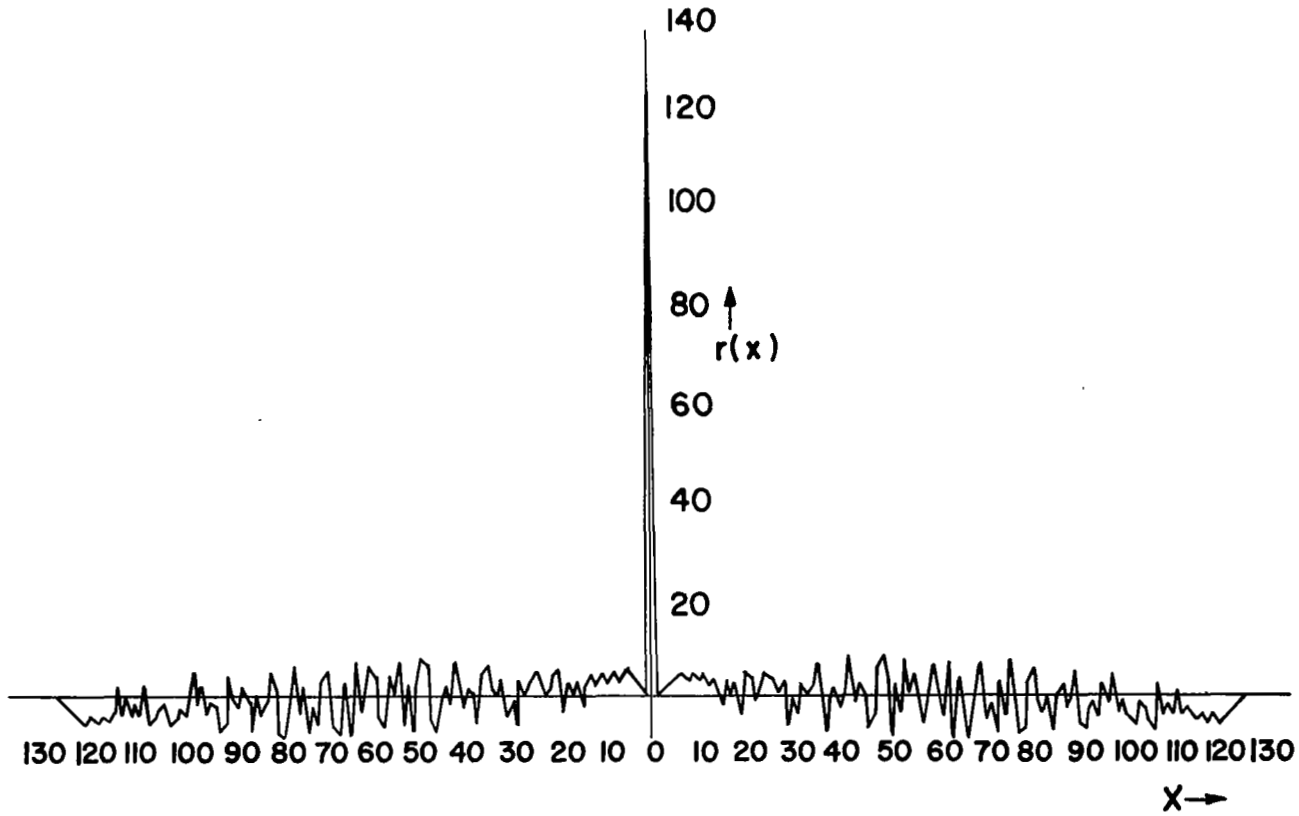

FIG.7. AUTO-CORRELATION FUNCTION OF 127 BIT PSEUDO RANDOM CODE.

$$\Psi(L,t) = I_m \sum_n X(n)\, B_n(t)$$

$$\cdot\, e^{j\omega_o t}\, e^{-j\omega_o t_o \sqrt{1 - P^2}}\, e^{j\theta_o (t - t_n)} \qquad (69)$$

We could at this point take the magnitude of (69) and obtain the cross-correlation function of it with $r(x)$. However, an easier route to follow is that described by Pindyck [2] which is, briefly, as follows:

As before, we can write:

$$\Psi(L,t) = \int_{-\infty}^{\infty} \bar{\Psi}(0,\omega) e^{j\Phi(\omega)}\, d\omega \qquad (70)$$

where $\bar{\Psi}(0,\omega)$ is the Fourier transform of (63)

$$\bar{\Psi}(0,\omega) = \frac{1}{2\pi} \int_{-\infty}^{\infty} m(t)\, e^{j\omega_o t}\, e^{-j\omega t}\, dt \qquad (71)$$

Inserting (71) into (70) and using the Taylor Series (24) for $\Phi(\omega)$ (which we now know can be used to represent the output for all times), normalizing and simplifying gives: (See Appendix VI for details.)

$$\Psi(L,t) = I_m \left[a(t)\, e^{j\omega_o t} \right] \qquad (72)$$

where $a(t)$ is a complex amplitude function defined by

$$a(t) = \frac{(1+j)}{2} e^{-j\beta(\omega_o)L}$$

$$\cdot \int_{-\infty}^{\infty} m\left[t - t_g + \frac{ut_R}{\sqrt{2}}\right] e^{-j\frac{\pi}{2}u^2} du \qquad (73)$$

and is slowly varying compared to ω_o .

As a check, we note that if a single stepped carrier turned on at $t = 0$ is considered (i.e., $m(t) = 1(t)$) then (72) with (73) reduces to (44) (or (47)) as should be.

Suppose we now examine the operation of the correlation receiver as described by Fig. 8. As indicated, the incoming signal is split evenly into two channels; mixed (multiplied) with $\sin \omega_o t$ and $\cos \omega_o t$; respectively, passed through a low pass filter; multiplied by a replica of the transmitted envelope, $m(t - t_c)$, delayed in time by t_c (subscript c for correlation time); integrated over an infinite time period (in practice, over a time period long enough to bring the signal sufficiently out of the noise will suffice), and displayed on an oscilloscope. The oscilloscope screen then will display a quantity proportional to the normalized cross-correlation function, $y(\tau)$, defined by

$$y(\tau) \equiv \frac{|R(\tau + \tau_g)|}{T} \qquad (74)$$

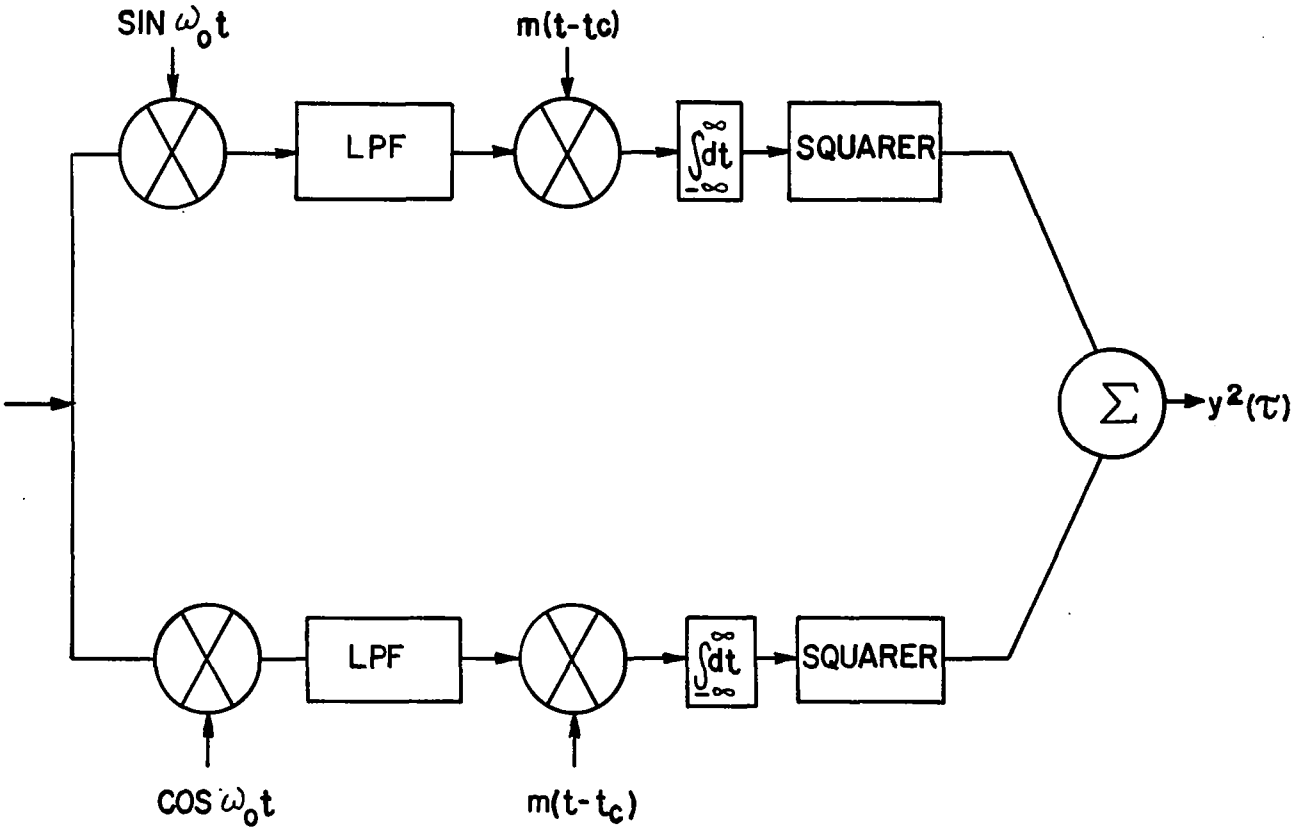

FIG.8 CORRELATION RECEIVER

as derived in Appendix VII where τ is the correlation time normalized with respect to the bit length, $\tau = t_c/T$, and $\tau_g = t_g/T$ with t_g defined by (35), and which becomes

$$y(\tau) = \sqrt{\frac{I_c^2(\tau) + I_s^2(\tau)}{2}} \tag{75}$$

with

$$I_c(\tau) = \frac{1}{\beta} \int_{-(N+\tau)}^{N-\tau} r(x) \Big|_{x=\tau+v} \cos\left[\frac{\pi}{2}\left(\frac{v}{\beta}\right)^2\right] dv \tag{76a}$$

$$I_s(\tau) = \frac{1}{\beta} \int_{-(N+\tau)}^{N-\tau} r(x) \Big|_{x=\tau+v} \sin\left[\frac{\pi}{2}\left(\frac{v}{\beta}\right)^2\right] dv \tag{76b}$$

where $r(x)$ is the auto-correlation function of the transmitted code as given by (68).

Inspection of (75) reveals that $y(\tau)$ is even with respect to τ ($y(-\tau) = y(\tau)$) and hence $\tau = 0$ is the center of the display. Thus the centers of the correlation curves occur at the absolute time of $t = t_g$, i.e., the group arrival time. Also, it is seen that $y(\tau)$ only contains one parameter, namely the distortion parameter β. As will be seen, the distortion parameter, β, will vary from slightly over zero to approximately 2. Computed curves of $y(\tau)$

versus τ , with β as a parameter, are given in Fig. 9. The form for computation follows that outlined by Pindyck [2] but an independent program was used, as described in Appendix VIII. If $\beta = 0$, (75) reduces to $r(x)$ as should be, and as given in Appendix VII. (It is noted here that if a Triple Folded Barker Code is used rather than the 127 Bit code considered, very similar correlation curves result, as shown in Appendix IX.)

c. Plasma Diagnostics with Single Carrier

The curves of Fig. 9 can now be used to measure $\bar{n}(\rho)$ of the particular path on a given day (the path length, L , can be considered constant over a day's period and is specified by the normalized offset distance $\rho = R_\perp / R_o$ and θ) by associating the observed shape of the measured $y(\tau)$ curve with the calculated curves of Fig. 9, to determine β . Then from (62), (57), and (58) we get

$$\bar{n}(\rho) = \frac{2c}{81} \beta^2(\rho)\, T^2\, f_o^3 \qquad (77)$$

Thus since T and f_o are specified, we determine $\bar{n}(\rho)$ from the measured β . Then from this value of $\bar{n}(\rho)$ we can deduce the radial number density variation $n(r)$ as will be discussed shortly.

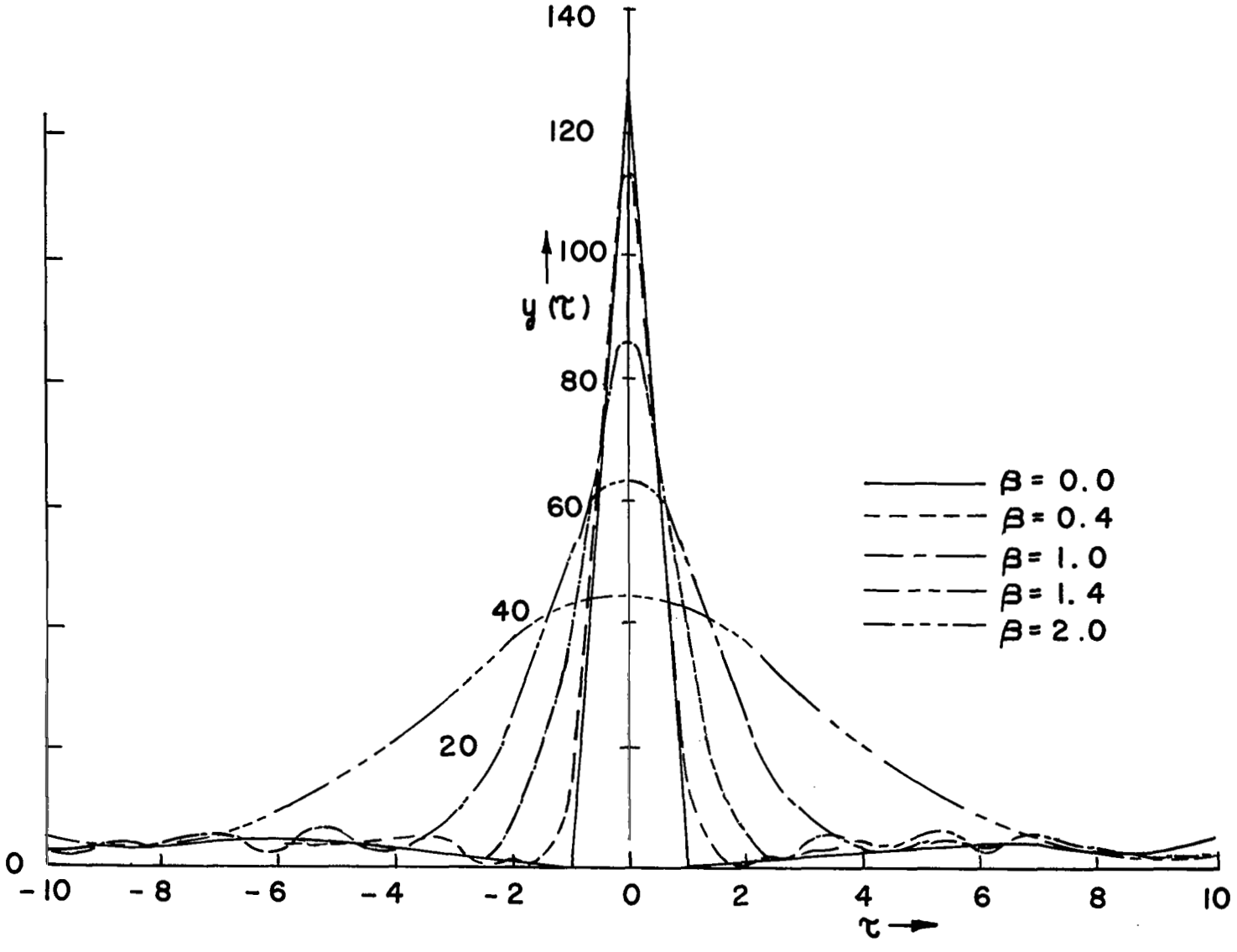

FIG.9 CORRELATION RECEIVER OUTPUT RESPONSE--COMPUTED

d. Plasma Diagnostics with Two (or More) Carriers

Since the deduced value of $\beta(\rho)$ as measured off the oscilloscope will degrade with increasing β, it is more accurate to determine $\bar{n}(\rho)$ by using two coded pulse trains, the first with carrier frequency f_{o_1} and the second with f_{o_2} where $f_{o_2} > f_{o_1}$, separated in time by T_s (where T_s is large enough so the first pulse train has completely decayed) and measuring, on the receiver scope, the differential time difference, ΔT, between the correlation centers (which we know will be peaks for $\beta \lesssim 2$) of these two trains. Since the centers occur at $\tau = 0$, this time difference is

$$-\Delta T = (t_{g_1} - t_{g_2}) - T_s = T_{d_2} - T_{d_1} \tag{78}$$

which becomes

$$\Delta T(\rho) = T_{d_1}\left[1 - \left(\frac{f_{o_1}}{f_{o_2}}\right)^2\right] = \frac{81\,\bar{n}(\rho)}{2c\,f_{o_1}^2}\left[1 - \left(\frac{f_{o_1}}{f_{o_2}}\right)^2\right] \tag{79}$$

Thus, in principle (disregarding noise effects, as will be discussed), the quantity $\bar{n}(\rho)$ can be measured as accurately as one can measure time.

V. OBTAINMENT OF n(r) VARIATION FROM KNOWLEDGE OF $\bar{n}(\rho)$

We have thus shown how, for any given point on the trajectory, pulsed carriers can be used to determine the average

integrated columnar electron density, $\bar{n}(\rho)$, for that particular path. Now, following the ingenious recognition by Harrington [3] one can deduce the actual $n(r)$ variation from a continuous record of measurements of $\bar{n}(\rho)$ as follows:

Consider the geometry as defined by Fig. 2, a typical propagation path of length L is shown. Now, the quantity we can measure is $\bar{n}(\rho)$ which, from (57), becomes in terms of various radii (normalized with respect to the radius of the Sun, R_o):

$$\bar{n}(\rho) = R_o\left[\int_{\rho}^{r_S} + \int_{\rho}^{r_E} \frac{n(r)rdr}{\sqrt{r^2-\rho^2}}\right] \tag{80}$$

Adding and subtracting contributions from r_S to ∞ and r_E to ∞ gives

$$\bar{n}(\rho) = 2R_o \int_{\rho}^{\infty} \frac{n(r)rdr}{\sqrt{r^2-\rho^2}} - \Delta \tag{81}$$

where

$$\Delta = +\left[\int_{r_S}^{\infty} + \int_{r_E}^{\infty} \frac{n(r)rdr}{\sqrt{r^2-\rho^2}}\right] R_o \tag{82}$$

Since $r_E \approx 215$, and $n(r)$ is very small for r_S large, it follows that to a first approximation Δ can be ignored.

Hence, to this approximation, we have $n(r)$ in the form of an Abel integral equation:

$$\bar{n}(\rho) = 2R_o \int_{\rho}^{\infty} \frac{n(r)rdr}{\sqrt{r^2 - \rho^2}} \tag{83}$$

which has the known solution [3] (see Appendix X)

$$n(r) = -\frac{1}{R_o \pi} \partial_r \left\{ \int_{r}^{\infty} \frac{r\bar{n}(\rho)d\rho}{\rho\sqrt{\rho^2 - r^2}} \right\} \tag{84}$$

Thus, if the quantity $\bar{n}(\rho)$ is measured at sufficiently fine increments of ρ (say for daily points along the trajectory) so as to get a smooth continuous function, one can perform the integration and differentiation operation of (84) to determine the $n(r)$ variation. Thus, $\bar{n}(\rho)$ and $n(r)$ are Abel transforms of one another.

To account for the fact that r_S and r_E (especially the former) are not infinite, one could correct the result (84) by subtracting the Δ term of (82) using the $n(r)$ distribution obtained from (84) in (82).

VI. EXAMPLE FOR DIAGNOSTICS USING V.H.F. CARRIERS

To demonstrate what type of correlation curves one can anticipate to receive, an example at V.H.F. carrier frequencies with an assumed $1/r^2$ electron density is now given.

At any given instant of time along the trajectory (determined by solving the mechanics problem), as shown in Fig. 10, the position of the satellite is defined by the angle θ and the radius R_s. Alternatively, a value of $R_\perp$ (or $\rho = R_\perp/R_o$) and R_s also specifies the location of the satellite. Now, from (80) and (56) it follows that (renormalizing distance with respect to $R_E \approx 215R_o$)

$$T_d = \frac{R_E\, k}{2f_o^2 c}\left[\int_{u_\perp}^{u_s} + \int_{u_\perp}^{1} \frac{un(u)du}{\sqrt{u^2 - u_\perp^2}}\right] \tag{85}$$

where $u = \frac{R}{R_E}$, $u_\perp = \frac{R_\perp}{R_E}$, and $u_s = \frac{R_s}{R_E}$, $k = \frac{e^2}{4\pi^2 \epsilon_v m}$

$= \frac{f_p^2(r)}{n(r)} \approx 81$.

Now, if we assume that $n(r)$ varies as:

$$n(r) = \frac{K}{r^2} \quad \text{electrons/meter}^3 \tag{86}$$

which is, as is seen from Fig. 1, valid for $\rho \gtrsim 6$, with $K = 10^{12}$. Using the fact that

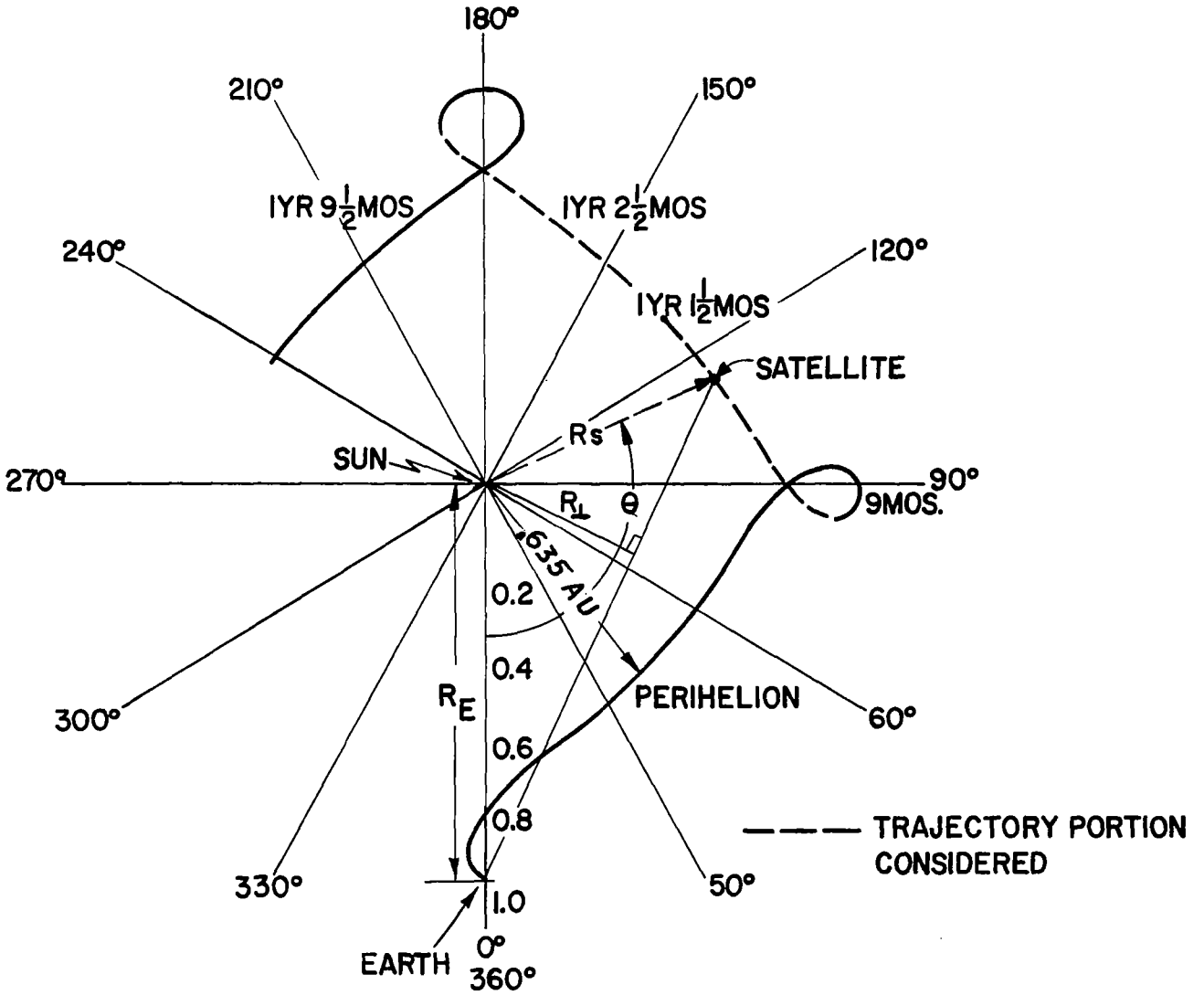

FIG. 10. MOTION OF SOLAR PROBE SATELLITE RELATIVE TO THE EARTH.

$$\int \frac{dx}{x\sqrt{x^2 - a^2}} = \pm\frac{1}{a} \arccos\left|\frac{a}{x}\right|, \quad x^2 > a^2 \tag{87}$$

(85) gives

$$T_d = (0.4349\ K)\left(\frac{1}{f_o^2}\right)\left\{\frac{\arccos\ \frac{u_\perp}{u_s} + \arccos\ (u_\perp)}{u_\perp}\right\} \tag{88}$$

This result is interesting in that the first quantity in parentheses depends only on the assumed electron density variation ($n(r) = K/r^2$), the second only on the carrier frequency, and the third only on the satellite location (assuming that $n(r) \sim 1/r^2$).

Computations for T_d using Fig. 10, made over that portion of the trajectory shown and representing the locations of the satellite trajectory between extreme values of R_s (and ρ), corresponding to $85^\circ \lesssim \theta \lesssim 187^\circ$, were made and are given in Table II and plotted in Fig. 11, for $f_o = 75$ mHz. The corresponding values of rise time, t_R , as given by (58) are also shown here, as well as the corresponding value of ρ . It is seen that t_R varies from approximately 2 to 25 μsec, as θ varies from 85° to 179° .

If now [1] a bit length of $T = 25.6$ μsec is used (causing $NT = 3.2512$ millisecs), it is seen that β ($\beta = \frac{t_R}{\sqrt{2}\,T}$) will vary from slightly over zero to approximately two for the trajectory range of $85^\circ \leq \theta \leq 179+^\circ$

TABLE II.

TABULATIONS OF T_d , t_R , AND β FOR SINGLE CARRIER FREQUENCY (f_o = 75 MHZ) AND ΔT FOR DUAL CARRIER FREQUENCY (f_o = 70 AND 80 MHZ)

θ^o	ρ	u_s	$u_\perp$	T_d MILLI-SECS.	t_R μ SEC.	β	ΔT MILLI-SECS.	$(S_o)_{in}$ WATTS TIMES 10^{-16}	$(S_o)_{in}$ DBM	S BAND Δf MHZ
85.0	154.2	.9241	.7172	.1576	2.050	.0566	.0424	5.354	-122.72	23.749
97.5	120.0	.7379	.5586	.2354	2.505	.0692	.0633	5.1869		19.4356
113.0	91.93	.6552	.4276	.3618	3.106	.0858	.09735	4.637	-123.35	15.674
134.0	63.77	.6207	.2966	.6174	4.058	.1121	.1661	3.982	-124.0	11.947
153.0	40.03	.6345	.1862	1.110	5.441	.1503	.2986	3.485		8.948
164.0	25.21	.6759	.1172	1.891	7.102	.1962	.5088	3.258		6.855
173.5	11.86	.7310	.0552	4.246	10.641	.2939	1.1424	3.003	-125.23	4.575
178.0	4.45	.7586	.02068	11.636	17.615	.4866	3.131	2.887		2.764
179.0	2.22	.7655	.01034	23.488	25.027	.6914	6.319			1.945
180.0	0	.7703	0	∞	∞	∞	∞	2.799		0
181.0	2.22	.7724	.02068	11.655	17.630	.4870	3.0415			2.762
184.0	8.90	.8207	.04137	5.734	12.365	.3415	1.543	2.694		3.94
187.0	14.83	.9380	.06897	3.383	9.498	.2623	.9102	2.484	-126.04	5.13

selected, as also tabulated in Table II and plotted in Fig. 11. Actually β will be infinite at $\theta = 180^{o}$, so the value $\beta = 2$ will be reached for θ slightly over 179^{o}. Hence, the computed $y(\tau)$ correlation curves of Fig. 9 will apply to this case. At a given carrier, measured curves of $y(\tau)$ should then be compared with those of Fig. 9 to see if indeed they can be matched, thus validating the assumed plasma density assumption of $n(r) = K/r^2$. Various values of K can be taken until a closer match is obtained.

Now, if several pulse trains, each at a different frequency are used, and if a spacing between pulse trains of $T_s = 1$ second is used, this is more than ample to insure that the correlation curves are well separated. In the proposed scheme [1] the difference in differential time, ΔT, between the 70 and 80 mHz correlation curve centers is to be measured. From (79) and (77), it follows that this time (now denoted by ΔT_{13}) can be expressed as:

$$\Delta T_{13} = (\beta_1^2 T^2 f_{o_1}) \left[1 - \left(\frac{f_{o_1}}{f_{o_3}}\right)^2\right]$$

$$= \frac{81\bar{n}}{2cf_{o_1}^2} \left[1 - \left(\frac{f_{o_1}}{f_{o_3}}\right)^2\right] \qquad (89)$$

where β_1 is the β value measured at $f_{o_1} = 70$ mHz,

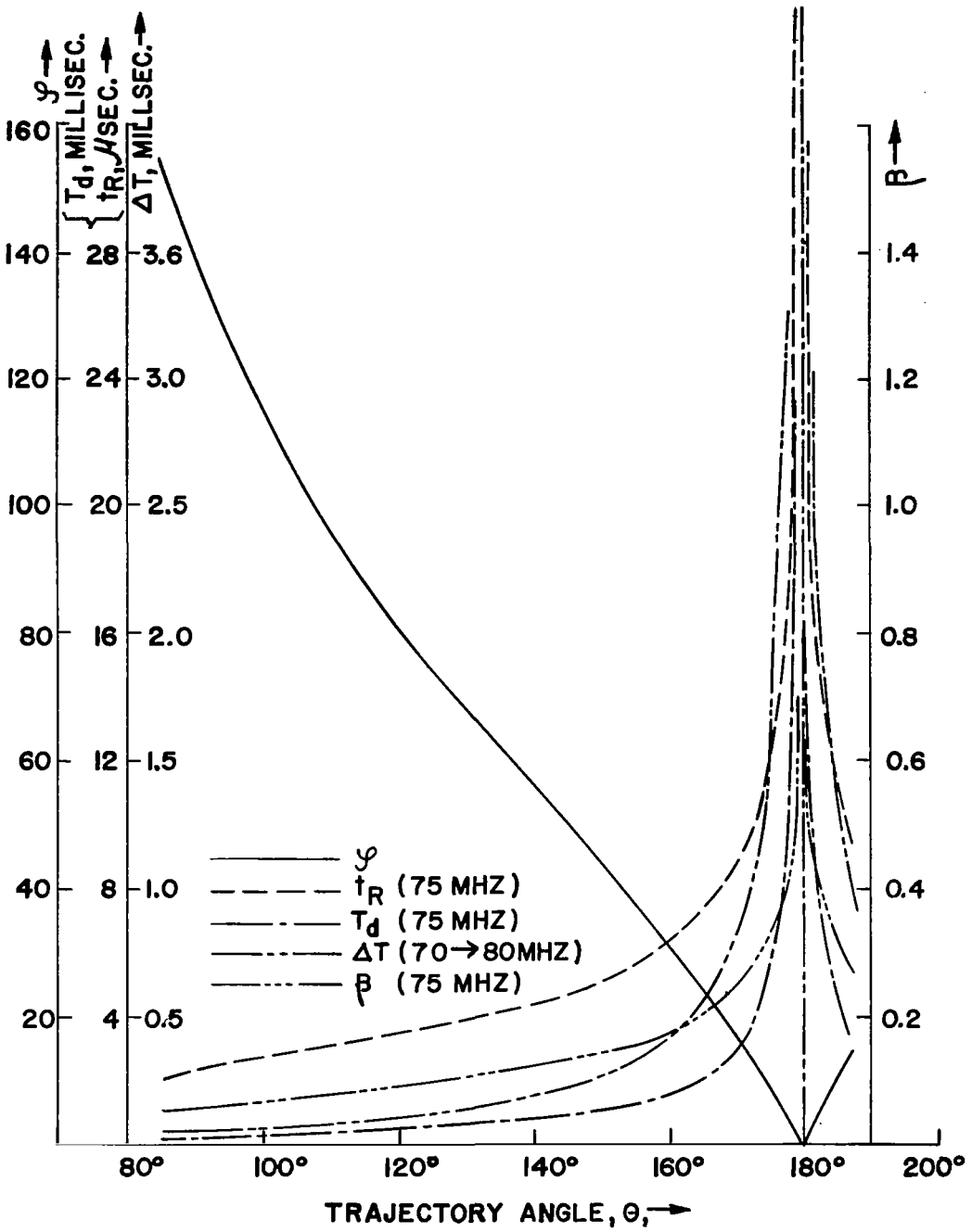

FIG. II. DEPENDENCE OF SINGLE FREQUENCY RISE TIME, DELAY TIME, AND DISTORTION PARAMETER, AND DUAL FREQUENCY DIFFERENTIAL DELAY TIME ON TRAJECTORY.

and $f_{o_3} = 80$ mHz ; hence since T , f_{o_1} , and f_{o_3} are held constant, it follows that $\Delta T_{13} \sim \beta_1^2$. A plot of ΔT_{13} versus trajectory angle is also shown in Fig. 11, and tabulated in Table II, and it is seen that ΔT_{13} varies between approximately 0.04 and 6.4 millisecs. These time differences can be measured quite readily, hence allowing experimental determination of β or $\bar{n}(\rho)$. Here again various values of K can be put into the assumed $n(r) = K/r^2$ relation to obtain various theoretical values of β until closer agreement with experiment is realized. In this way K can be determined. (The effect of noise and the consequent error in the ΔT measurement will be discussed in what follows.)

Thus, by measuring either the shape of $y(\tau)$ at a single carrier frequency, or the differential time separation of the centers of the $y(\tau)$ curves at two carriers, one can determine a measured value of β and compare it with those predicted in Fig. 11. If the values of K can be found to match these two, and K is relatively constant with respect to satellite trajectory, this would then verify the validity of the $n(r) = K/r^2$ assumption.

VII. EFFECTS OF NOISE ON MEASUREMENT ACCURACY

a. R.M.S. Error in Location Time of Correlation Peak -- Heuristic Derivation

In the preceding, the output normalized correlation function, $y(\tau)$, was determined and computed as a function of the normalized correlation time τ $\left(\tau = \frac{t_c + t_g}{T}\right)$ with the distortion parameter, β, as a parameter. Curves of $y(\tau)$ are given in Fig. 9. These curves would be those observed in the absence of noise for an infinite bandwidth receiver. In reality neither of these ideals exist and this will result in errors in the measurement accuracy of β and hence the integrated plasma, integrated electron density, $\bar{n}(\rho)$.

The effect of noise is depicted in Fig. 12 which shows that the peak can be displaced from its no noise position. Now, to locate the position of the maximum peak, τ_o, (here $\tau_o = 0$ in the absence of noise) one can tune the receiver to some arbitrary but identical level on each side of the peak (since the peak will be more difficult to locate especially for larger β's where it is very round) say at positions τ_s^+ and τ_s^- (only τ_s^- is shown in Fig. 12), and obtain τ_o as

$$\tau_o = \tfrac{1}{2}(\tau_s^+ + \tau_s^-) \tag{90}$$

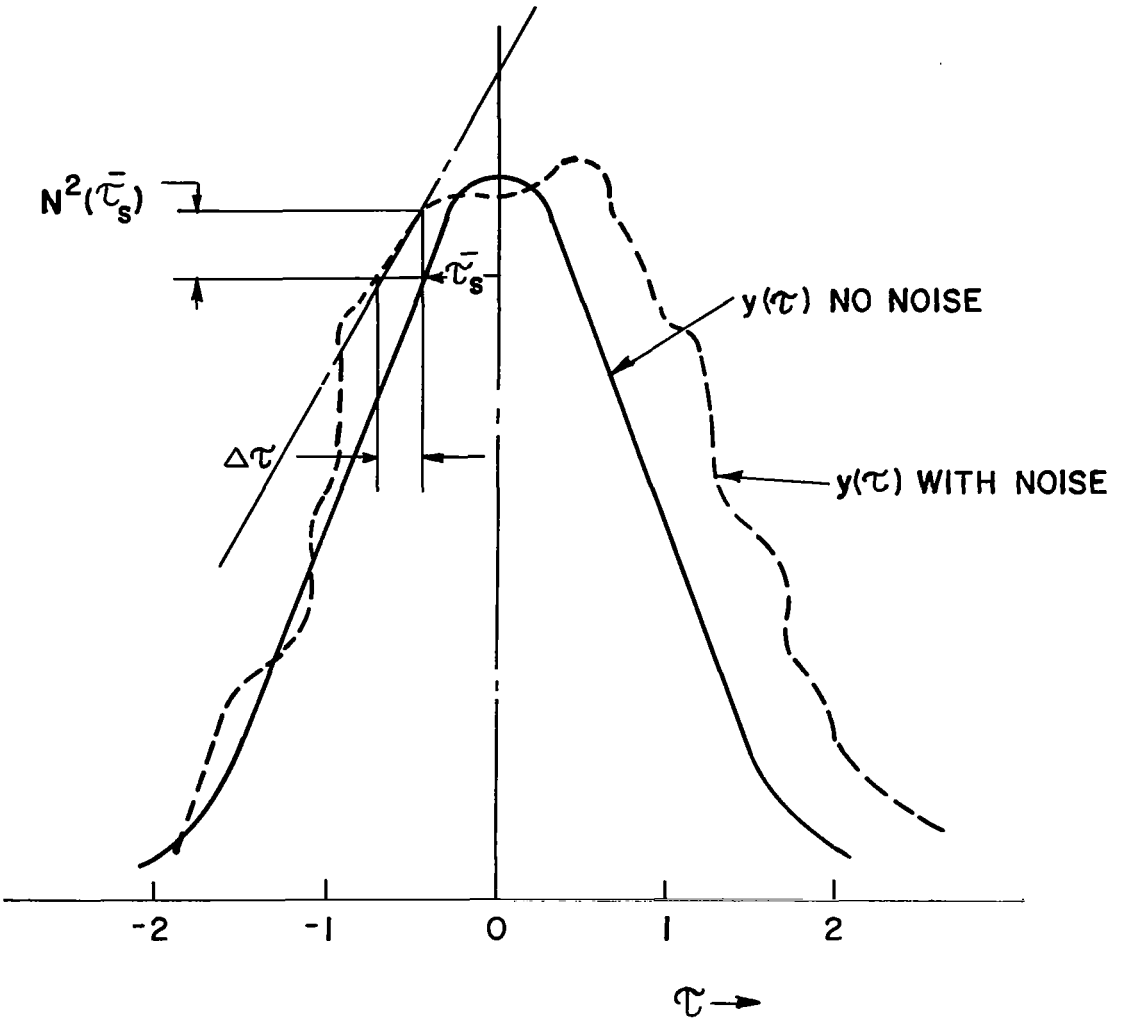

FIG. 12. EFFECT OF NOISE ON LOCATION OF PEAK CORRELATION OUTPUT.

However, due to the noise, τ_s is actually displaced by some amount, say $\Delta\tau$, and the correlation function rather than being $y(\tau_s)$ is $y(\tau_s) + N^2(\tau_s)$ (recognizing that the correlation function is really a power entity). Now for a large signal to noise ratio at the output of the receiver, we can anticipate that the shape or rates of change of $y(\tau)$ will not change too much [15] with or without noise, hence equating the slope of $y(\tau)$ with and without noise gives, as seen from Fig. 12

$$\text{Slope at } \tau = \tau_s^- = y'(\tau_s^-) \approx \frac{N^2(\tau_s^-)}{\Delta\tau} \tag{91}$$

Now if we take τ_s^- small then we recognize from the curves of Fig. 9 and associated computed values of $y(\tau)$ as a function of β that near τ equal zero we can write

$$y(\tau) \approx y_o e^{-k\tau^2} \approx y_o(1 - k\tau^2) \tag{92}$$

where

$$y_o = y(\tau)\Big|_{\tau = 0} \tag{93}$$

and k depends on β in the manner shown in Table III and plotted in Fig. 13, as obtained from Fig. 9 and the computed values (see Appendix XI for details).

TABLE III. THE FACTOR k FOR CORRELATION OUTPUT CURVES.

β	k	$\frac{1}{2k}$
0	∞	0
0.05	3.90	0.128
0.10	3.50	0.143
0.15	3.00	0.167
0.25	2.40	0.2083
0.40	1.90	0.2632
0.75	1.15	0.4348
1.00	0.75	0.667
1.25	0.315	1.59
1.40	0.20	2.50
1.75	0.12	4.17
2.00	0.10	5.00
2.50	0.05	10.00
3.00	0.025	20.00

But from (92) and the fact that $y'(\tau)\Big|_{\tau=0} = y'(0) = 0$ (since the top of the peak for no noise present is a smooth curve for β finite) gives

$$y''(\tau) = -2y_o k \qquad (94)$$

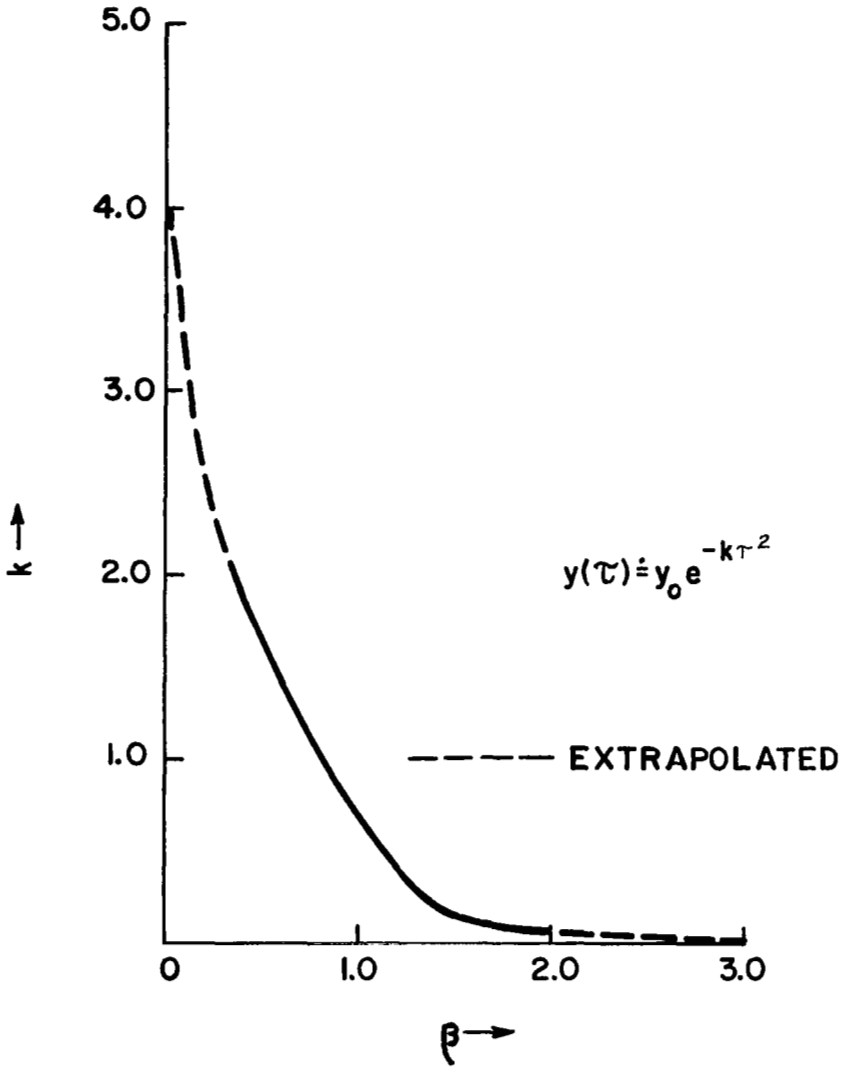

FIG. 13. DEPENDENCE OF THE FACTOR k ON THE DISTORTION PARAMETER.

hence since $y''(\tau)$ is independent of τ,

$$y''(\tau) = y''(0) = -2y_o k \quad , \tag{95}$$

i.e.

$$k = \frac{-y''(0)}{2y_o} \tag{96}$$

Hence from (92)

$$y'(\tau) = -2ky_o\tau = +y''(0)\tau \tag{97}$$

Hence from (91) the error $\Delta\tau$ is

$$\Delta\tau = \frac{N^2(\tau_s^-)}{y''(0)\tau_s^-} \tag{98}$$

But τ_s^- is arbitrary, hence if we choose it equal to $-\Delta\tau$ we obtain

$$(\Delta\tau)^2 = \frac{N^2(\Delta\tau)}{-y''(0)} \tag{99}$$

Integrating to obtain the mean square or R.M.S. error then gives

$$\overline{(\Delta\tau)^2} = \frac{N_o}{y''(0)} = \frac{1}{-\left(\frac{y_o}{N_o}\right)\left(\frac{y''(0)}{y_o}\right)} \tag{100}$$

But y_o/N_o is the output (power) signal to noise ratio, hence letting $y_o = S_o$

$$\left(\frac{S_o}{N_o}\right)_{out} \overline{(\Delta\tau)^2} = \frac{-y_o}{y''(0)} \tag{101}$$

But from (96)

$$\left(\frac{S_o}{N_o}\right)_{out} \overline{(\Delta\tau)^2} = + \frac{1}{2k} \tag{102}$$

This is the sought relationship and since we know the dependence of k on β via Table III or Fig. 13, we can obtain a plot of $\left(\frac{S_o}{N_o}\right)_{out} \overline{(\Delta\tau)^2}$ versus β, as shown in Fig. 14. Hence, from Fig. 14 for a given satellite location on the trajectory, i.e., a given β, and for a known output signal to noise power ratio, the R.M.S. error in the correlation peak can be determined.

It remains to determine the ultimate error in average electron density and to relate it to the output to input signal to noise ratio.

b. R.M.S. Error in Integrated Electron Density Measurement

Suppose we now relate the error $\overline{(\Delta\tau)^2}$ to the error in the integrated columnar electron density, $\bar{n}(\rho)$. From (79), letting $\Delta T = T_p$ (differential time between peaks)

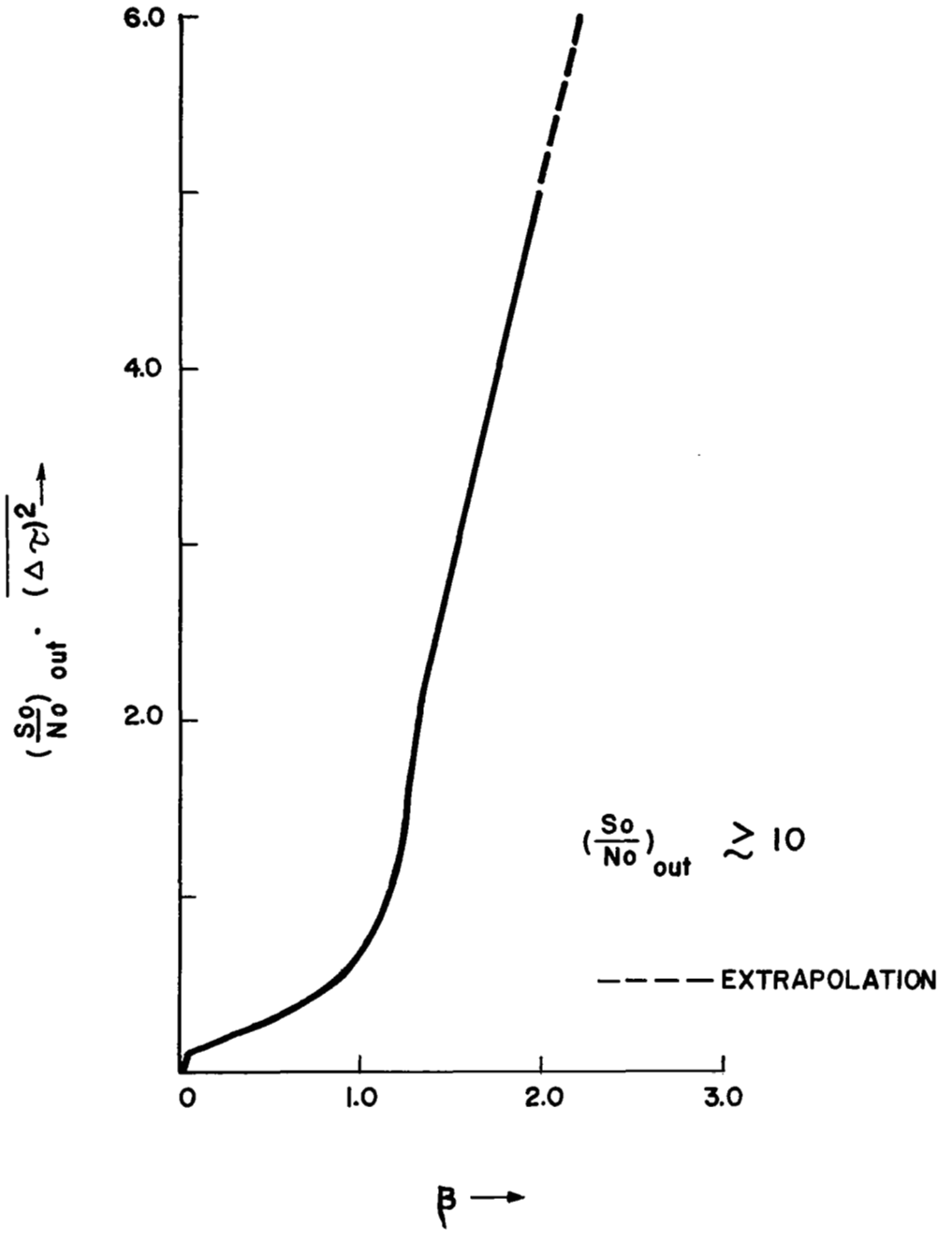

FIG. 14 R.M.S. ERROR IN CORRELATION PEAK LOCATION TIME.

the percentage error made in determining $\bar{n}$ is equal to that made in measuring T_p, i.e.

$$\frac{\Delta \bar{n}}{\bar{n}} = \frac{\Delta T_p}{T_p} = \frac{\Delta \tau_p}{\left(\frac{T_p}{T}\right)} \tag{103}$$

where $\tau_p = T_p/T$.

Now, the error in measuring τ_p is the composite of the error made in locating the correlation peak at the first carrier, $\Delta \tau_1$, and error made in locating the correlation peak at the second carrier, $\Delta \tau_2$. These errors can be found from Fig. 14 and, for a given $(S_o/N_o)_{out}$ depend only on β. But from (62), (58), and (56) we can write

$$\frac{\beta_1}{\beta_2} = \sqrt{\frac{t_{R_1}}{t_{R_2}}} = \sqrt{\frac{T_{d_1} f_{o_2}}{T_{d_2} f_{o_1}}} = \left(\frac{f_{o_2}}{f_{o_1}}\right)^{3/2} \tag{104}$$

That is, the higher frequency, f_{o_2} $(f_{o_2} > f_{o_1})$ has the lower β and the smaller error for a fixed bit length and output signal to noise ratio.

The total R.M.S. error made, $\Delta\tau_p$, is the square root of the sum of the squares, or

$$\overline{(\Delta\tau_p)^2} = \overline{(\Delta\tau_1)^2} + \overline{(\Delta\tau_2)^2} \tag{105}$$

and since $f_{o_1}/f_{o_2} < 1$, the second quantity is bounded by

unity, hence

$$\overline{(\Delta\tau_p)^2} \lesssim 2\overline{(\Delta\tau_1)^2} \tag{106}$$

For simplicity we will take the errors as equal and write:

$$\overline{(\Delta\tau_p)^2} \approx \overline{2(\Delta\tau_1)^2} \tag{107}$$

Now, using (89) to determine T_p

$$\frac{T_p}{T} = \beta_1^2(Tf_{o_1})\left[1 - \left(\frac{f_{o_1}}{f_{o_3}}\right)^2\right] \tag{108}$$

(where f_{o_3} now replaces f_{o_2}) we can then write, after multiplying both sides of (103) by $(S_o/N_o)_{out}$, using (107), and taking the R.M.S. of both sides

$$\frac{\overline{(\Delta\bar{n})^2}}{(\bar{n})^2}\left(\frac{S_o}{N_o}\right)_{out} = \frac{\overline{2(\Delta\tau_1)^2}\left(\frac{S_o}{N_o}\right)_{out}}{\left(\frac{T_p}{T}\right)^2} \tag{109}$$

Using the plot of Fig. 14 or Table III to obtain the product of $\overline{(\Delta\tau_1)^2}\left(\frac{S_o}{N_o}\right)_{out}$ and using (108) to obtain $\left(\frac{T_p}{T}\right)^2$, which for $f_{o_1} = 70$ mHz , and $f_{o_3} = 80$ mHz , with $T = 25.6\ \mu$sec is

$$\frac{T_p}{T} \approx 420\,\beta_1^2 \tag{110}$$

we obtain the percent squared R.M.S. error in $\bar{n}$ as plotted in Fig. 15, and tabulated in Table IV.

Fig. 15 reveals that for $S_o/N_o \gtrsim 10$ that the maximum percent R.M.S. error made in measuring $\bar{n}$ is less than 5% for all $\beta \gtrsim 0.08$. This is indeed an acceptably small percentage error. In what follows we will see how an output signal to noise ratio of 10 or more can be realized.

c. Determination of Output Signal to Noise Ratio

It can be shown (pp. 422 and 412) [16] , that the correlation receiver of Fig. 8 acts like a matched filter detector. The latter has the property that the maximum peak signal to noise power ratio, $(S_o/N_o)_{out}$, is equal to twice the ratio of the energy contained in the input signal/input noise power per cycle of bandwidth, E_{IN}/N_{IN} , i.e.

$$\left(\frac{S_o}{N_o}\right)_{out_{max}} = 2\left(\frac{E_{IN}}{N_{IN}}\right) \tag{111}$$

where

E_{IN} = Peak Input Energy (Joules) at Antenna Terminals

$$= \frac{(P_T NT)G_T}{4\pi R^2} A_R \tag{112}$$

TABLE IV.

MEASUREMENT ERROR IN $\bar{n}$

β	$\left(\frac{S_o}{N_o}\right)_{out} \cdot \frac{\overline{(\Delta \bar{n})^2}}{(\bar{n})^2}$
0.00	———
0.05	$2.3220 \cdot 10^{-1}$
0.10	$1.6210 \cdot 10^{-2}$
0.15	$3.7400 \cdot 10^{-3}$
0.25	$6.0450 \cdot 10^{-4}$
0.40	$1.1656 \cdot 10^{-4}$
0.75	$1.5570 \cdot 10^{-5}$
1.00	$7.5600 \cdot 10^{-6}$
1.25	$7.3800 \cdot 10^{-6}$
1.40	$7.3700 \cdot 10^{-6}$
1.75	$5.0480 \cdot 10^{-6}$
2.00	$3.5430 \cdot 10^{-6}$
2.50	$2.9020 \cdot 10^{-6}$
3.00	$2.8000 \cdot 10^{-6}$

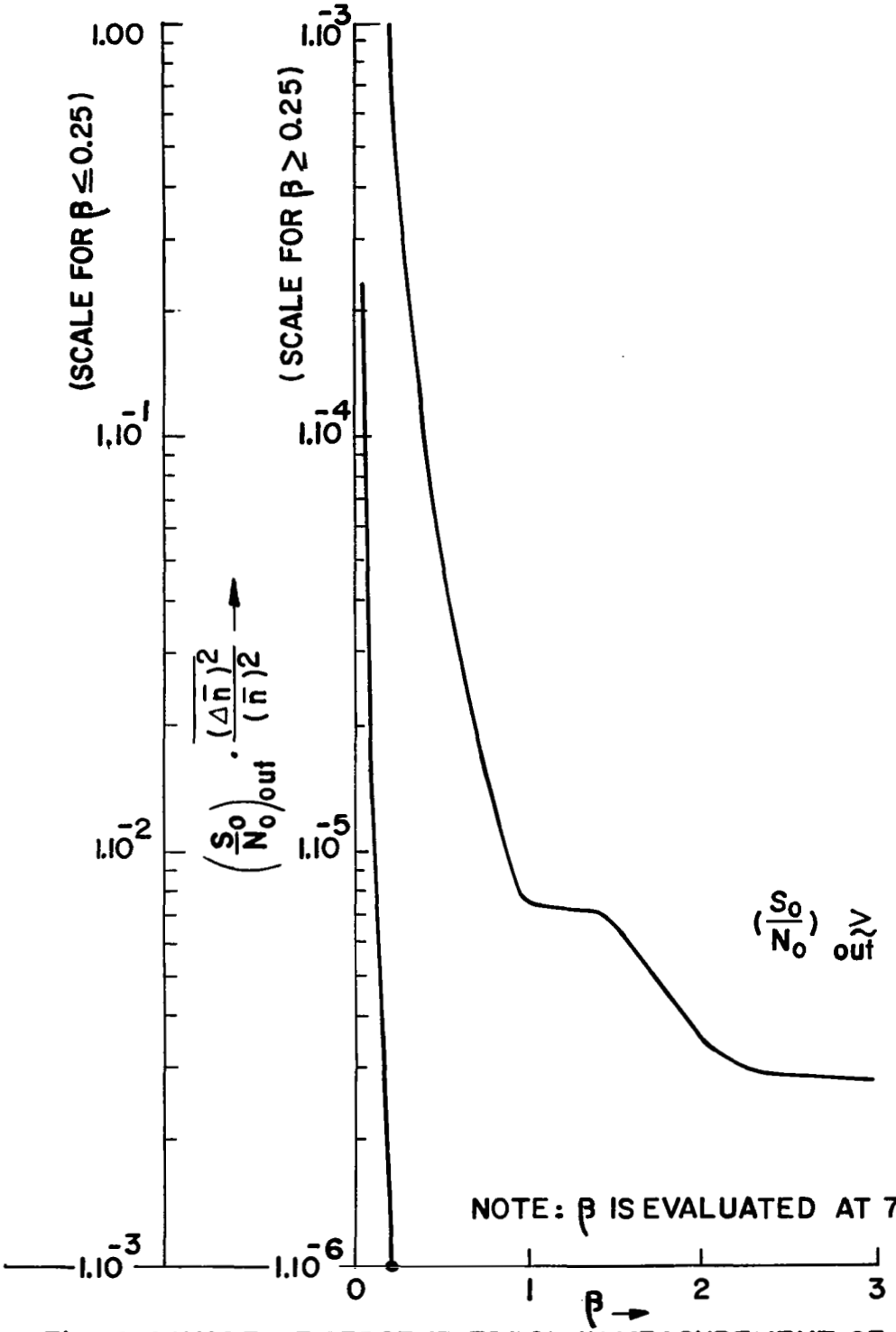

FIG. 15. SQUARE OF PERCENT ERROR IN MEASUREMENT OF INTEGRATED COLUMNAR ELECTRON DENSITY FOR DUAL FREQUENCY (70 AND 80 MHZ.) EXPERIMENT.

N_{IN} = Noise Energy

= Noise Power per Cycle of Bandwidth = $K T_I$ (113)

A_R = Effective Collecting Area of Receiving Antenna

$= \frac{G_R \lambda_v^2}{4\pi}$

R = Distance from Transmitter (Satellite) to Receiver (Earth)

P_T = Peak Transmitter Power, Watts

NT = Duration of Coded Pulse Train of P_T Peak Power (N = 127 , T = 25.6 μ sec)

G_T = Gain of Transmitting Antenna

G_R = Gain of Receiving Antenna

K = Boltzman's Constant = $1.37 \cdot 10^{-23}$ Joules/Degree Kelvin

T_I = Total Input Noise Temperature of Receiver $T_A + T_e$, Degrees Kelvin

T_A = Effective Noise Temperature of Antenna, Degrees Kelvin

T_e = Effective Noise Temperature of First R.F. Stage of Receiver, Degrees Kelvin

1. Received Signal Energy, E_{IN}

For P_T = 2,000 watts , N = 127 , T = 25.6 μ sec , f_o = 75 mHz (λ_v = 4 meters) , G_T = 1 , and a 50 Db. receiving antenna gain ($G_R = 10^5$) , and using the geometry of Fig. 10 to obtain R as a function of θ , the variation of $E_{IN}(\theta)$ is as given in Table V.

TABLE V.

COMPUTATIONS OF INPUT ENERGY LEVELS ($T = 2650^{\circ}K$)

θ°	E_{IN} JOULES	N_{IN} JOULES	$\frac{E_{IN}}{N_{IN}}$	$\frac{E_{IN}}{N_{IN}}$ DB.
85.0	$1.741 \cdot 10^{-18}$	$3.6305 \cdot 10^{-20}$	47.95	16.80
97.5	$1.686 \cdot 10^{-18}$	$3.6305 \cdot 10^{-20}$	46.94	16.65
113.0	$1.5076 \cdot 10^{-18}$	$3.6305 \cdot 10^{-20}$	41.525	16.20
134.0	$1.2946 \cdot 10^{-18}$	$3.6305 \cdot 10^{-20}$	36.659	15.62
153.0	$1.1330 \cdot 10^{-18}$	$3.6305 \cdot 10^{-20}$	31.208	14.95
164.0	$1.0592 \cdot 10^{-18}$	$3.6305 \cdot 10^{-20}$	29.175	14.68
173.5	$.9763 \cdot 10^{-18}$	$3.6305 \cdot 10^{-20}$	26.892	14.30
178.0	$.9386 \cdot 10^{-18}$	$3.6305 \cdot 10^{-20}$	25.853	14.10
180.0	$.9100 \cdot 10^{-18}$	$3.6305 \cdot 10^{-20}$	25.065	13.90
184.0	$.8759 \cdot 10^{-18}$	$3.6305 \cdot 10^{-20}$	24.126	13.82
187.0	$.8076 \cdot 10^{-18}$	$3.6305 \cdot 10^{-20}$	22.245	13.48

The received noise energy, N_{IN}, at the antenna terminals, if we consider that this energy will be passed through the first R.F. stage and associated antenna network having an effective noise temperature T_e, is given by (113).

Plots of antenna noise temperature [17], T_A, are shown in Figs. 16a and 16b and also [18] Fig. 17.

The receiver front end noise temperature, T_e, is usually expressed in terms of the noise factor (or noise figure if expressed in decibels), F_N, by $F_N = 1 + (T_e/T_o)$ where $T_o = 290^oK$; for example, if $T_e = 290^oK$, $F_N = 2$ or a 3 Db. noise figure. **Receivers can be built with noise** temperatures as low as 30^oK for parametric amplifiers and essentially a few degrees Kelvin for maser amplifiers in the microwave region [17], and some typical results [18] are shown in Fig. 18. For operation in the V.H.F. region of 70 or 80 mHz, a value of T_e of 850^oK (i.e. a noise figure of about 6 Db.) (the assumed M.I.T. value) is seen to be more than reasonable (if we extrapolate the transistor curves of Fig. 18 down to 75 mHz).

From Fig. 16 (or an extrapolation of Fig. 17) we see that an antenna noise temperature of $T_A = 1{,}800^oK$ is an average type value at 75 mHz (although it can go as high as slightly over $10{,}000^oK$ under severe cosmic noise conditions). Thus taking $T_A = 1{,}800^oK$, $T_E = 850^oK$, we get

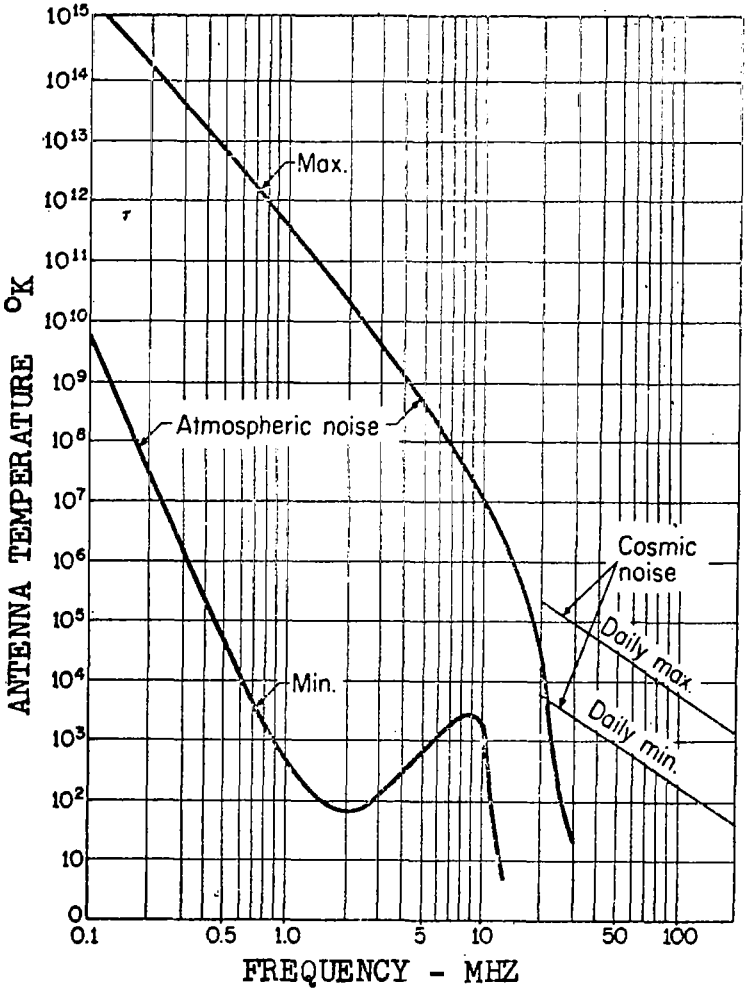

FIG. 16a. NOISE TEMPERATURE AT MEDIUM AND HIGH FREQUENCIES (E.C. HAYDEN).

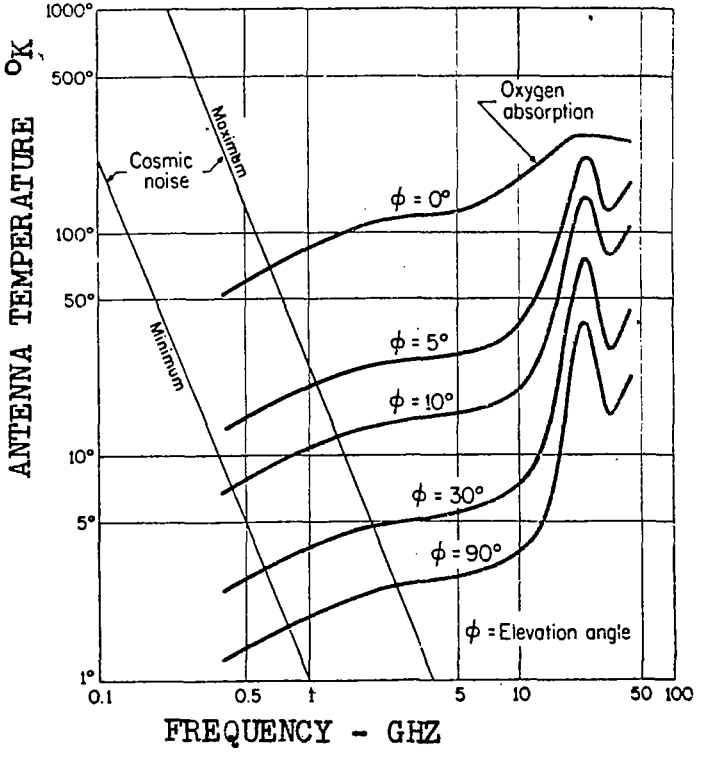

FIG. 16b. NOISE TEMPERATURE AT MICROWAVE FREQUENCIES (PIERCE-KOMPFNER, AFTER D.C. HUGG).

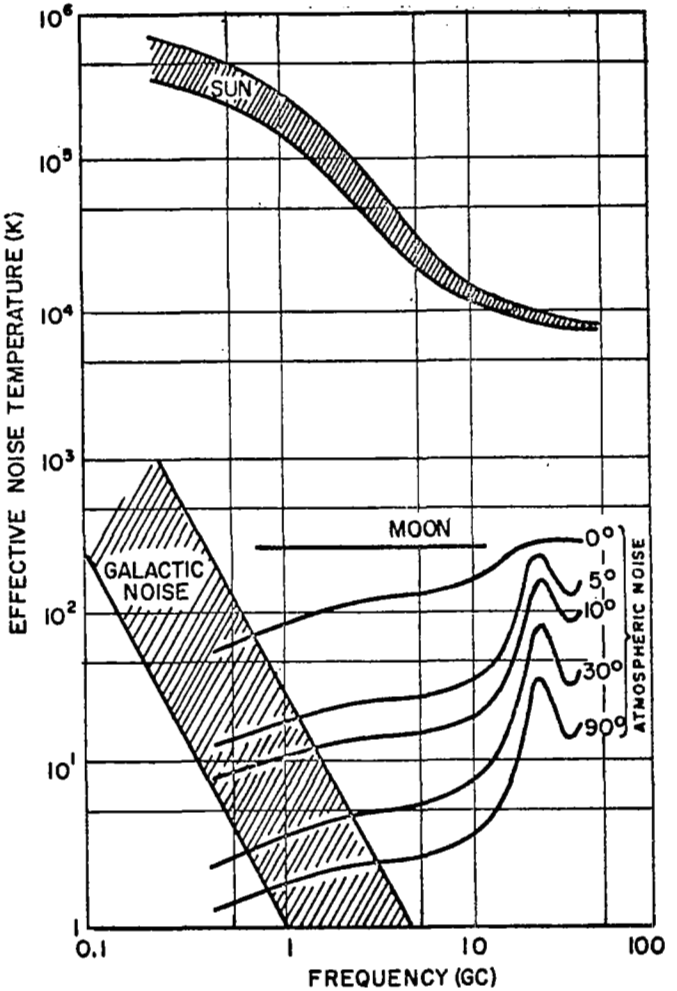

Variation of effective galactic and atmospheric noise temperatures. Degrees on atmospheric noise curves indicate angle above horizon. Minimum noise from these sources is found in the frequency range from 1 to 10 gigahertz.

NOISE TEMPERATURE LIMITS OF IDEAL LOW-NOISE ANTENNA FOR VERTICAL AND HORIZONTAL ELEVATIONS

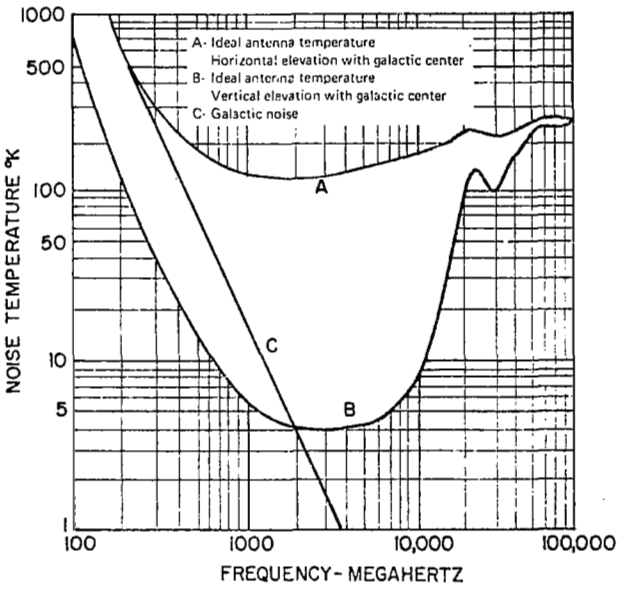

FIG. 17. ANTENNA NOISE TEMPERATURE.

CHARACTERISTIC NOISE TEMPERATURE BOUNDARIES FOR VARIOUS AMPLIFIER TYPES.

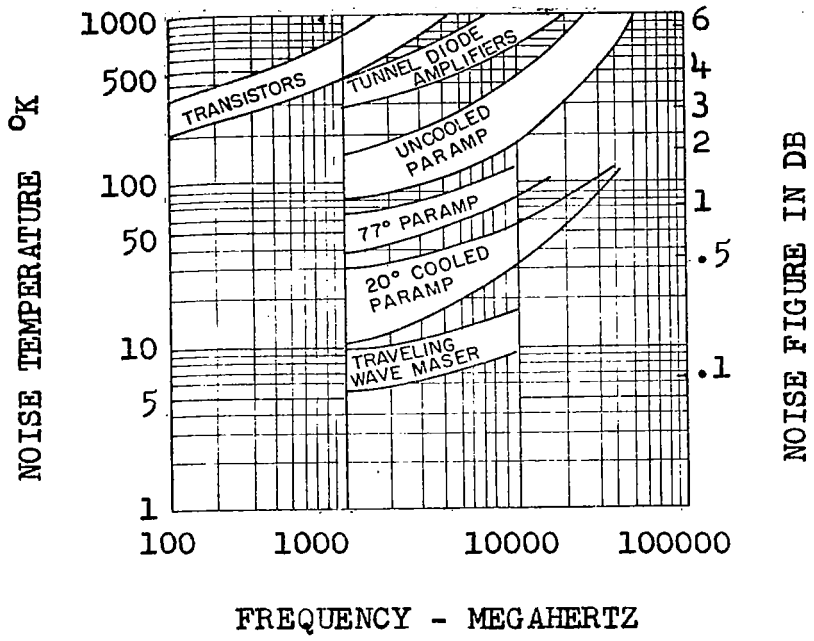

FIG. 18. TYPICAL FRONT END RECEIVER AMPLIFIER NOISE TEMPERATURE. [18]

$$N_{IN} = 3.631 \cdot 10^{-20} \quad \text{Joules} \qquad (114)$$

From the results of Table V, for E_{IN}, and (114) for N_{IN} we can then determine the input energy signal to noise ratio, E_{IN}/N_{IN}, as a function of trajectory angle, θ, or the corresponding distortion parameter, β, which depends on θ (for $f_{o_2} = 75$ mHz and $T = 25.6$ μsec) as shown in Fig. 11. The result is also tabulated in Table V and shows that $E_{IN}/N_{IN} \gtrsim 22$ (i.e. $10 \log_{10} E_{IN}/N_{IN} \gtrsim 13.5$ Db.) over the entire trajectory considered.

Hence, from (111) we see that the maximum $(S_o/N_o)_{out}$ is at least 44. Thus, assuming the correlation receiver can be built properly, it certainly is reasonable to assume that $(S_o/N_o)_{out} \gtrsim 10$. Hence, from Fig. 15, as previously noted, the corresponding accuracy with which the integrated electron density can be measured will be at least 5% for all $\beta \gtrsim 0.08$. This is indeed satisfactory.

d. Selection of Receiver Front End Bandwidth

The designer of the receiver must realize that the front end bandwidth, B, must be great enough to pass the signal with little distortion. However, as B is increased the input noise power, $N_{o_{IN}} = KT_IB$, increases degrading the input signal to noise power ratio. As this ratio is decreased more correlation must be performed by the receiver

to extract the signal from the noise. This correlation requires more circuitry and hence more expense. This aspect is considered in detail in Appendix XII. In any case, the output signal to noise power ratio can be made to exceed 10.

e. Effect of Antenna and Transmission Line, Etc. Bandwidths

If the bandwidths of the antenna, transmission line, and associated connectors, etc., at both the receiving and transmitting end of the path are made much greater than the rise time bandwidth, B_R, as plotted in Fig. XII-1 of Appendix XII, then little additional distortion will occur. The maximum B_R is about 75 kHz, hence for a carrier of 75 mHz, this represents a percentage bandwidth ($100\ B_R/f_o$) of about 0.1%. Certainly it is reasonable to expect that both antennas can be designed to have their impedance, and radiation characteristics flat over this percentage bandwidth, similarly for the bandwidth of the transmission lines and associated connectors.

Thus the main problem in the antennas' bandwidth is (as in the front end receiver characteristic) to determine what small compensation should be made in the measured correlation curves due to their finite bandwidth, this compensation decreasing with increasing bandwidth above B_R; the actual β factor will be smaller than that measured by the receiver due to the finite bandwidth.

VIII. CONCLUSIONS AND RECOMMENDATIONS

From the preceding, the following main conclusions are made:

(1) The proposed dual frequency (70 and 80 mHz) propagation experiment to measure the solar corona electron density variation, $n(r)$, by measuring the differential time difference, ΔT, between the correlation peaks of coded pulse trains at these two frequencies, is conceptually valid.

(2) Specifically, from a measurement of ΔT, one determines $\bar{n}(\rho)$ from (79), and $n(r)$ from (84).

(3) The percent R.M.S. error made in measuring $\bar{n}(\rho)$ (and hence $n(r)$) is less than 5% for all values of the distortion parameter, β, such that $\beta \gtrsim 0.08$ (corresponding to a satellite location from inferior conjunction to superior conjunction) provided the receiver output signal to noise power ratio, $(S_o/N_o)_{out}$, is such that $(S_o/N_o)_{out} \gtrsim 10$. The error dependence on β is given in Fig. 15.

(4) However, to practically realize the performance of the experiment requires two state of the art engineering efforts: the design and construction of the 50 Db. gain receiving antenna at 70 and 80 mHz, and the design and construction of the correlation receiver which must provide a high $(S_o/N_o)_{out}$ with a low $(S_o)_{in} \approx -125$ DBM, as discussed in Appendix XII.

Some supplementary conclusions and recommendations are:

(5) The actual pseudo random code used, as long as it is sharply peaked, is not critical as far as the shape of received output correlation curves is concerned, as shown in Appendix IX.

(6) The effect of the ionosphere is to slightly increase the distortion parameter, β , (Appendix XIII).

(7) The effects of refraction of the solar corona are too small to be ascertained by standard computational-graphical methods, (Appendix XIV).

(8) It is recommended that prior to performing an actual solar experiment, that a waveguide simulation experiment similar to that discussed in Appendix XV be performed. This experiment could be done at relatively low cost and be used to both ascertain the validity of the method and to calibrate the receiver system.

(9) The communication bandwidth of the solar corona at S-Band is large enough to handle quality T.V. signals (Appendix XVI).

(10) The dual frequency experiment can be performed at S-X Band. This experiment has the advantage of using existing (or modification of existing) antenna sites and of introducing a smaller noise error compared to the V.H.F. case. However, it has the disadvantage, for similar power levels, of requiring larger correlation codes requiring a more complex correlation receiver than for V.H.F. (Appendix XVII).

(10) Both A.M. and N.B.F.M. can be used to modulate a continuous wave carrier to diagnose a plasma (Appendix XVIII). Schemes of this type may be worthwhile to investigate for solar corona diagnostics.

APPENDIX I

SOLUTION TO WAVE EQUATION IN SLIGHTLY NONHOMOGENEOUS SOLAR CORONA

Consider

$$\partial_\xi^2 \bar{\Psi} + \beta_p^2(\xi)\bar{\Psi} = 0 \tag{1}$$

Suppose we write

$$\bar{\Psi} = Ae^{-j\int_0^\xi v(x)dx} \tag{2}$$

where $v(x)$ is as yet unknown, then (letting $v' = \partial_\xi v$)

$$\partial_\xi^2 \bar{\Psi} = \bar{\Psi}(v' + v^2) \tag{3}$$

and (1) becomes

$$jv' + v^2 = +\beta_p^2(\xi) \tag{4}$$

which is the Ricatti equation.

Suppose now that $\beta_p^2(\xi)$ is a constant $= \beta_o^2$, then v has the solution v_o

$$v_o = +\beta_o \tag{5}$$

(we ignore the backward wave $v_o = -\beta_o$ solution here) and, therefore,

$$\bar{\Psi} = Ae^{-j\beta_o \xi} \tag{6}$$

Hence, if β_p is not constant but is slowly varying (as will be defined), we would expect that

$$v_o(\xi) = +\beta_p(\xi) \tag{7}$$

may be a good approximation.

Let's see if this is so. From (4)

$$v = +\sqrt{\beta_p^2(\xi) - jv'} \tag{8}$$

which if (7) holds becomes

$$v = +\sqrt{v_o^2 - jv_o'} = v_o\sqrt{1 - j\frac{v_o'}{v_o^2}} \tag{9}$$

Expanding

$$v = v_o\left\{1 - j\frac{v_o'}{2v_o^2} - \frac{(v_o')^2}{8v_o^4} + \text{----------}\right\} \tag{10}$$

therefore, if

$$\left|\frac{v_o'}{2v_o^2}\right| << 1 \tag{11}$$

we see that $v \approx v_o$ will be a good solution.

Now, from (7)

$$v_o' = \partial_\xi \beta_p(\xi) = \beta_p' \tag{12}$$

Here

$$\left.\begin{aligned} \beta_p &= j\beta_v n(\xi) \\ n(\xi) &= \sqrt{\epsilon_r} = \sqrt{1 - \frac{\omega_p^2(\xi)}{\omega^2}} \\ \beta_v &= \frac{\omega}{c} \end{aligned}\right\} \tag{13}$$

Hence, the inequality (11) becomes:

$$\left| \frac{n'(\xi)}{2\beta_v n^2(\xi)} \right| << 1 \tag{14}$$

Now, the "wavelength" in the media is

$$\lambda = \frac{\lambda_v}{n} \tag{15}$$

$$\beta_p = \frac{2\pi}{\lambda} = \beta_v n \tag{16}$$

and since $\partial_\xi = \beta \frac{\partial}{\partial(\theta)}$, where $\theta = \frac{2\pi}{\lambda}$, (14) can be expressed as:

$$\left| \frac{\left(\frac{d\beta}{\beta}\right)}{2d\theta} \right| << 1 \tag{17}$$

i.e., if β changes by a small amount in a distance of a wavelength, then (7) will be valid.

In terms of the dielectric constant variation per wavelength, this becomes

$$\left| \frac{1}{8\pi \epsilon_r} \frac{d\epsilon_r}{d\left(\frac{\xi}{\lambda}\right)} \right| << 1 \tag{18}$$

Now, since $\epsilon_r = 1 - \frac{f_p^2(\xi)}{f^2}$ and if $f^2 >> f_p^2$, then

$$\epsilon_r \approx 1 \tag{19}$$

and

$$\frac{d\epsilon_r}{d\left(\frac{\xi}{\lambda}\right)} \approx -2\left(\frac{f_p}{f}\right)^2 \frac{\partial\left(\frac{f_p}{f}\right)}{\partial\left(\frac{\xi}{\lambda}\right)} \tag{20}$$

but since $\epsilon_r \approx 1$, $\lambda \approx \lambda_v$, hence $\frac{\partial\left(\frac{f_p}{f}\right)}{\partial\left(\frac{\xi}{\lambda}\right)} \approx \frac{\partial\left(\frac{f_p}{f}\right)}{\partial\left(\frac{\xi}{\lambda_v}\right)}$.

Now, from Fig. 1 of the text it is seen that for $3 \leq r \leq 215$, $f_{p\,max} \approx 5$ mHz. As such, $(f_p/f)^2 << 1$ will hold if $f \gtrsim 15$ mHz, i.e., if $\lambda_v \lesssim 20$ meters. Thus since, from Fig. 1, $\frac{\Delta\left(\frac{f_p}{f}\right)}{\Delta r} \lesssim \frac{1}{f} \frac{(5 \cdot 10^6 - 3 \cdot 10^4)}{215 - 3} \approx \frac{2.5 \cdot 10^4}{f}$, where f is in cycles. But,

$$\frac{\Delta\left(\frac{f_p}{f}\right)}{\Delta\left(\frac{R}{\lambda_v}\right)} = \left(\frac{\lambda_v}{R_o}\right)\frac{\Delta\left(\frac{f_p}{f}\right)}{\Delta r}$$

and since $R_o \approx 6.96 \cdot 10^8$ meters then for $f \gtrsim 15$ mHz,

$\frac{\Delta\left(\frac{f_p}{f}\right)}{\Delta\left(\frac{R}{\lambda_v}\right)} \leq \frac{1}{2} \cdot 10^{-10}$, therefore, $\left|\frac{1}{8\pi\epsilon_r}\frac{d\epsilon_r}{d\left(\frac{\xi}{\lambda_v}\right)}\right| < \frac{1}{2} \cdot 10^{-10}$

since the change of ϵ_r along the path, ξ, is even less than that along the radial distance, R. Hence (17) certainly is satisfied for $3 \lesssim r \lesssim 215$ and $f \geq 15$ mHz.

Therefore, (1) has the solution:

$$\bar{\Psi} = \bar{\Psi}_o e^{-j\int_0^{\xi}\beta_p(x)dx} \qquad (21)$$

where $\bar{\Psi}_o$ is the value of $\bar{\Psi}$ at $\xi = 0$ (i.e., at the transmitter). This is a form of a W.K.B. solution. [19]

APPENDIX II

OUTPUT CONTRIBUTION AT LOWER FREQUENCIES

From (18) of the text, we have that the contribution at the lower frequencies (i.e. between $-\omega_m \leq \omega \leq \omega_m$) is

$$\Delta\Psi(L,t) = \int_{-\omega_m}^{\omega_m} \left[\bar{\Psi}(L,\omega)e^{j\omega t} - \bar{\Psi}_o e^{j\Phi(\omega)}\right]d\omega \quad (1)$$

where $\bar{\Psi}(L,\omega)$ is the solution (which is not known) to (1) of the text at $\xi = L$, and $\bar{\Psi}_o$ is the input transform of (7) of the text, which is, from (5) of Appendix III

$$\bar{\Psi}_o = \frac{\omega_o}{2\pi(\omega_o^2 - \omega^2)} \quad (2)$$

Now, we note that for any steady state frequency, ω , the effect of the plasma will be a pure phase shift if $\omega > \hat{\omega}_p$, and will be both a phase shift and attenuation if $\omega < \hat{\omega}_p$, in either case the magnitude of the steady state component will then not exceed its input value, i.e.

$$\left|\bar{\Psi}(L,\omega)\right| \leq \left|\bar{\Psi}_o\right|_{max} \quad \text{any } \omega \quad (3)$$

Hence, from (1)

$$|\Delta\Psi| \leq 4\left|\bar{\Psi}_o\right|_{max} \omega_m \tag{4}$$

and hence from (2) and $\omega_m = 3\hat{\omega}_p$

$$|\Delta\Psi| \lesssim 2\frac{\hat{f}_p}{f_o} \tag{5}$$

Now for a carrier of V.H.F. (say 70 mc.) or higher, for a solar distance of $\rho \gtrsim 3$, $\hat{f}_p \approx 5$ mc., hence

$$|\Delta\Psi| \lesssim \frac{1}{10} \tag{6}$$

(the inequality improving with increasing carrier frequency). Hence the low frequency contribution is neglected compared to the higher frequency contributions.

APPENDIX III

A CONCISE REVIEW OF THE PROPAGATION OF A STEPPED CARRIER WAVE THROUGH A HOMOGENEOUS PLASMA†

At any distance, L, down the plasma the output is:

$$e_o(t,L) = \int_{-\infty}^{\infty} \overline{e_i}(\omega) e^{j\Phi(\omega)} \, d\omega \tag{1}$$

where

$$\Phi(\omega) = \omega t - \beta(\omega) L \tag{2}$$

$$\beta(\omega) = \frac{1}{c} (\omega^2 - \omega_p^2)^{\frac{1}{2}} \tag{3}$$

Let the input at $L = 0$ be a stepped carrier

$$e_i(t) = 1(t) \sin \omega_o t \tag{4}$$

Hence*

†It is noted here that an exact solution to this problem has been obtained (Rubinowicz [20], Gajewski [21], Knop [22], in the form of a Convergent Series of Bessel functions; however, for path lengths much greater than a free space wavelength, the series converges too slowly to be useful. Hence, the asymptotic solutions reviewed here must be used.

*It is recognized that, strictly speaking, the Fourier Transform of $1(t) \sin \omega_o t$ does not exist, but this is overcome by introducing a damping factor $e^{-\alpha t}$, $\alpha > 0$, and then letting α become arbitrarily small in the result for $\overline{e_i}(\omega)$.

$$\overline{e_i}(\omega) = \frac{1}{2\pi}\int_{-\infty}^{\infty} e_i(t)e^{-j\omega t}dt = \frac{1}{2\pi}\frac{\omega_o}{\omega_o^2 - \omega^2} \qquad (5)$$

Let $y = \omega/\omega_o$, $\rho = t/t_o$, $\eta = \omega_o t_o$, $P = \omega_p/\omega_o$,

$A(y) = \omega_o\overline{e_i}(\omega) = 1/2\pi\left[1/(1 - y^2)\right]$, therefore,

$$e_o(\rho,\eta) = \int_{-\infty}^{\infty} A(y)e^{j\eta f(y)}dy \qquad (6)$$

where

$$f(y) = \begin{cases} y\left[\rho - \sqrt{1 - \frac{P^2}{y^2}}\right] & y^2 > P^2 \\ y\left[\rho + j\sqrt{\frac{P^2}{y^2} - 1}\right] & y^2 < P^2 \end{cases} \qquad (7)$$

For y not near ± 1 , $A(y)$ is sufficiently regular, and hence for large η ($\eta \to \infty$) the method of stationary phase [23, 24] gives (for $f''(y_s) \neq 0$),

$$e_o(\rho,\eta) = \sum_n A(y_{s_n})e^{j\eta f(y_{s_n})}\sqrt{\frac{2\pi j}{\eta f''(y_{s_n})}} + O\left(\frac{1}{\eta}\right) \qquad (8)$$

where y_{s_n} are the stationary phase points, determined by $f'(y_s) = \partial_y f(y) = 0$, here

$$y_s = \pm \frac{\rho P}{\sqrt{\rho^2 - 1}} \tag{9}$$

Hence

$$f(y_s) = \pm P \sqrt{\rho^2 - 1} \tag{10}$$

$$f''(y_s) = \pm \frac{(\rho^2 - 1)^{3/2}}{P} \tag{11}$$

i.e., there are two stationary phase points, their sum, (8), giving

$$e_o(\rho, \eta) = \sqrt{\frac{2P}{\pi\eta}} \frac{(\rho^2 - 1)^{1/4}}{\rho^2(1 - P^2) - 1} \cos\left\{\eta P \sqrt{\rho^2 - 1} + \frac{\pi}{4}\right\}$$

$$\text{for} \quad \rho \neq 1 \,, \quad \rho \neq \frac{1}{\sqrt{1 - P^2}} \tag{12}$$

as long as y_s is not near unity (which from (9) means that ρ is not near or equal to $1/\sqrt{1 - P^2} \equiv \rho_g$) and as long as $f''(y_s)$ is not near zero (which from (11) means that ρ is not near or equal to unity). If ρ is near unity, $|y_s|$ is near ∞ . Hence we can get $e_o(\rho, \eta)$ for $\rho \longrightarrow 1$ by letting $y^2 \longrightarrow \infty$ initially in (6). This gives

$$e_o(\rho, \eta) \underset{\rho \to 1}{=} \frac{1}{2\pi} \int_{-\infty}^{\infty} -\frac{1}{y^2} e^{j\eta y \left[\rho - 1 + \frac{1}{2}\frac{P^2}{y^2}\right]} dy \tag{13}$$

which can be cast in the form of a known inverse Laplace Transform [25] of $\mathcal{L}^{-1}\left\{e^{-st_o}\left[\frac{e^{-b/s}}{s^2}\right]\right\}$, where $b = \frac{\omega_p^2 t_o}{2}$, hence one obtains the Sommerfeld result

$$e_o(\rho,\eta) \underset{\rho\to 1}{=} \frac{\sqrt{u}}{P^2\eta} J_1(\sqrt{u})\, 1(\rho - 1) \qquad (14)$$

where $u = 2P^2\eta^2(\rho - 1)$.

Now as the point, y_s, nears unity, the main signal solution is valid since there we expanded about $\omega = \omega_o$ (i.e., about $y = 1$). This corresponds to the time $\rho = \rho_g = \frac{1}{\sqrt{1 - P^2}}$. Then as y_s passes through unity and approaches zero, the pole contribution at $y_s = \pm 1$ (i.e., the steady state solution, $\sin\left[\eta(P - \sqrt{1 - P^2})\right]$, comes in which then has added to it the stationary phase contribution for $y_s > 1$ as again given by (12); the sum of these two is referred to as the Posterior Transient.

Thus in summary the solution (for large η) can be broken down into four regions of time as follows:

$$e_o(\rho,\eta) = \begin{cases} \text{Sommerfeld Solution} = (14), & \rho \to 1 \\ \text{Anterior Transient Solution} = (12), & 1 < \rho < \rho_g \\ \text{Main Signal Solution} = (47) \text{ of Text}, & \rho \to \rho_g \\ \text{Posterior Transient} = \text{Steady State} + (12), & \rho_g < \rho < \infty \end{cases} \tag{15}$$

A more thorough coverage of the splitting up of the solution in this manner is given in the excellent paper by Haskell and Case. [12]

It is to be stressed here, however, that as shown in the text the main signal solution is valid for, essentially, all times since its amplitude is essentially zero in the regions of time of $\rho < 1$, the Sommerfeld and Anterior Transient Solutions, and is essentially unity in the Posterior Transient Solution. Stating the same result in other words: Sommerfeld, Anterior Transient, and the transient portion of the Posterior Transient Solution have, in the solar plasma case, essentially, zero amplitude.

Hence,

$$e_o(\rho,\eta)\Big|_{\text{Solar Case}} \approx \text{Main Signal Solution} \quad -\infty \lesssim \rho \lesssim \infty \tag{16}$$

APPENDIX IV

PROOF OF $|t - t_g| << t_o\overline{P^2}$

Denoting y by ω/ω_o, ω_s/ω_o by y_s, t/t_o by ρ, and t_g/t_o by ρ_g, we have from (31) of the text

$$|y_s - 1| << 1 \tag{1}$$

i.e.

$$y_s = 1 + \Delta \qquad (|\Delta| << 1) \tag{2}$$

i.e.

$$y_s^2 \approx 1 + 2\Delta \tag{3}$$

But from (33) of the text

$$y_s^2 = \frac{\overline{P^2}}{2(\rho - 1)} \tag{4}$$

hence

$$(\rho - 1) = \frac{1}{2}\frac{\overline{P^2}}{y_s^2} \tag{5}$$

Therefore, using (3)

$$\rho - 1 = \frac{1}{2}\frac{\overline{P^2}}{(1 + 2\Delta)} \approx \frac{1}{2}\overline{P^2}(1 - 2\Delta) \tag{6}$$

i.e.

$$t - t_o = \frac{1}{2} t_o \overline{P^2}(1 - 2\Delta) \tag{7}$$

But, from (35) of the text

$$t_g - t_o = \frac{1}{2} t_o \overline{P^2} \tag{8}$$

Subtracting (7) and (8)

$$t - t_g = \frac{1}{2} t_o \overline{P^2}(-2\Delta) = -t_o \overline{P^2} \Delta \tag{9}$$

i.e.

$$\left| t - t_g \right| << t_o \overline{P^2} \tag{10}$$

APPENDIX V

ALTERNATE DERIVATION OF RISE TIME

Another way to derive t_R is to realize that the frequency range, Δf, represented by the signal as the time changes from $t_g - (t_R/2)$ to $t_g + (t_R/2)$, is governed by (33) of the text. This equation can be written as:

$$(t - t_o) = \frac{t_o P^2}{2\left(\frac{\omega}{\omega_o}\right)^2} \tag{1}$$

Now, when $t = t_g$ we know $\omega = \omega_o$, therefore

$$(t_g - t_o) = \frac{t_o P^2}{2} \tag{2}$$

Thus,

$$(t - t_g) = \frac{t_o P^2}{2}\left[\frac{1}{\left(\frac{\omega}{\omega_o}\right)^2} - 1\right] \tag{3}$$

Hence, since $\frac{\omega}{\omega_o} = 1 \pm \frac{1}{2}\frac{\Delta\omega}{\omega_o}$ at $t = t_g \pm \frac{t_R}{2}$, we get, since $\left|\frac{\Delta\omega}{\omega_o}\right| << 1$,

$$t_R = t_o P^2 \frac{\Delta\omega}{\omega_o} \tag{4}$$

But $\Delta\omega = 2\pi\Delta f$ and $\Delta f = 1/t_R$, hence

$$t_R = \sqrt{\frac{P^2 t_o}{f_o}} \tag{5}$$

But $t_o = (2T_d)/P^2$, hence

$$t_R = \sqrt{\frac{2T_d}{f_o}} \tag{6}$$

which is identical to (58) of the text.

Thus, the definitions of rise time in terms of rate of change of phase or in terms of the reciprocal of the frequency interval required to represent this time change are equivalent.

APPENDIX VI

SIMPLIFICATION OF $\Psi(L,t)$ EXPRESSION [2]

We have

$$\Psi(L,t) = \int_{-\infty}^{\infty} \bar{\Psi}(0,\omega) e^{-j\beta_p(\omega)L} e^{j\omega t} d\omega \qquad (1)$$

but

$$\bar{\Psi}(0,\omega) = \frac{1}{2\pi} \int_{-\infty}^{\infty} m(t') e^{j\omega_o t'} e^{-j\omega t'} dt' \qquad (2)$$

Let

$$\beta_p(\omega) = \beta_p(\omega_o) + \beta_p'(\omega_o)(\omega - \omega_o) + \beta_p''(\omega_o) \frac{(\omega - \omega_o)^2}{2} + \text{---------} \qquad (3)$$

therefore,

$$\Psi(L,t) = \frac{1}{2\pi} \int_{-\infty}^{\infty} e^{-jL\left[\beta_p(\omega_o) + \beta_p'(\omega_o)(\omega-\omega_o) - \left|\beta_p''(\omega_o)\right| \frac{(\omega-\omega_o)^2}{2} + \text{----}\right]} \cdot d\omega \int_{-\infty}^{\infty} m(t') e^{j\left[\omega t + (\omega_o - \omega) t'\right]} dt' \qquad (4)$$

Interchanging the order of integration, and letting $\Omega = \omega - \omega_o$, and noting that $\beta_p''(\omega_o) < 0$, gives

$$\Psi(L,t) = \frac{e^{j\left[\omega_o t - \beta(\omega_o)L\right]}}{2\pi}$$

$$\cdot \int_{-\infty}^{\infty}\int_{-\infty}^{\infty} m(t')e^{j\Omega\left(\left[t-t'-\beta_p'(\omega_o)L\right]+\frac{1}{2}\left|\beta_p''(\omega_o)\right|L\Omega\right)}$$

$$\cdot\, d\Omega dt' \tag{5}$$

Letting

$$\pi\xi^2 = \left|\beta_p''(\omega_o)L\right|\left[\Omega - \frac{\left[t' - t + \beta_p'(\omega_o)L\right]}{\left|\beta_p''(\omega_o)\right|L}\right]^2 \tag{6}$$

therefore,

$$d\Omega = \sqrt{\frac{\pi}{\left|\beta_p''(\omega_o)\right|L}}\; d\xi \tag{7}$$

and

$$\frac{\left|\beta_p''(\omega_o)L\right|}{2}\Omega^2 = -\Omega\left[t - t' - \beta_p'(\omega_o)L\right]$$

$$-\frac{1}{2}\frac{\left[t' - t + \beta_p'(\omega_o)L\right]^2}{\left|\beta_p''(\omega_o)\,L\right|} + \frac{\pi}{2}\xi^2 \tag{8}$$

hence

$$\Psi(L,t) = \frac{e^{j[\omega_o t - \beta(\omega_o)L]}}{2\pi} \cdot \int_{-\infty}^{\infty} \sqrt{\frac{\pi}{|\beta_p''(\omega_o)|\,L}}\, m(t')\, e^{-j\frac{[t'-t+\beta_p'(\omega_o)L]^2}{2|\beta_p''(\omega_o)L|}}\, dt' \cdot \int_{-\infty}^{\infty} e^{j\frac{\pi}{2}\xi^2}\, d\xi \tag{9}$$

But

$$\int_{-\infty}^{\infty} e^{j\frac{\pi}{2}\xi^2}\, d\xi = (1+j) \tag{10}$$

Letting

$$\frac{\pi}{2}u^2 = \frac{[t' - t + \beta_p'(\omega_o)L]^2}{2|\beta_p''(\omega_o)|L} \tag{11}$$

then gives

$$\Psi(L,t) = \frac{(1+j)}{2}\, e^{j\Phi(\omega_o)} \int_{-\infty}^{\infty} m\left[t - t_g + \frac{ut_R}{\sqrt{2}}\right] e^{-j\frac{\pi}{2}u^2}\, du \tag{12}$$

where

$$\left.\begin{aligned} \Phi(\omega_o) &= \omega_o t - \beta_p(\omega_o)L \\ t_g &= \beta_p'(\omega_o)L \\ \Phi''(\omega_o) &= -\beta_p(\omega_o)L \\ t_R &= \sqrt{2\pi\Phi''(\omega_o)} = \sqrt{2\pi|\beta_p''(\omega_o)|\,L} \end{aligned}\right\} \tag{13}$$

(recalling that $\Phi(\omega) \equiv \omega t - \beta_p(\omega)L$).

Shortening the notation into a complex amplitude and a carrier gives

$$\Psi(L,t) = a(t)\, e^{j\omega_o t} \tag{14}$$

where

$$a(t) = \frac{(1+j)}{2}\, e^{-j\beta(\omega_o)L} \cdot \int_{-\infty}^{\infty} m\left[t - t_g + \frac{ut_R}{\sqrt{2}}\right] e^{-j\frac{\pi}{2}u^2}\, du \tag{15}$$

APPENDIX VII

CORRELATION RECEIVER OUTPUT [2]

Referring to Fig. 8, it follows that the sine channel first gives, denoting $\Psi(L,t)$ by $e(t) = I_m\left\{a(t)e^{j\omega_o t}\right\}$, $a(t) = a_r(t) + ja_i(t)$

$$e(t)\sin\omega_o t = a_r(t)\sin^2\omega_o t + a_i \sin\omega_o t\cos\omega_o t$$

$$= \frac{a_r(t)}{2}(1 - \sin 2\omega_o t) + \frac{a_i(t)}{2}\sin 2\omega_o t \tag{1}$$

which when passed through the L.P.F. (eliminating the $\sin 2\omega_o t$ terms)

$$e_{L.P.}(t) = \frac{a_r(t)}{2} \tag{2}$$

Multiplying by $m(t - t_c)$ and integrating gives

$$\tfrac{1}{2} R_r(t_c) = \int_{-\infty}^{\infty} \frac{a_r(t)}{2} m(t - t_c)dt \tag{3}$$

Similarly, the cosine channel gives

$$\tfrac{1}{2} R_i(t_c) = \int_{-\infty}^{\infty} \frac{a_i(t)}{2} m(t - t_c)dt \tag{4}$$

Squaring and adding gives the correlation output, $Y(t_c)$

$$Y^2(t_c) \equiv \frac{R_r^2(t_c)}{4} + \frac{R_i^2(t_c)}{4} = \frac{1}{4} \left| R(t_c) \right|^2 \tag{5}$$

where

$$R(t_c) = \int_{-\infty}^{\infty} a(t)\, m(t - t_c)dt \tag{6}$$

But here (Appendix VI)

$$a(t) = \frac{(1 + j)}{2} e^{-j\beta(\omega_o)L} \int_{-\infty}^{\infty} m\left[t - t_g + \frac{ut_R}{\sqrt{2}}\right] e^{-j\frac{\pi}{2}u^2} du \tag{7}$$

Therefore, substituting (7) into (6), reversing the order of integration and letting $t_c' = t_c - t_g$, gives

$$\left|R(t_c' + t_g)\right| = \left| \frac{1}{\sqrt{2}} \int_{-\infty}^{\infty} e^{-j\frac{\pi}{2}u^2} \left\{ \int_{-\infty}^{\infty} m\left[t - t_g - t_c'\right] \cdot m\left[(t - t_g) + \frac{ut_R}{\sqrt{2}}\right] dt \right\} du \right| \tag{8}$$

We recognize the quantity in curly brackets as the auto-correlation function of $m(t)$ evaluated at the correlation time $t_c' + ut_R$, as is seen by letting $t' = t - t_g + ut_R$, giving

$$\left\{ \quad \right\} = \int_{-\infty}^{\infty} m(t')\, m\left[t' - \left(t_c' + \frac{ut_R}{\sqrt{2}}\right)\right] dt' \equiv R_m\left(t_c' + \frac{ut_R}{\sqrt{2}}\right) \quad (9)$$

Hence (dropping the primes on t_c)

$$\left|R(t_c + t_g)\right| = \frac{1}{\sqrt{2}} \left| \int_{-\infty}^{\infty} e^{-j\frac{\pi}{2}u^2} R_m\left(t_c + \frac{ut_R}{\sqrt{2}}\right) du \right| \quad (10)$$

normalizing times with respect to the bit length, T , i.e. let $\tau = t_c/T$, $\tau_g = t_g/T$, $\beta = t_R/(\sqrt{2}\,T)$, gives, after letting $v = \beta u$, the normalized cross-correlation output

$$y(\tau) \equiv \frac{\left|R(\tau + \tau_g)\right|}{T} \quad (11)$$

where

$$y(\tau) = \sqrt{\frac{I_c^2(\tau) + I_s^2(\tau)}{2}} \quad (12)$$

$$I_c(\tau) = \frac{1}{\beta} \int_{-\infty}^{\infty} r(x) \Big|_{x = \tau + v} \cos\left[\frac{\pi}{2}\left(\frac{v}{\beta}\right)^2\right] dv \quad (13)$$

$$I_s(\tau) = \frac{1}{\beta} \int_{-\infty}^{\infty} r(x) \Big|_{x = \tau + v} \sin\left[\frac{\pi}{2}\left(\frac{v}{\beta}\right)^2\right] dv \quad (14)$$

with

$$r(x) = \int_{-\infty}^{\infty} m(w - x)\, m(w)\, dw \quad , \quad r(-x) = r(x) \tag{15}$$

where

$$\beta = \frac{t_R}{T\sqrt{2}} \tag{16}$$

We note for the N bit code discussed in the text, the limits of x need only range from $-N \leq x \leq N$, hence v will vary from $-(N + \tau)$ to $+(N - \tau)$ in (13) and (14).

Also we note

$$y(-\tau) = y(\tau) \tag{17}$$

and that if $\beta = 0$ (letting $u = \frac{v}{\beta}$)

$$I_c(\tau)\Big|_{\beta=0} = \lim_{\beta \to 0} \int_{-\frac{(N+\tau)}{\beta}}^{\frac{N-\tau}{\beta}} r(x)\Big|_{x=\tau+u\beta} \cos\frac{\pi}{2}u^2\, du \tag{18}$$

which for* $\tau < N$ becomes

---

*We note that for $\tau > N$ and $\beta = 0$, $I_c(\tau) = I_s(\tau) = 0$ since upper and lower limits of these integrals both become $-\infty$; therefore $y(\tau) = 0$ for $\tau > N$ and $\beta = 0$ which is also what $r(\tau)$ is, hence $y(\tau) = r(\tau)$ for all τ for $\beta = 0$.

$$I_c(\tau)\Big|_{\beta=0} = r(\tau)\int_{-\infty}^{\infty}\cos\frac{\pi}{2}u^2\,du = r(\tau) \qquad (19)$$

Similarly, $I_s(\tau)\Big|_{\beta=0} = r(\tau)$, hence

$$y(\tau)\Big|_{\beta=0} = r(\tau) \qquad (20)$$

which is as should be since for no distortion the cross-correlation becomes the auto-correlation.

Note on Computation of $y(\tau)$

Following Pindyck [2] , $y(\tau)$ can also be computed as follows. We note that we can write $r(x)$ as:

$$r(x) = (a_k x + b_k) \qquad k \le x \le k+1 \ , \quad k = \text{integer} \qquad (21)$$

where a_k and b_k are constants for each k^{th} interval, but vary for each interval, as can be obtained from a plot of $r(x)$, or from (68) of the text.

From (21), we must call the interval between $x = 0$ and $x = 1$ the 0^{th} interval, it follows that since $r(-x) = r(x)$ we must then choose

$$\left.\begin{aligned} -a_{(k-1)} &= a_{-k} \\ b_{(k-1)} &= b_{-k} \end{aligned}\right\} \qquad (22)$$

Substituting (1) into (11)

$$y(\tau) = \frac{1}{\beta\sqrt{2}} \left| \int_{-(N+\tau)}^{N-\tau} (a_k x + b_k) \Big|_{x=\tau+v} e^{-j\frac{\pi}{2}\left(\frac{v}{\beta}\right)^2} dv \right| \qquad (23)$$

Performing the integration over v by performing over each k^{th} interval (noting that $v = x - \tau$) and then summing over all intervals

$$y(\tau) = \frac{1}{\beta\sqrt{2}} \left| \sum_{k=-N}^{N-1} a_k \int_{k-\tau}^{k+1-\tau} v\, e^{-j\frac{\pi}{2}\left(\frac{v}{\beta}\right)^2} dv + (a_k\tau + b_k)\beta \int_{\frac{k-\tau}{\beta}}^{\frac{k+1-\tau}{\beta}} e^{-j\frac{\pi}{2}\left(\frac{v}{\beta}\right)^2} d\left(\frac{v}{\beta}\right) \right| \qquad (24)$$

Recognizing the first integration as an exact one, and the second as cosine and sine Fresnel integrals since

$$\int_{\frac{k-\tau}{\beta}}^{\frac{k+1-\tau}{\beta}} = \int_{\frac{k-\tau}{\beta}}^{0} + \int_{0}^{\frac{k+1-\tau}{\beta}} = -\int_{0}^{\frac{k-\tau}{\beta}} + \int_{0}^{\frac{k+1-\tau}{\beta}}$$

gives

$$y(\tau) = \frac{1}{\beta\sqrt{2}} \left| \sum_{k=-N}^{k=N-1} \left[j \frac{\beta^2 a_k}{\pi} \left\{ \cos\left[\frac{\pi}{2}\left(\frac{k+1-\tau}{\beta}\right)^2\right] - j \sin\left[\frac{\pi}{2}\left(\frac{k+1-\tau}{\beta}\right)^2\right] - \cos\left[\frac{\pi}{2}\left(\frac{k-\tau}{\beta}\right)^2\right] + j \sin\left[\frac{\pi}{2}\left(\frac{k-\tau}{\beta}\right)^2\right] \right\} + \beta(a_k\tau + b_k) \cdot \left\{ \left[C(U) - C(L)\right] - j\left[S(U) - S(L)\right] \right\} \right] \right| \quad (25)$$

where

$$\left.\begin{aligned} C(X) &= \int_0^X \cos\frac{\pi}{2} u^2 \, du \\ S(X) &= \int_0^X \sin\frac{\pi}{2} u^2 \, du \end{aligned}\right\} \quad (26)$$

$$\left.\begin{aligned} U &= \frac{k+1-\tau}{\beta} \\ L &= \frac{k-\tau}{\beta} \end{aligned}\right\} \quad (27)$$

Separating into real and imaginary parts and simplifying

$$y(\tau) = \frac{1}{\sqrt{2}}\left\{\left[\sum_{k=-N}^{N-1} P_k(\tau)\right]^2 + \left[\sum_{k=-N}^{N-1} Q_k(\tau)\right]^2\right\}^{1/2} \qquad (28)$$

where

$$P_k(\tau) = \left\{\frac{\beta a_k}{\pi}\left[\sin\left\{\frac{\pi}{2}\left(\frac{k+1-\tau}{\beta}\right)^2\right\} - \sin\left\{\frac{\pi}{2}\left(\frac{k-\tau}{\beta}\right)^2\right\}\right]\right.$$
$$\left. + (a_k\tau + b_k)\left[C\left(\frac{k+1-\tau}{\beta}\right) - C\left(\frac{k-\tau}{\beta}\right)\right]\right\} \qquad (29)$$

$$Q_k(\tau) = \left\{\frac{\beta a_k}{\pi}\left[\cos\left\{\frac{\pi}{2}\left(\frac{k+1-\tau}{\beta}\right)^2\right\} - \cos\left\{\frac{\pi}{2}\left(\frac{k-\tau}{\beta}\right)^2\right\}\right]\right.$$
$$\left. - (a_k\tau + b_k)\left[S\left(\frac{k+1-\tau}{\beta}\right) - S\left(\frac{k-\tau}{\beta}\right)\right]\right\} \qquad (30)$$

But we now note that since $y(-\tau) = y(\tau)$, therefore, replacing τ by $-\tau$ in (29) and (30) gives (28) where now

$$P_k(\tau) = \left\{\frac{\beta a_k}{\pi}\left[\sin\left\{\frac{\pi}{2}\left(\frac{k+1+\tau}{\beta}\right)^2\right\} - \sin\left\{\frac{\pi}{2}\left(\frac{k+\tau}{\beta}\right)^2\right\}\right]\right.$$
$$\left. - (a_k\tau - b_k)\left[C\left(\frac{k+1+\tau}{\beta}\right) - C\left(\frac{k+\tau}{\beta}\right)\right]\right\} \qquad (31)$$

$$Q_k(\tau) = \left\{ \frac{\beta a_k}{\pi} \left[\cos\left\{ \frac{\pi}{2}\left(\frac{k+1+\tau}{\beta}\right)^2 \right\} - \cos\left\{ \frac{\pi}{2}\left(\frac{k+\tau}{\beta}\right)^2 \right\} \right] + (a_k\tau - b_k)\left[S\left(\frac{k+1+\tau}{\beta}\right) - S\left(\frac{k+\tau}{\beta}\right) \right] \right\} . \quad (32)$$

Check Case of $\beta = 0$

Suppose we let $\beta \to 0$; examination of (29) and (30) shows that the first terms vanish with $\beta = 0$ and that if $k > \tau$ then both $\frac{k-\tau}{\beta}$ and $\frac{k+1-\tau}{\beta}$ will approach $+\infty$ and since $C(\infty) = \frac{1}{2}$ then $P_k(\tau) = 0$. Similarly, for $k > \tau$, $Q_k(\tau) = 0$.

However, if $k < \tau$ and $k + 1 > \tau$ i.e. if $k < \tau < k + 1$ then $\frac{k+1-\tau}{\beta} \to +\infty$, $\frac{k-\tau}{\beta} \to -\infty$ and hence since $C(\infty) = \frac{1}{2}$, $C(-\infty) = -\frac{1}{2}$, it follows that $P_k(\tau) = a_k\tau + b_k$; similarly $P_k(\tau) = -(a_k\tau + b_k)$ hence

$$y(\tau)\Big|_{\beta = 0} = \frac{1}{\sqrt{2}} \left\{ (a_k\tau + b_k)^2 + (a_k + b_k)^2 \right\}^{\frac{1}{2}}$$

$$= a_k\tau + b_k \quad , \qquad k < \tau < k + 1 \qquad (33)$$

which is as it should be.

APPENDIX VIII

PROGRAMMING OF CORRELATION FUNCTION

Computer Program for Computing $y(\tau)$

The program described here is a FORTRAN (level G) program written for the IBM S/360 Computer. Nearly all internal computing by this program is done in double precision floating point form.

The main functions of the program are to compute:

(i) a table of auxiliary quantities: m_k , r_k , a_k , b_k;

(ii) $y(\tau)$ for the values of β and τ specified by the input.

The amount and type of printed output to be produced by the program is determined by a write-flag, denoted by IWR, whose value is specified as an input quantity.

BLOCK DIAGRAM OF THE PROGRAM

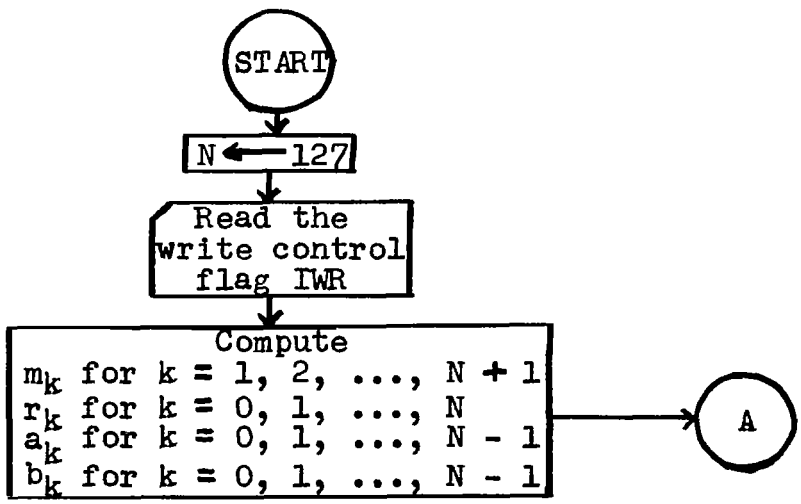

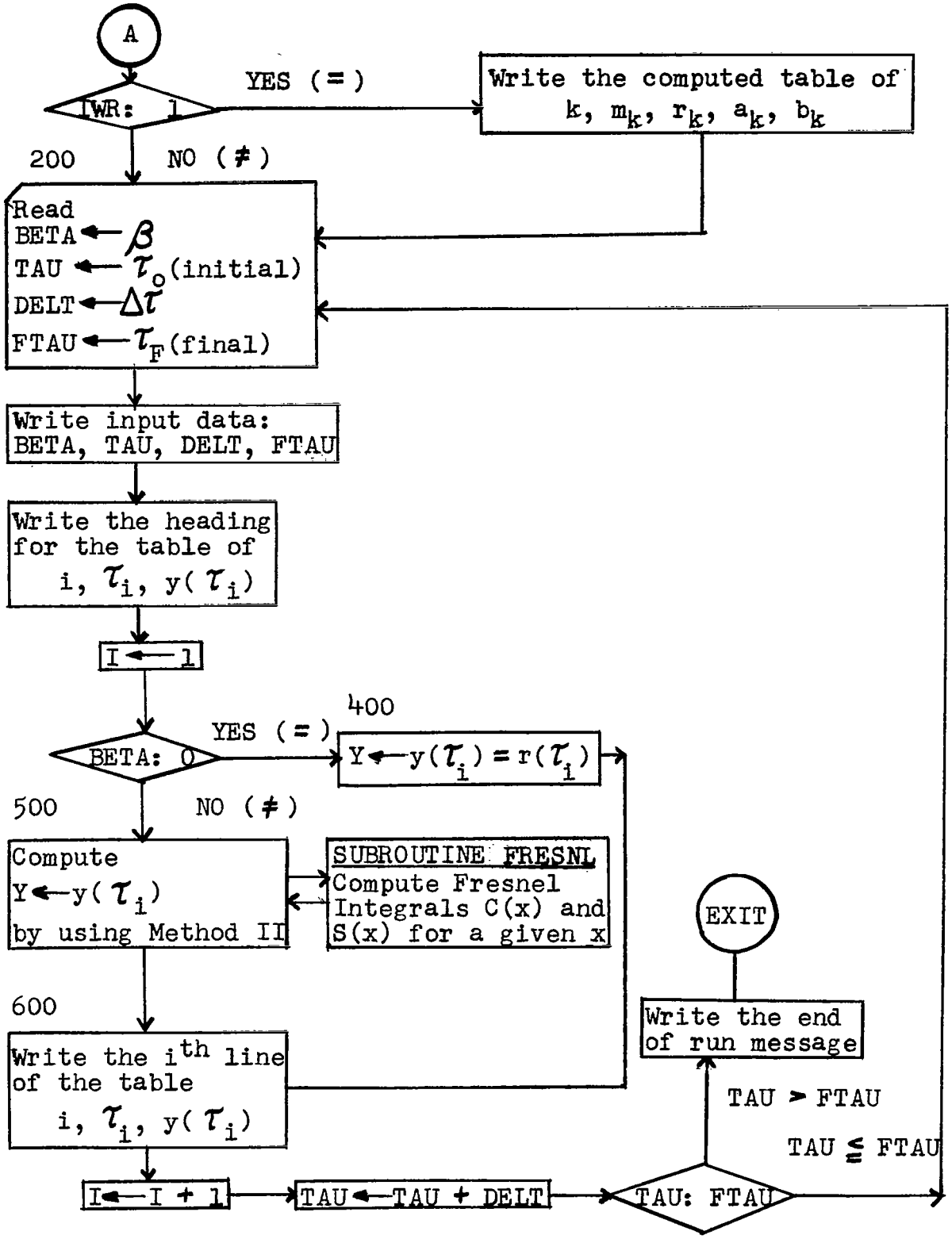
A
IWR: 1
YES (=)
Write the computed table of k, m_k, r_k, a_k, b_k
200
NO (≠)
Read
BETA ← β
TAU ← τ_o (initial)
DELT ← $\Delta\tau$
FTAU ← τ_F (final)
Write input data: BETA, TAU, DELT, FTAU
Write the heading for the table of i, τ_i, $y(\tau_i)$
I ← 1
400
BETA: 0
YES (=)
$Y \leftarrow y(\tau_i) = r(\tau_i)$
500
NO (≠)
Compute $Y \leftarrow y(\tau_i)$ by using Method II
SUBROUTINE FRESNL
Compute Fresnel Integrals C(x) and S(x) for a given x
600
Write the i^{th} line of the table i, τ_i, $y(\tau_i)$
I ← I + 1
TAU ← TAU + DELT
TAU: FTAU
TAU > FTAU
TAU ≦ FTAU
EXIT
Write the end of run message

Input Data

Card #1 (Format: II)

IWR ← Write Control Flag

= 0 for standard output only (i, τ_i, $y(\tau_i)$);

= 1 for standard output and the table of m_k, r_k, a_k, b_k;

= 2 for standard output and intermediate results in the computation of each $y(\tau_i)$.

Card #2 (Format: 4G10.0)

BETA ← β

TAU ← τ_o (= initial τ)

DELT ← $\Delta\tau$

FTAU ← τ_F (= final τ)

Sample Output

Sample output, obtained by using IWR = 0, and the listing of the source program are attached at the end of this appendix.

Computational Method

For $\beta = 0$, set $y(\tau) = r(\tau)$. For $\beta \neq 0$, the so-called Method II is used. This method depends on Fresnel integrals

$$C(x) = \int_0^x \cos\left(\frac{\pi}{2} u^2\right) du$$

and

$$S(x) = \int_0^x \sin\left(\frac{\pi}{2} u^2\right) du$$

For $x > 100$, the method described [11], (p. 324) is used. For $x \leq 100$, the method developed by J. Boersma [26], is used. The latter method is a special case of the τ-Method of Lanczos.

According to its author, the maximum error in the Boersma's technique is $< 1.6 \times 10^{-9}$. Intensive numerical testing tends to indicate that the maximum error in the other method, for $x > 100$, is in the order of magnitude of 10^{-8}.

Print Outs

For the sake of completeness the print outs of the $\beta = 0$ results are given in Table VIII-1, i.e., the auto-correlation results for (66) of the text, where the $x(n)$ are defined by (63) and (64).

The $y(\tau)$ results for $\beta > 0$ are not tabulated here, but are plotted in Fig. 9 of the text.

TABLE VIII-1.

AUTO-CORRELATION COEFFICIENTS (a_k AND b_k),

AND AUTO-CORRELATION FUNCTION, r_k,

FOR N = 127 PSEUDO RANDOM CODE

k	r_k	a_k	b_k
0	127.00000	-127.00000	127.00000
1	0.00001000	1.0000000	-1.0000000
2	1.0000000	1.0000000	-1.0000000
3	2.0001000	1.0000000	-1.0000000
4	3.0001000	1.0000000	-1.0000000
5	4.0000000	1.0000000	-1.0000000
6	5.0000000	-1.0000000	11.000000
7	4.0000000	-1.0000000	11.000000
8	3.0000000	1.0000000	-5.0000000
9	4.0000000	-1.0000000	13.000000
10	3.0000000	1.0000000	-7.0000000
11	4.0000000	-1.0000000	15.000000
12	3.0000000	-1.0000000	15.000000
13	2.0000000	1.0000000	-11.000000
14	3.0000000	-5.0000000	73.000000
15	-2.0001000	5.0000000	-77.000000
16	3.0000000	-3.0000000	51.000000
17	0.00000000	3.0000000	-51.000000
18	3.0000000	-7.0000000	129.00000
19	-4.0000000	9.0000000	-175.00000
20	5.0001000	-1.0000000	25.000000
21	4.0000000	-3.0000000	67.000000
22	1.0000000	-1.0000000	23.000000
23	-0.00001000	5.0000000	-115.00000
24	5.0000000	-1.0000000	29.000000
25	4.0000000	-1.0000000	29.000000
26	3.0000000	-3.0000000	81.000000
27	-0.00000000	3.0000000	-81.000000
28	3.0000000	-9.0000000	255.00000
29	-6.0001000	7.0000000	-209.00000
30	1.0001000	-5.0000000	151.00000
31	-4.0001000	7.0000000	-221.00000
32	3.0000000	-3.0000000	99.000000
33	0.00001000	1.0000000	-33.000000
34	1.0001000	5.0000000	-169.00000

TABLE VIII-1.

(CONTINUED)

k	r_k	a_k	b_k
35	5.0000000	-1.0000000	41.000000
36	5.0000000	-11.000000	401.00000
37	-6.0000000	7.0000000	-265.00000
38	1.0000000	1.0000000	-37.000000
39	2.0000000	-5.0000000	197.00000
40	-3.0000000	3.0000000	-123.00000
41	0.00000000	7.0000000	-287.00000
42	7.0000000	-9.0000000	385.00000
43	-2.0000000	5.0000000	-217.00000
44	3.0000000	-3.0000000	135.00000
45	-0.00000000	-7.0000000	315.00000
46	-7.0000000	3.0000000	-145.00000
47	-4.0000000	11.000000	-521.00000
48	7.0000000	1.0000000	-41.000000
49	3.0000000	-7.0000000	351.00000
50	1.0000000	-9.0000000	451.00000
51	-3.0000000	11.000000	-569.00000
52	3.0000000	-7.0000000	367.00000
53	-4.0000000	11.000000	-587.00000
54	7.0000000	-7.0000000	385.00000
55	0.00000000	5.0000000	-275.00000
56	5.0000000	-9.0000000	509.00000
57	-4.0000000	-3.0000000	167.00000
58	-7.0000000	11.000000	-645.00000
59	4.0000000	3.0000000	-173.00000
60	7.0000000	-5.0000000	307.00000
61	2.0000000	-7.0000000	429.00000
62	-5.0000000	13.000000	-811.00000
63	3.0000000	-17.000000	1079.0000
64	-9.0000000	13.000000	-841.00000
65	4.0000000	-7.0000000	459.00000
66	-3.0000000	-5.0000000	327.00000
67	-3.0000000	3.0000000	-209.00000
68	-5.0000000	11.000000	-753.00000
69	6.0000000	-3.0000000	213.00000
70	3.0000000	-9.0000000	633.00000
71	-6.0000000	5.0000000	-361.00000
72	-1.0000000	-7.0000000	503.00000
73	-8.0000000	11.000000	-811.00000
74	8.0000000	-7.0000000	521.00000

TABLE VIII-1.

(CONTINUED)

k	r_k	a_k	b_k
75	-4.0000000	11.000000	-829.00000
76	7.0000000	-9.0000000	691.00000
77	-2.0000000	-7.0000000	537.00000
78	-9.0000000	1.0000000	-87.000000
79	-8.0000000	11.000000	-877.00000
80	3.0000000	3.0000000	-237.00000
81	6.0000000	-7.0000000	573.00000
82	-1.0000000	-3.0000000	245.00000
83	-4.0000000	5.0000000	-419.00000
84	1.0000000	-9.0000000	757.00000
85	-8.0000000	7.0000000	-603.00000
86	-1.0000000	3.0000000	-259.00000
87	2.0000000	-5.0000000	437.00000
88	-3.0000000	1.0000000	-91.000000
89	-2.0000000	7.0000000	-625.00000
90	5.0000000	-11.000000	995.00000
91	-6.0000000	-1.0000000	85.000000
92	-7.0000000	5.0000000	-467.00000
93	-2.0000000	1.0000000	-95.000000
94	-1.0000000	-3.0000000	281.00000
95	-4.0000000	7.0000000	-669.00000
96	3.0000000	-5.0000000	483.00000
97	-2.0000000	7.0000000	-681.00000
98	5.0000000	-9.0000000	887.00000
99	-4.0000000	3.0000000	-301.00000
100	-1.0000000	-3.0000000	299.00000
101	-4.0000000	-1.0000000	97.000000
102	-5.0000000	-1.0000000	97.000000
103	-6.0000000	5.0000000	-521.00000
104	-1.0000000	-1.0000000	103.00000
105	-2.0000000	-3.0000000	313.00000
106	-5.0000000	-1.0000000	101.00000
107	-6.0000000	9.0000000	-969.00000
108	3.0000000	-7.0000000	759.00000
109	-4.0000000	3.0000000	-331.00000
110	-1.0000000	-3.0000000	329.00000
111	-4.0000000	5.0000000	-559.00000
112	1.0000000	-5.0000000	561.00000
113	-4.0000000	1.0000000	-117.00000
114	-3.0000000	-1.0000000	111.00000

TABLE VIII-1.

(CONTINUED)

k	r_k	a_k	b_k
115	-4.0000000	-1.0000000	111.00000
116	-3.0000000	1.0000000	-121.00000
117	-4.0000000	-1.0000000	113.00000
118	-5.0000000	1.0000000	-123.00000
119	-4.0000000	-1.0000000	115.00000
120	-3.0000000	-1.0000000	115.00000
121	-6.0000000	1.0000000	-127.00000
122	-5.0000000	1.0000000	-127.00000
123	-4.0000000	1.0000000	-127.00000
124	-3.0000000	1.0000000	-127.00000
125	-2.0000000	1.0000000	-127.00000
126	-1.0000000	1.0000000	-127.00000
127	-0.0000000		

APPENDIX IX.

THE TRIPLE FOLDED BARKER CODE

To show that the shape of the distorted cross-correlation curves are not critically dependent on the detailed nature of the auto-correlation input, $r(x)$, (provided it has a sharp well-defined peak), we consider the case of an 11 Bit, triple folded, Barker code.

This code consists of an 11 bit code, $x(n)$, defined by

$$x(n) = \left\{ \begin{array}{ll} 1 & 1 \leq n \leq 3 \\ -1 & 4 \leq n \leq 6 \\ 1 & n = 7 \\ -1 & 8 \leq n \leq 9 \\ 1 & n = 10 \\ -1 & n = 11 \end{array} \right\} \qquad (1)$$

which is then "folded" on itself to give the 121 bit code of $m(t)$, where

$$m(t) = \sum_{n=1}^{121} A(n)\, x(n) \left[1(t) - 1(t - nT)\right] \qquad (2)$$

where T is the fundamental bit time (here $T = 25.6\ \mu$sec.), and

$$A(n) = \left\{ \begin{array}{ll} 0 & n < 0 \\ 1 & 1 \leq n \leq 33 \\ 1 & 67 \leq n \leq 77 \\ -1 & 78 \leq n \leq 99 \\ 1 & 100 \leq n \leq 110 \\ -1 & 111 \leq n \leq 121 \\ 0 & n > 121 \end{array} \right\} \quad (3)$$

with

$$x(n + 11) = x(n)$$

The auto-correlation function of this code then is

$$r(x) = \sum_{n=1}^{121 - x} x(n)\, A(n)\, x(n + x)\, A(n + x) \quad (4)$$

which gives

$$\left. \begin{array}{ll} r(0) = 121 & \\ r(x) = +1 & x = \text{even integer} \\ r(x) = 0 & x = \text{odd integer} \\ r(-x) = r(x) & \\ r(x) = 0\,, \quad |x| > 121 & \end{array} \right\} \quad (5)$$

Thus it resembles the r(x) of the 127 bit pseudo random code except its peak is 121 and all its lobes are plus unity. A sketch of it is shown in Fig. IX-1.

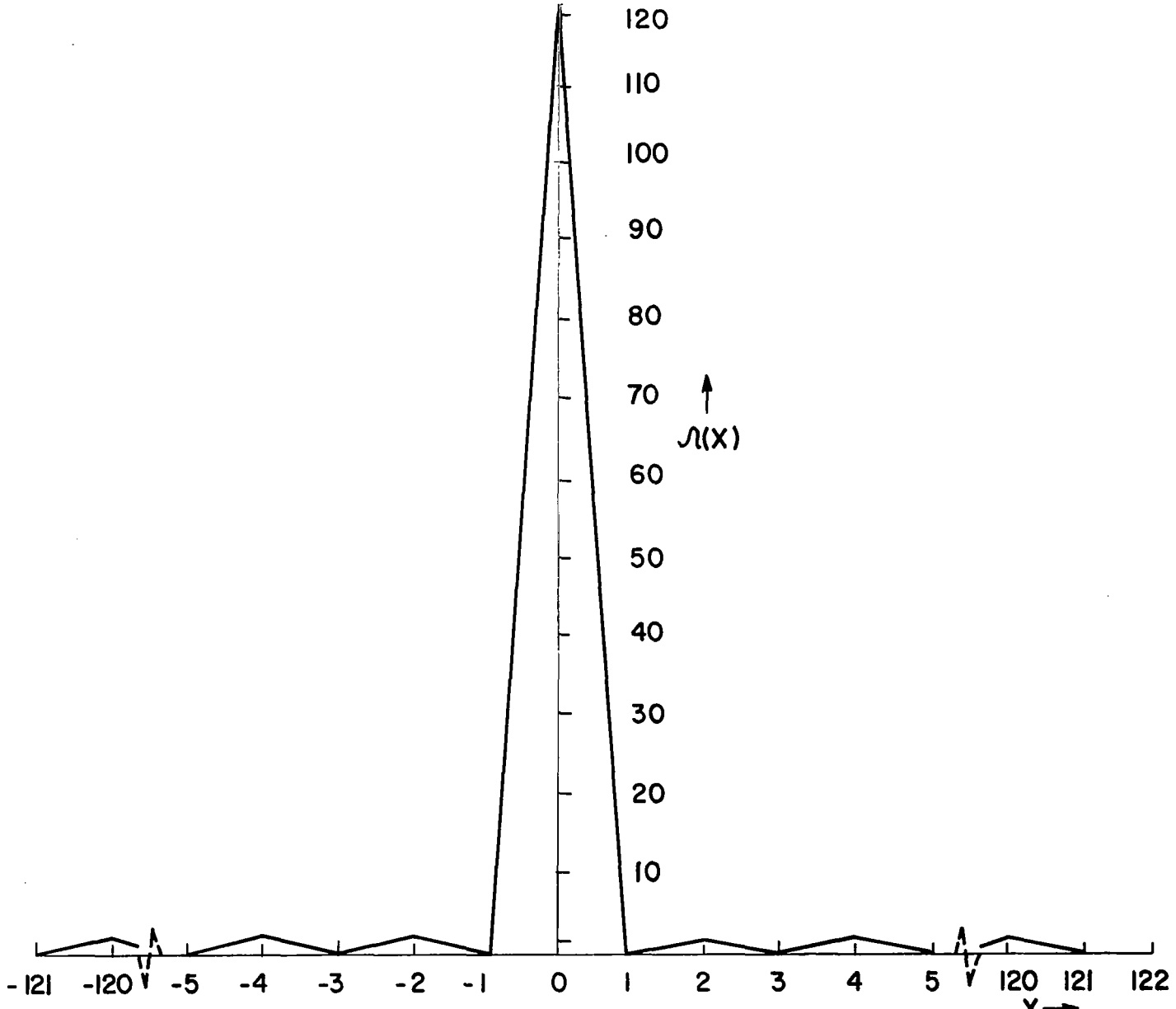

FIG. IX-1. AUTO CORRELATION FUNCTION OF TRIPLE FOLDED BARKER CODE.

Computation of $y(\tau)$

To compute the received cross-correlation function, $y(\tau)$, the same program as described in Appendix VIII is used, except the a_k and b_k coefficients are altered to fit the new $r(x)$, and N is changed from 127 to 121. Thus $y(\tau)$ is computed from (28) of Appendix V.

Computation for $y(\tau)$ for the case of $\beta = 2$ were made and are tabulated in Table IX-1.

These values are so close to the same case ($\beta = 2$) for the $N = 127$ pseudo random code of Fig. 9 of the text that they are not drawn in for the sake of clarity. Indeed, if normalized to the on-axis values, the corresponding curves would nearly overlap.

TABLE IX-1.

$y(\tau)$ COMPUTATIONS FOR $\beta = 2$

FOR THE TRIPLE FOLDED BARKER CODE

τ	$y(\tau)$
0.0	43.051
2.0	35.011
4.0	18.018
6.0	5.247
8.0	7.317
10.0	2.047

Conclusions

From the above, it is concluded that the shape of the cross-correlation curves, $y(\tau)$, are not critically dependent on the type of pseudo random code used provided it has a sharp peak of nearly the same magnitude and is approximately the same length.

APPENDIX X

PROOF THAT RADIAL AND OFFSET ELECTRON DENSITIES ARE ABEL TRANSFORM PAIRS

If $Y(\rho)$ is related to $X(r)$ by (83) of the text (letting $Y(\rho) = \frac{\bar{n}(\rho)}{2R_o}$, and $X(r) = n(r)$)

$$Y(\rho) = \int_{\rho}^{\infty} \frac{X(r)rdr}{\sqrt{r^2 - \rho^2}} \tag{1}$$

then we wish to show that the solution for $X(r)$ is:

$$X(r) = -\frac{2}{\pi} \frac{\partial}{\partial r} \left[\int_{r}^{\infty} \frac{rY(\rho)d\rho}{\rho\sqrt{\rho^2 - r^2}} \right] \tag{2}$$

Thus $Y(\rho)$ and $X(r)$ are Abel Transforms of each other.

Proof:

By changing variables,

$$\frac{1}{\rho^2} = \alpha \tag{3}$$

$$\frac{1}{r^2} = \beta \tag{4}$$

$$dr = -\tfrac{1}{2}\beta^{-3/2}\, d\beta \tag{5}$$

hence (1) becomes

$$2\alpha^{-\frac{1}{2}}\, Y(\alpha) = \int_0^{\alpha} \frac{X(\beta)\,\beta^{-3/2}\,d\beta}{\sqrt{\alpha-\beta}} \tag{6}$$

Let

$$F(\alpha) = 2\alpha^{-\frac{1}{2}}\, Y(\alpha) \tag{7}$$

and

$$f(\beta) = X(\beta)\,\beta^{-3/2} \tag{8}$$

then (6) can be simplified as

$$F(\alpha) = \int_0^{\alpha} \frac{f(\beta)\,d\beta}{\sqrt{\alpha-\beta}} \tag{9}$$

We now recognize that (7) is of the Abel form [27, 28]

$$F(x) = \int_0^{x} f(\xi)(X-\xi)^{-a}\,d\xi \qquad 0 < a < 1 \tag{10}$$

where in our case $a = \frac{1}{2}$.

If we take the Laplace transformation [29] on both sides of (10) and use the Convolution Theorem,

$$\mathcal{L}^{-1}(\bar{f}\,\bar{g}) = \int_0^{x} f(\xi)\, g(X-\xi)\,d\xi \tag{11}$$

(where here $g = x^{-a}$), (10) reads:

$$\mathcal{L}\left[F(x)\right] = \mathcal{L}(x^{-a})\,\mathcal{L}\left[f(x)\right] \tag{12}$$

where

$$\mathcal{L}\left[g(x)\right] = \int_0^\infty g(x)\, e^{-px}\, dx \tag{13}$$

Now, since

$$\mathcal{L}(x^{-a}) = \int_0^\infty x^{-a}\, e^{-px}\, dx = p^{a-1}\,\Gamma(1-a) \tag{14}$$

and

$$\mathcal{L}(x^{a-1}) = \int_0^\infty x^{a-1}\, e^{-px}\, dx = p^{-a}\,\Gamma(a) \tag{15}$$

Hence (12) becomes

$$\frac{1}{p}\,\mathcal{L}\left[f(x)\right] = \frac{\mathcal{L}\left[F(x)\right]\,\mathcal{L}\left[x^{a-1}\right]}{\Gamma(a)\,\Gamma(1-a)} \tag{16}$$

By knowing [11] (p. 256),

$$\Gamma(a)\,\Gamma(1-a) = \frac{\pi}{\sin a\pi} \tag{17}$$

(16) gives

$$\frac{1}{p}\,\mathcal{L}\left[f(x)\right] = \frac{\sin a\pi}{\pi}\,\mathcal{L}\left[F(x)\right]\,\mathcal{L}(x^{a-1}) \tag{18}$$

Taking the inverse Laplace Transform of both sides of (18) gives, using (11)

$$\frac{1}{2\pi j}\int_{c-j\infty}^{c+j\infty}\frac{e^{px}}{p}\,\mathcal{L}[f(x)]\,dp = \frac{\sin a\pi}{\pi}\int_0^x (X-\xi)^{a-1}F(\xi)d(\xi) \tag{19}$$

Differentiating both sides with respect to x, gives

$$f(x) = \frac{\sin a\pi}{\pi}\frac{d}{dx}\int_0^x (X-\xi)^{a-1}F(\xi)d\xi \tag{20}$$

But since $a = \frac{1}{2}$, (20) can be written in the following form:

$$f(\beta) = \frac{1}{\pi}\frac{d}{d\beta}\int_0^\beta \frac{F(\alpha)}{\sqrt{\beta-\alpha}}\,d\alpha \tag{21}$$

Using (7) and (8), we obtain

$$X(\beta)\beta^{-3/2} = \frac{1}{\pi}\frac{d}{d\beta}\int_0^\beta \frac{2Y(\alpha)\alpha^{-\frac{1}{2}}d\alpha}{\sqrt{\beta-\alpha}} \tag{22}$$

Using (3) and (4) gives

$$X(r)r^3 = \frac{1}{\pi}\frac{\partial}{\partial_r}\left[\bar{\bar{f}}(\beta,r)\right]\frac{\partial r}{\partial\beta} \tag{23}$$

where

$$\bar{\bar{f}}(\beta,r) = \int_0^{\beta} \frac{2Y(\alpha)\alpha^{-\frac{1}{2}}d\alpha}{\sqrt{\beta-\alpha}} = -4\int_{\infty}^{r} \frac{Y(\rho)\rho^{-2}d\rho}{\sqrt{\frac{1}{r^2}-\frac{1}{\rho^2}}} \tag{24}$$

$$\frac{\partial r}{\partial \beta} = -\tfrac{1}{2} r^3 \tag{25}$$

therefore,

$$X(r) = -\frac{2}{\pi}\frac{\partial}{\partial r}\left[\int_r^{\infty} \frac{Y(\rho)r\,d\rho}{\rho\sqrt{\rho^2-r^2}}\right] \tag{26}$$

which proves that (2) is correct. Therefore, $Y(\rho)$ and $X(r)$ are transformable with each other. Either one of them can be found as long as the other one is known by going through the integration-differentiation operations as indicated by (1) and (2).

APPENDIX XI

DETERMINATION OF THE k FACTOR

We have

$$\frac{y}{y_o} \approx e^{-k\tau^2} \tag{1}$$

Hence

$$k = \frac{-\ln\left(\frac{y}{y_o}\right)}{\tau^2} = \frac{\ln\left(\frac{y_o}{y}\right)}{\tau^2} \tag{2}$$

but $y_o/y = 1 + x$, $x = (y_o/y) - 1$ and $x^2 << 1$, therefore

$$k \approx \frac{\ln(1+x)}{\tau^2} \approx \frac{x}{\tau^2} = \frac{\frac{y_o}{y} - 1}{\tau^2} \tag{3}$$

Tabulations of k versus τ obtained from the computed values of $y(\tau)$, as also tabulated in Table XI-1, then give the values of k indicated, as plotted in Fig. 13 of the text, and other values read off this curve as tabulated in Table III of the text.

TABLE XI-1.

TABULATIONS OF k VERSUS β

β = 0.40	y(τ)	k	
0	113.06366	------	
.25	100.5837	1.9851	
.50	64.328	3.030	Take k ≈ 1.90
.75	29.104	5.128	

β = 1.00	y(τ)	k	
0	85.6044	-------	
.2	83.0387	.77225	
.4	75.8889	.80012	Take k ≈ 0.75
.6	65.2865	.8645	

β = 1.40	y(τ)	k	
0	63.130757	-------	
.2	62.62638	.20125	
.4	61.10134	.20631	Take k = 0.20
.6	58.66586	.21138	

β = 2.00	y(τ)	k	
0	43.573874	-------	
.4	43.800 *	.11037	Take k = 0.10
.6	43.400 *	.07511	

* From Fig. 9 of text.

APPENDIX XII

DISCUSSION OF RECEIVER DESIGN

The text has shown that the measurement error will be small since the output signal to noise power ratio of a properly designed correlation receiver will be greater than ten. Now, it is desirable to adjust the receiver bandwidth, B, to as small a value as possible without introducing distortion, so as to have a higher signal to noise, $(S_o/N_o)_{in} = (S_o)_{in} / (KT_I B)$, power ratio to minimize the correlation time required and associated receiver expense.

The designer of the receiver, however, must also realize that the bandwidth of all its stages must be sufficient to pass the received coded pulse train signal without distorting it. A conventional engineering rule [30] is that the bandwidth of an amplifier stage, B, (as measured between the lower and upper 3 Db. points) be some fraction, usually 0.35, of the reciprocal of the rise time, t_R, i.e.

$$B = 0.35\, B_R \quad \text{cycles/sec.} \tag{1}$$

where B_R = Rise Time Bandwidth $= 1/t_R$, B = Receiver Bandwidth. We note that B_R can be written as

$$B_R = \frac{1}{T\sqrt{2}\left(\frac{t_R}{\sqrt{2}\,T}\right)} = \frac{1}{\sqrt{2}\,\beta T} \tag{2}$$

where β is the distortion parameter as defined by (62) of the text, and T is the bit duration (here $T = 25.6\ \mu$sec.). Hence,

$$BT = \frac{0.35}{\sqrt{2}\beta} = \frac{0.2475}{\beta} \tag{3}$$

A plot of BT (and also B in Kcps) versus β is given in Fig. XII-1 , and tabulated in Table XII-1.

To justify reducing the bandwidth, B , below $.35\ B_R$ we can introduce the concept of a mean square, or effective bandwidth, B_e .

First, we recognize [10], (p. 115) that the output correlation function $y(\tau)$ has a spectral density $G(\omega T)$ which is the Fourier transform of $y(\tau)$, i.e.

$$G(\omega T) = \int_{-\infty}^{\infty} y(\tau)\, e^{-j\omega T\tau}\, d\tau \tag{4}$$

and, therefore,

$$y(\tau) = \frac{1}{2\pi} \int_{-\infty}^{\infty} G(\omega T)\, e^{j\omega T\tau}\, d(\omega T) \tag{5}$$

hence

$$y''(0) = -\frac{1}{2\pi} \int_{-\infty}^{\infty} (\omega T)^2\, G(\omega T)\, d(\omega T) \tag{6}$$

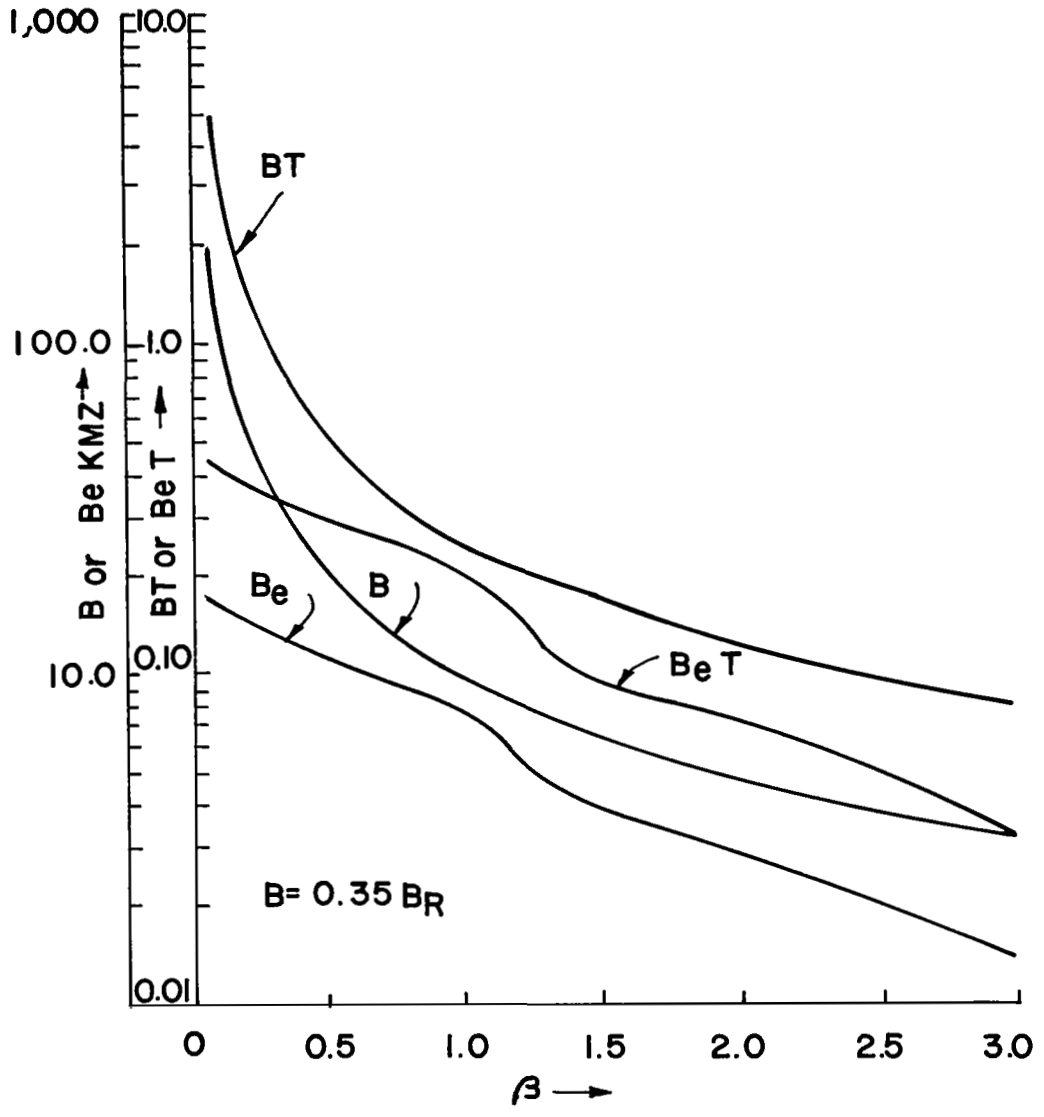

FIG. XII - 1 RISE TIME AND EFFECTIVE BAND WIDTH DEPENDENCE ON DISTORTION PARAMETER

TABLE XII-1.

RISE TIME AND EFFECTIVE BANDWIDTH COMPUTATIONS

β	k	0.35 $B_R T$	$B_e T$	0.35 B_R KC.	B_e KC.
0.00	∞	∞	∞	∞	∞
0.05	3.90	4.95	0.445	193.36	17.38
0.10	3.50	2.475	0.421	96.67	16.45
0.15	3.00	1.650	0.390	64.45	15.23
0.25	2.40	0.990	0.349	38.67	13.63
0.40	1.90	0.6188	0.310	24.17	12.11
0.75	1.15	0.330	0.2414	12.89	9.43
1.00	0.75	0.2475	0.195	9.67	7.62
1.25	0.315	0.1980	0.126	7.73	4.92
1.40	0.20	0.1768	0.1007	6.91	3.93
2.00	0.10	0.1238	0.07118	4.84	2.78
2.50	0.05	0.0990	0.05033	3.87	1.96
3.00	0.025	0.0825	0.03559	3.23	1.39

The total output signal energy, y_o, at $\tau = 0$, is $(S_o)_{out}$ and must be distributed over the entire spectrum, i.e.

$$y_o = (S_o)_{out} = \frac{1}{2\pi} \int_{-\infty}^{\infty} G(\omega T)\, d(\omega T) \tag{7}$$

We can now define (following Gabor and Woodyard and as discussed by Pindyck [2], p. 24, see also Reference 15, p. 467) an effective mean square bandwidth, $(B_e T)$ as (B_e in cycles/sec. and T in sec.)

$$(B_e T)^2 \equiv \frac{\int_{-\infty}^{\infty} (\omega T)^2 G(\omega T) d(\omega T)}{(2\pi)^2 \int_{-\infty}^{\infty} G(\omega T) d(\omega T)} = \frac{1}{(S_o)_{out} (2\pi)^3} \cdot \int_{-\infty}^{\infty} (\omega T)^2\, G(\omega T)\, d(\omega T) \tag{8}$$

Hence (6) becomes

$$y''(0) = -(2\pi)^2 (B_e T)^2 S_o \tag{9}$$

and ((100) of the text gives (since $y_o = (S_o)_{out}$)

$$\overline{\Delta\tau^2} = \frac{1}{4\pi^2 \left(\frac{S_o}{N_o}\right)_{out} (B_e T)^2} \tag{10}$$

The result (10) is an alternative expression for the R.M.S. error we make in locating the peak of the correlation curve centered at $\tau = 0$, and is only valid for large signal to noise ratios $\left[(S_o/N_o)_{out} >> 1\right]$. It is this result that is given in earlier work [2] (see p. 24, (22b) where there it is assumed $(S_o/N_o)_{out} = 2(S_o/N_o)_{in}$). (Also, in that work, since extensive curves of $y(\tau)$ were not available, the factor $y''(0)$ was calculated by means of (5), i.e. by first performing integration of (4) to obtain $G(\omega T)$ then multiplying by $(\omega T)^2$ and integrating via (6); the results obtained were questionable and inconclusive. In this report $y''(0)$ was obtained as previously discussed by a much more direct procedure since extensive curves of $y(\tau)$ were first obtained.)

Now, from (8) we can write

$$(B_e T)^2 = -\frac{1}{4\pi^2}\,\frac{y''(0)}{y_o} \tag{11}$$

But the ratio of $y''(0)/y_o$ has already been found (namely from (96) of the text), hence

$$(B_e T) = \frac{1}{\pi\sqrt{2}}\sqrt{k} \tag{12}$$

where the factor k is plotted as a function of β in Fig. 13 and tabulated in Table III of the text. Hence, we can obtain $(B_e T)$ versus β as also plotted in Fig. XII-1

and also tabulated in Table XII-1. (B_e in Kcps is also plotted in this figure.

From Fig. XII-1 we see $B_e < 0.35\ B_R$; this suggests that we may get by with using a bandwidth less than $0.35\ B_R$ and still not get too much distortion since if $B > B_e$ and if the energy is mostly concentrated in the bandwidth B_e , most of the energy will get through.

Choosing B -- Effect on Input Signal to Noise Power Ratio.

From the above, we see that B must be chosen large enough ($B \geq 0.35\ B_R$ or possibly in the range $B_e < B < 0.35 B_R$) to insure faithful reproduction of the wave form, but we want B as small as possible to limit the input noise power ($kT_I B$) such that the input signal to noise ratio is as high as we can make it so that the receiver need not perform as much correlation (i.e. integration).

Suppose we choose B at the limits B_e and $0.35\ B_R$ and examine the resulting Input Signal to Noise Power Ratio as a function of satellite position (note that $(S_o)_{in} = E_{in}/NT$). The results are tabulated in Table XII-2. It is seen that $(S_o/N_o)_{in} < 1$ for either choice but is larger for $B = B_e$.

Thus, the correlation receiver expense can be minimized for the lower bandwidth choice $B = B_e$, but at the cost of more signal distortion, which, somehow, would have to be

TABLE XII-2.

COMPUTATIONS OF INPUT SIGNAL TO NOISE POWER RATIO, $\left(\frac{S_o}{N_o}\right)_{in}$

θ^o	β	$(S_o)_{in}$ WATTS	t_R μ SEC.	$B = .35B_R = 0.35B_R$ KCPS	$(N_o)_{in}$ $B = .35B_R$ WATTS	$\left(\frac{S_o}{N_o}\right)_{in}$ $B = .35B_R$	B_e KCPS	$\left(\frac{S_o}{N_o}\right)_{in}$ $B = B_e$
85.0	.0566	$5.354 \cdot 10^{-16}$	2.050	170.7	$6.197 \cdot 10^{-15}$	.084	17.36	.8496
97.5	.0692	$5.1869 \cdot 10^{-16}$	2.505	139.72	$5.0725 \cdot 10^{-15}$	.1025	16.80	.8525
113.0	.0858	$4.637 \cdot 10^{-16}$	3.106	112.685	$4.091 \cdot 10^{-15}$	.1133	16.45	.7761
134.0	.1121	$3.982 \cdot 10^{-16}$	4.058	86.249	$3.131 \cdot 10^{-15}$	.1272	15.98	.6865
153.0	.1503	$3.485 \cdot 10^{-16}$	5.441	64.326	$2.335 \cdot 10^{-15}$	.1493	15.23	.6306
164.0	.1962	$3.258 \cdot 10^{-16}$	7.102	49.282	$1.789 \cdot 10^{-15}$	.1821	14.31	.6271
173.5	.2939	$3.003 \cdot 10^{-16}$	10.641	32.892	$1.1941 \cdot 10^{-15}$	.2515	13.20	.6267
178.0	.4866	$2.887 \cdot 10^{-16}$	17.615	19.869	$.7213 \cdot 10^{-15}$	.4002	11.46	.6939
180.0	∞	$2.799 \cdot 10^{-16}$	∞	0	0	-----	0	-----
184.0	.3415	$2.694 \cdot 10^{-16}$	12.365	12.306	$1.0276 \cdot 10^{-15}$	.2621	12.59	.5893
187.0	.2623	$2.484 \cdot 10^{-16}$	9.498	36.850	$1.338 \cdot 10^{-15}$	.1857	13.34	.5130

calibrated out, if possible, of the output of the receiver, $y(\tau)$. This writer prefers choosing $B = 0.35\ B_R$ and accepting the lower input signal to noise power ratio and building a more expensive receiver (i.e., one capable of performing more correlation) whose output need not calibrate out any distortion due to the receiver. In either case, sufficient correlation would have to be performed so that the output signal to noise power ratio would exceed 10 so as to validate the low error findings of the text. This should not be much of a problem, as previously indicated in the text, since the maximum output signal to noise ratio power should be capable of being at least 44.

APPENDIX XIII

EFFECT OF IONOSPHERE ON SOLAR PROBE EXPERIMENT

In the text, the distribution of $f_p(r)$ as shown in Fig. 1, did not include the presence of the ionosphere which extends from approximately 50 kilometers above the earth to several earth radii (mean earth radius = 6371 kilometers) with a distribution [17] (pp. 668-670) typified by Fig. XIII-1.

Thus the actual $f_p(r)$ distribution should be as sketched in Fig. XIII-2.

However, the solution to the scalar wave equation even in this ionospheric layer can still be taken as the W.K.B. solution since the inequality (18) of Appendix I,

$$\Delta = \left| \frac{1}{8\pi} \frac{d\epsilon_r}{d\left(\frac{\xi}{\lambda}\right)} \right| \tag{1}$$

is still much less than unity. This is seen as follows: From Fig. XIII-1, we see that f_p varies from roughly zero to 10 mHz (hence ϵ_r varies from roughly unity to 0.98, for $f_o \approx 70$ mHz) in a distance of $\Delta\xi = 300$ km, hence since $\lambda \approx \lambda_v \approx \frac{300}{70}$ meters, we have

$$\Delta \approx \frac{1}{8\pi} \frac{(.02)}{\frac{300 \cdot 10^3}{\left(\frac{300}{70}\right)}} \approx 10^{-8} << 1 \quad .$$

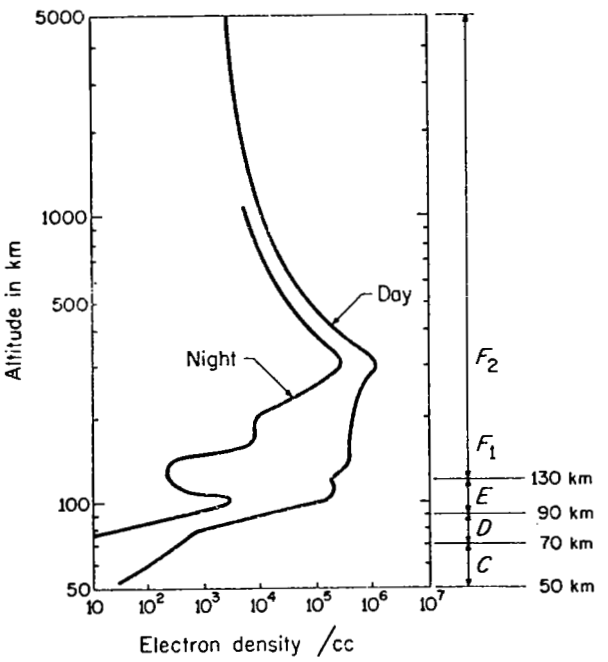

FIG. XIII-1. TYPICAL IONOSPHERE ELECTRON PROFILES.

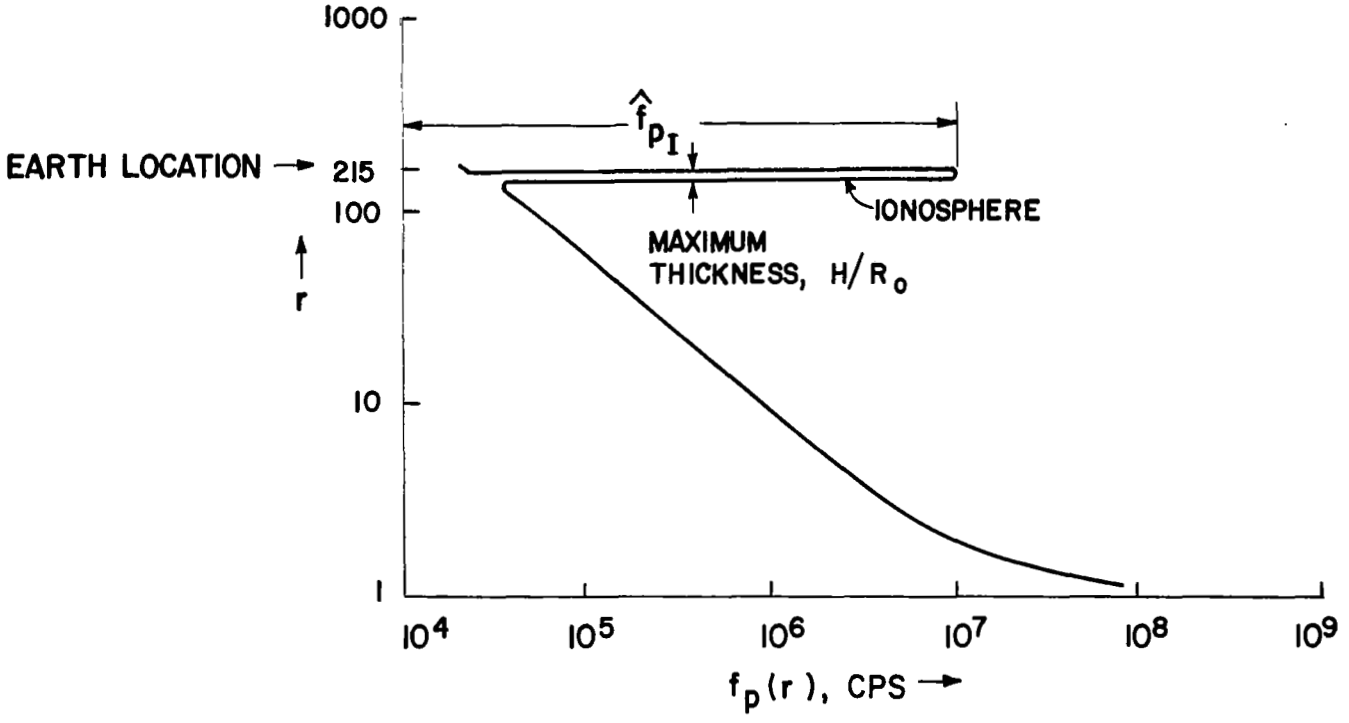

FIG. XIII-2. SKETCH OF PLASMA FREQUENCY VARIATION IN SOLAR CORONA INCLUDING IONOSPHERE.

As such the effect of the ionosphere is merely to increase the averaged or integrated squared plasma frequency factor by the additional amount over the ionosphere. Hence denoting by $\overline{P_I^2}$ the value of the normalized plasma factor with the ionosphere present and by $\overline{P^2}$ the value in the absence of the ionosphere, gives

$$\overline{P_I^2} = \overline{P^2} + \frac{1}{Lf_o^2} \int_{\xi_I}^{\xi_I + H} f_p^2(\xi)\, d\xi \tag{2}$$

where ξ_I is the effective distance of the top of the ionosphere, and H its maximum thickness. If we denote by $\hat{f}_{p_I}$ the maximum plasma frequency in the ionosphere then

$$\overline{P_I^2} \leqq \overline{P^2} \left(1 + \frac{\overline{\Delta P^2}}{\overline{P^2}}\right) \tag{3}$$

where

$$\overline{\Delta P^2} = \left(\frac{H}{L}\right) \left(\frac{\hat{f}_{p_I}}{f_o}\right)^2 \tag{4}$$

Hence, for a given carrier frequency, f_o, and path length, t_o, it follows from (54) of the text that the rise times and hence from (62) of the text, the distortion factors, for a fixed bit length, T, for ionosphere absent are related by

$$\frac{\beta_I}{\beta} \leq \sqrt{1 + \frac{\overline{\Delta P^2}}{\overline{P^2}}} \tag{5}$$

which from (56) of the text can be written in terms of the differential group delay time as

$$\frac{\beta_I}{\beta} \leq \sqrt{1 + \frac{\Delta T_d}{T_d}} \tag{6}$$

where

$$\Delta T_d \leq \frac{1}{2} \frac{H}{c} \frac{\hat{f}_{p_I}^2}{f_o^2} \tag{7}$$

Now since $H \approx 300$ km , and $\hat{f}_{p_I} \approx 10$ mHz, then for 75 mHz, $\Delta T_d \lesssim 0.01$ milliseconds. From Table II of the text we see that T_d ranges over $0.16 \lesssim T_d \leq \infty$ milliseconds for an offset distance $0 \lesssim \rho \lesssim 154$, and, therefore, (6) becomes

$$\frac{\beta_I}{\beta} \approx 1 + \frac{\Delta T_d}{2T_d} \lesssim 1.03 \approx 1 \tag{8}$$

Hence, the ionosphere has a negligible effect on the distortion of the signal. This is true for any carrier frequency satisfying $f_o^2 >> \hat{f}_{p_I}^2$ and $f_o^2 >> f_m^2$, since the f_o^2 terms cancel in the ratio of $(\Delta T_d)/T_d$ in (8).

Another way of expressing this result is that the effective bandwidth of the ionosphere, Δf_I , is much larger than that of the solar path, Δf , since from the definition, $\Delta f = 1/t_R$, (54) of the text gives:

$$\Delta f_I = \frac{1}{t_{R_I}} = \frac{1}{\sqrt{\frac{t_{o_I}(\overline{\Delta P^2})}{f_o}}} \quad \frac{1}{\sqrt{\frac{H}{c}\frac{(\overline{\Delta P^2})}{f_o}}} \tag{9}$$

$$\Delta f = \frac{1}{t_R} = \frac{1}{\sqrt{\frac{L}{c}\frac{\overline{P^2}}{f_o}}} \tag{10}$$

but using (56) of the text this can be expressed as

$$\frac{\Delta f_I}{\Delta f} = \sqrt{\frac{T_d}{\Delta T_d}} >> 1 \ . \tag{11}$$

Thus the additional distortion undergone by the wave as it traverses the ionosphere will be negligible as compared to that undergone by wave as it traversed the solar path.

The above is for normal (radial) incidence; for oblique incidence larger corrections would result. All of these would add incrementally to the signal rise time, (or effective $\overline{P^2}$) and should be added in with the incremental rise time introduced by the antennas, transmission lines, and receiver front end, when evaluating the receiver output response.

APPENDIX XIV

EFFECTS OF REFRACTION OF SOLAR CORONA -- GEOMETRICAL OPTICS SOLUTION

a. Introduction

Thus far, the effects of refraction (ray bending) have been neglected. In this appendix, this refractive bending due to the solar corona is shown to be trivial by using a simple and concise geometrical optics method.

b. Ray-Path Equation

By employing the electromagnetic theory approach to geometrical optics, the analytical formula obtained for describing electromagnetic ray paths in a inhomogeneous medium [31] is

$$\theta(r) = \theta_s + \int_{r_s}^{r} \frac{b\,dr}{r\sqrt{n^2(r)r^2 - b^2}} \qquad (1)$$

where θ_s and r_s are the initial angle and the initial distance of the ray path respectively, as measured from the origin of the coordinate system, and b is the ray parameter given by

$$n(r)r \sin \phi = b = \text{constant} \qquad (2)$$

and ϕ is the angle between the position vector $\mathbf{r}$ and the tangent at the point P on the ray (see Fig. XIV-1), and n(r) is the refractive index.

From Section II of the text, for the model of solar corona assumed, the refractive index is approximately given by

$$n^2(r) = 1 - \frac{k^2}{r^2} \tag{3}$$

where k can be found equal to 12×10^{-2} for $f_o = 75$ mc (see p. 48 of text).

By considering that the ray path starts from the satellite, the origin of the coordinate system can be taken at the center of the sun such that $\theta_s = 0$, and r_s equal to the normalized distance (with respect to the radius, R_o, of the Sun), between the sun and the satellite (i.e. $r_s = R_s/R_o$) as shown in Fig. XIV-1.

In terms of normalization distance (i.e. $r = R/R_o = (R/R_E)(R_E/R_o) = 215\ u$, and $r_s = R_s/R_o = (R_s/R_E)(R_E/R_o) = 215\ u_s$), (1), with refractive index given by (3) becomes

$$\theta(r) = \frac{b}{\sqrt{k^2 + b^2}} \left\{ \cos^{-1} \left| \frac{\sqrt{k^2 + b^2}}{215\ u} \right| - \cos^{-1} \left| \frac{\sqrt{k^2 + b^2}}{215\ u_s} \right| \right\}$$

$$\text{for } (215\ u)^2 > k^2 + b^2 , \quad (215\ u_s)^2 > k^2 + b^2 \tag{4}$$

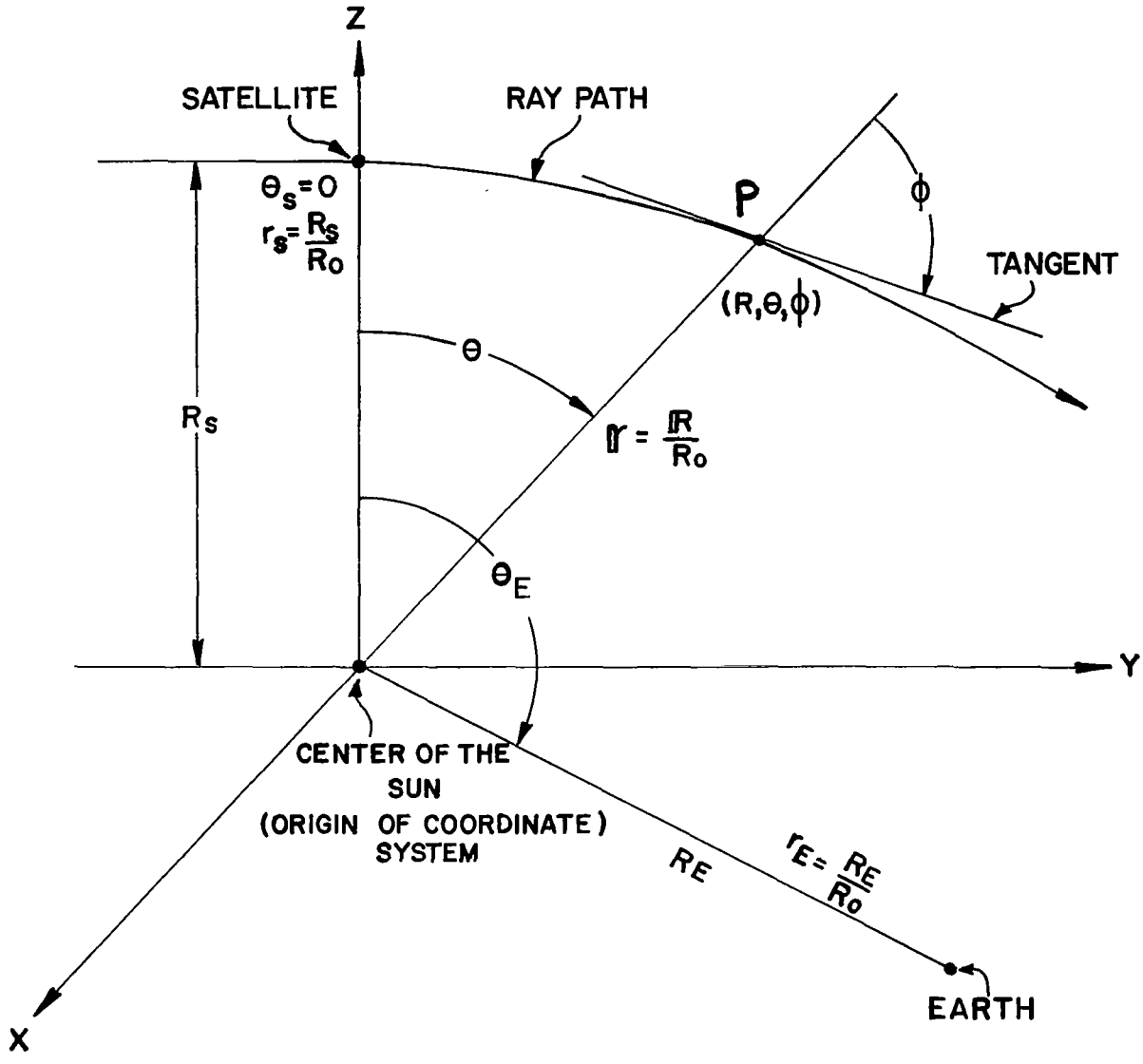

FIG. XIV-1. RAY PATH GEOMETRY SOLAR PROBE PROBLEM.

c. Effects of Refraction Due to Refractive Index $n(r)$ -- Comparison with Vacuum Case $n(r) = 1$

Since the equation, (4), of the ray path is known, it can be solved graphically for the parameter b by computing a curve of θ versus b for given values of k, u, and u_s (with the aid of all the information tabulated in Table II of the text). In other words, for a fixed satellite position (u_s) and a specified termination point (θ and u) the parameter b can be found. This has been done for five cases of θ, as shown in Fig. XIV-2. This gives, for example for $\theta = 85^\circ$, $b = 155$ from Fig. XIV-2-b, etc. Knowing that the ray parameter b and the initial angle, ϕ_s, starting from the satellite, due to the refractive bending is related by (2), the corresponding value of ϕ_s can thus be determined by

$$\phi_s = \sin^{-1}\left[\frac{b}{n(r_s)r_s}\right] \tag{5}$$

since b is now known from the θ versus b curves. For the satellite location ranging from $\theta = 85^\circ$ to 181.3°, the corresponding value of b ranges from 2.05 to 155, and the initial starting angles, ϕ_s, from 48.17° to 0.069°. The values of ϕ_s for the vacuum case ($k = 0$) can be found by simple geometrical relation and are also tabulated in Table XIV-1.

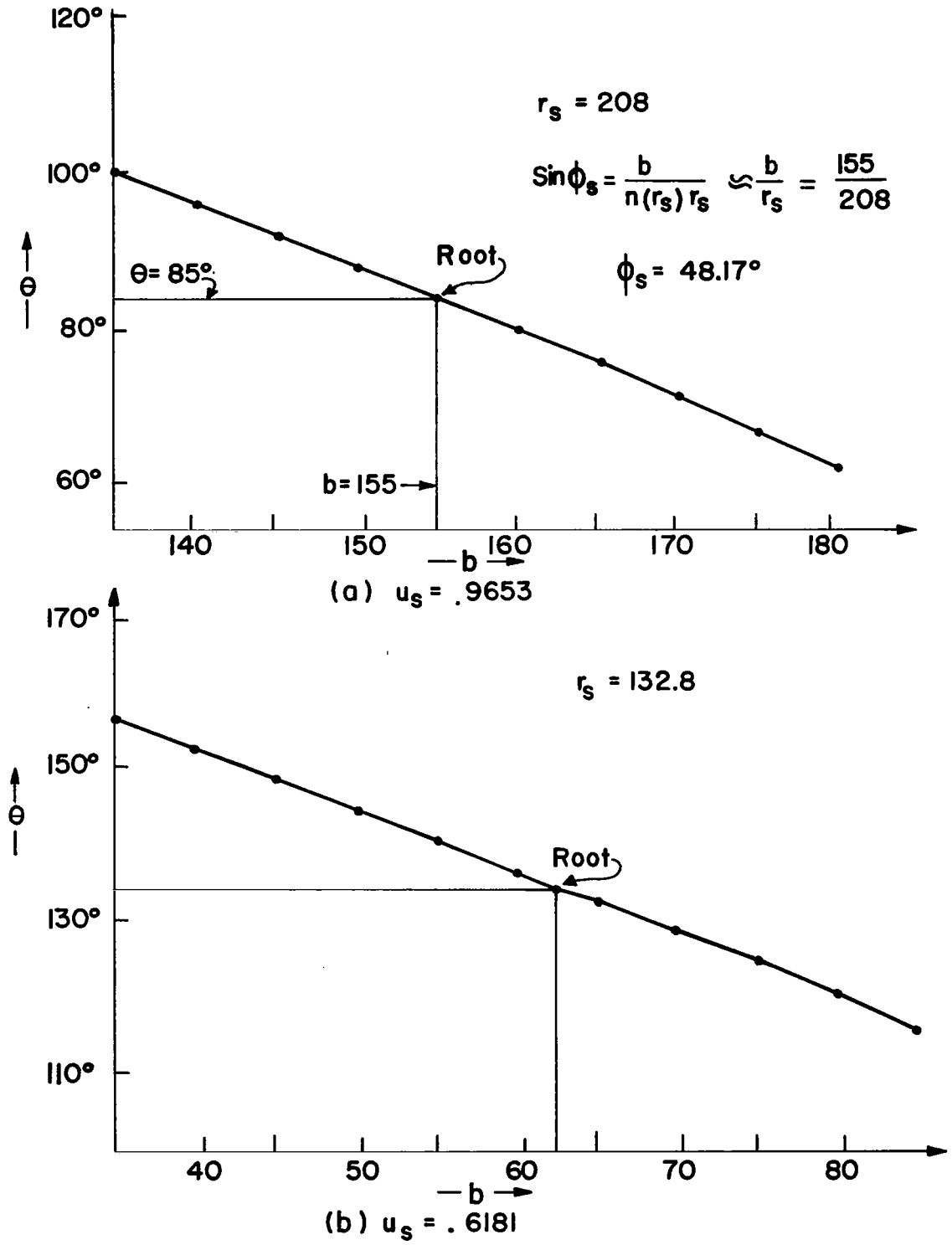

FIG. XIV-2. COMPUTED CURVES FOR RAY PATH PARAMETER b

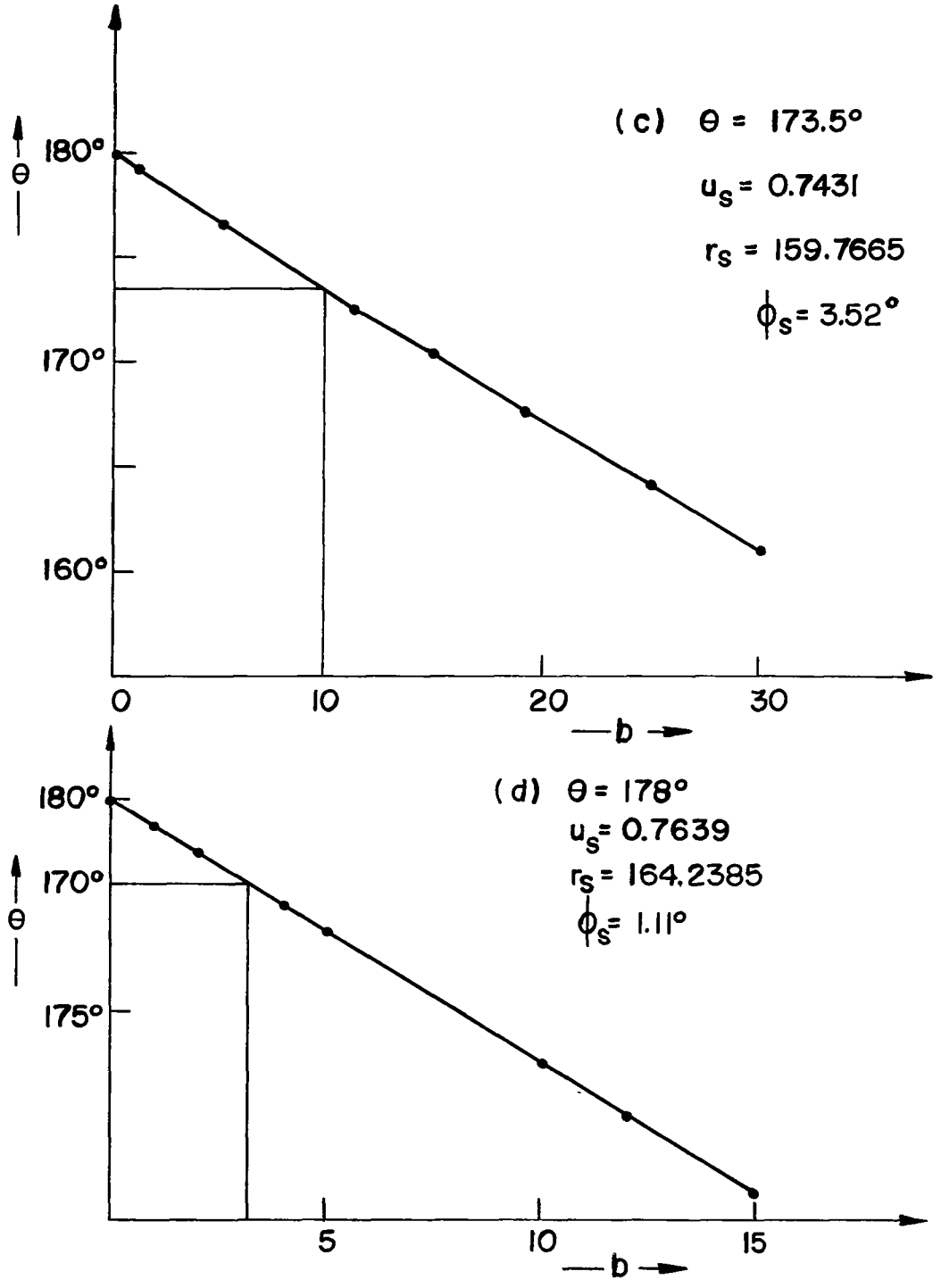

FIG. XIV-2. COMPUTED CURVES FOR RAY PATH PARAMETER b

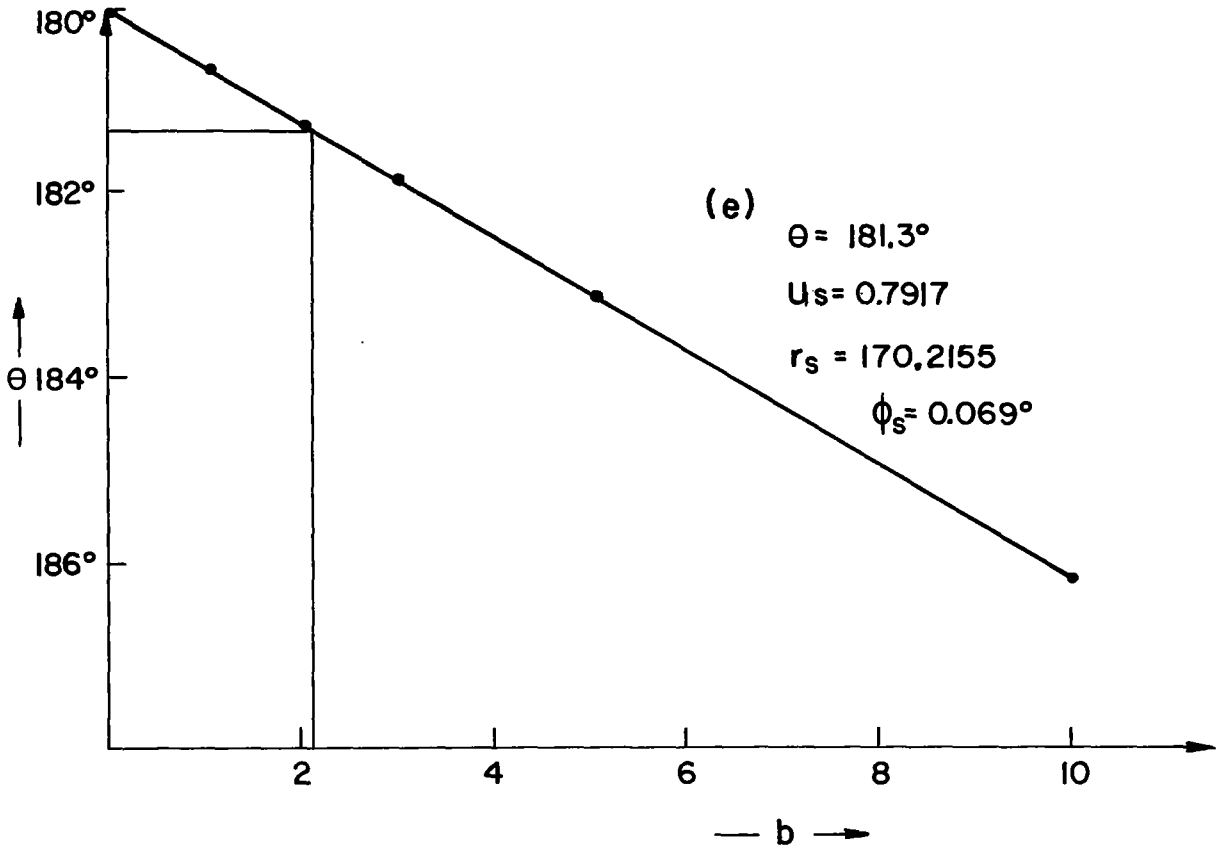

FIG. XIV-2. COMPUTED CURVES FOR RAY PATH PARAMETER b

TABLE XIV-1.

RAY STARTING ANGLES (ϕ_s AND ϕ_{sv}) CALCULATIONS

θ DEGREES	ρ	b	ϕ_s DEGREES	ϕ_{sv} DEGREES	u_s
85	155.28	155	48.17	48.6	0.9653
134	64.2	62.5	28.10	28.69	0.6181
173.5	8.96	9.8	3.52	3.74	0.7431
178	2.984	3.18	1.11	1.13	0.7639
181.3	1.492	2.05	0.069	0.073	0.7917

Although, we would expect, at least theoretically, (from (1)) that the **deviation** due to the bending of rays for the inhomogeneous case as compared to the vacuum straight line case would increase as b gets smaller and smaller, Table XIV-1 shows the **deviations** are still very small and cannot be noticed within the accuracy associated with the graphical procedure to obtain b. In other words, $\phi_{sv} \approx \phi_s$, within the accuracy of Fig. XIV-2. Therefore, the effects of refraction of the solar corona can be approximated by a model having the refractive index $n(r) \approx 1$ as far as the refraction is concerned.

d. Conclusions

Choosing θ_1 and θ_2 which are two angles extending from two extreme points of the earth from the center of the sun, the corresponding values of b (say b_1 and b_2) can be obtained from the curves of Fig. XIV-2. From (5), it follows:

$$\Delta\phi = \phi_2 - \phi_s \tag{6}$$

where $n(r_s)r_s \sin \phi_1 = b_1$, $n(r_s)r_s \sin \phi_2 = b_2$. For the vacuum case (straight line since $k = 0$)

$$\Delta\phi_v = \frac{\frac{D}{2}}{R_{s_E}} \tag{7}$$

where D = diameter of the earth. From the preceding, we would expect to obtain with high accuracy computations of ϕ_2 and ϕ_1 that (within the accuracy of Fig. XIV-2 it is the case)

$$\Delta\phi \approx \Delta\phi_v \tag{8}$$

This implies that the power received by the earth, the product of the flux density per unit solid angle, (which is the same for each case since it is radiated isotropically by the satellite) times the subtended angle, is essentially the same for both the vacuum and the $n(r) = 1 - \frac{k^2}{r^2}$ case, where $k^2 \ll 1$.

APPENDIX XV

WAVEGUIDE SIMULATION OF THE SOLAR CORONA

a. Basis of Simulation

To test the feasibility of the proposed correlation scheme to measure, essentially, the β of the solar corona path as a function of satellite position, it is desirable to insure that the designed system is indeed working correctly, i.e., to calibrate the system. To accomplish this, it is suggested that the pseudo random phase shift keyed carrier be injected into a run of waveguide having a length L_2 with a cutoff to carrier frequency of P_2, and the output be fed into the correlation receiver. To simulate the solar corona, the waveguide parameters, L_2 and P_2, must be chosen such that two conditions be satisfied:

(1) The β factor of the waveguide must be the same as that of the solar corona. Denoting the waveguide case by the subscript 2 and the solar corona case by the subscript 1, then we must have:

$$\beta_1 = \beta_2 \tag{1}$$

(2) The waveguide length, L_2; the carrier frequency for the waveguide case, f_{o2}; and the ratio of cutoff to carrier frequency, P_2, must be such that the waveguide

output will have the main signal type of response to a stepped carrier input, for essentially, all time (since this is the response for the solar case). This amounts to having the maximum value of the normalized time-distance factor for the waveguide case, $v_{2\ max}$, the same or greater than its maximum value for the solar case, $v_{1\ max}$, i.e.:

$$v_{2\ max} \geq v_{1\ max} \tag{2}$$

Let us now explicitly state these conditions. From (62), (54), and (56) of the text, it follows that (1) implies*

$$\frac{P_1 \sqrt{\frac{t_{o_1}}{2f_{o_1}}}}{T_1(1 - P_1^2)^{3/4}} = \frac{P_2\sqrt{\frac{t_{o_2}}{2f_{o_2}}}}{T_2(1 - P_2^2)^{3/4}} \tag{3}$$

* It is noted here that for the general case (where $P^2 << 1$ need not be satisfied), (29) of the text gives $\Phi''(\omega_o) = t_o(\omega_p^2/\omega_o^3)(1 - P^2)^{-3/2}$, giving, from (54) of the text, $t_R = \sqrt{t_o P^2/f_o}\,(1 - P^2)^{-3/4}$, and hence β is given by (3). Also, $\Phi'''(\omega_o) = -3t_o(\omega_p^2/\omega_o^4)(1 - P^2)^{-5/2}$, causing (31) of the text to become $|(\omega/\omega_o) - 1| << (1 - P^2)^{-1}$; (33) of the text to become $\omega_s/\omega_o = \pm (\rho P)/\sqrt{\rho^2 - 1}$, thus causing (36) of the text to become (5) and (50) of the text to become (6).

But since $P_1^2 << 1$ and using the notation $\eta_1 = 2\pi f_{o_1} t_{o_1}$ and $\eta_2 = 2\pi f_{o_2} t_{o_2}$, this becomes

$$\frac{P_1 \sqrt{\eta_1}}{f_{o_1} T_1} = \frac{P_2 \sqrt{\eta_2}}{f_{o_2} T_2 (1 - P_2^2)^{3/4}} \tag{4}$$

Let us now see what (2) implies. From (36) of the text we saw that we get the main signal response to a stepped carrier for*

$$\left| \frac{t - t_g}{t_o} \right| << \frac{P^2}{(1 - P^2)^{3/2}} \tag{5}$$

and since

$$v \equiv \frac{1}{P} \sqrt{\frac{\eta}{\pi}} \left(\frac{t - t_g}{t_o} \right) (1 - P^2)^{3/4} \tag{6}$$

It then follows that the main signal solution will exist for

$$|v| << \sqrt{\frac{\eta}{\pi}} \frac{P}{(1 - P^2)^{3/4}} \equiv v_{max} \tag{7}$$

Now for the solar case (Case 1), $P_1^2 << 1$, hence

$$v_{1\,max} \equiv P_1 \sqrt{\frac{\eta_1}{\pi}} \tag{8}$$

* See footnote, p. 160.

(We note that $v_{1\ max}$ reduces to, since $\eta_1 = 2\pi f_{o_1} t_{o_1}$, and $t_{o_1} = \frac{2T_d}{P_1^2}$, $v_{1\ max} = 2\sqrt{f_{o_1} T_{d_1}}$ which for the H.F. (Table II) experiment where $f_o \approx 70$ mHz and $T_{d_1} \gtrsim \frac{3}{2} \cdot 10^{-4}$ secs. gives $v_{1\ max} \gtrsim 200$; hence from Fig. 4a we see that the main signal can be used for, essentially, all times. Hence if we made $v_{2\ max} \geq v_{1\ max}$, we insure that the main signal solution exists for, essentially, all times for the waveguide case. Now we want to make L_2 as small as possible, therefore, we can get by with $v_{2\ max} = v_{1\ max}$, but from (7)

$$v_{2\ max} = \sqrt{\frac{\eta_2}{\pi}} \quad \frac{P_2}{(1 - P_2^2)^{3/4}} \tag{9}$$

therefore,

$$\sqrt{\eta_2} \quad \frac{P_2}{(1 - P_2^2)^{3/4}} = P_1 \sqrt{\eta_1} \tag{10}$$

Thus, (4) and (10) must be satisfied if the waveguide is to simulate the solar corona. Substituting $P_1 \sqrt{\eta_1}$ from (10) into (4) gives

$$f_{o_1} T_1 = f_{o_2} T_2 \tag{11}$$

Letting

$$M = f_{o_1} T_1 = \#\ \text{of cycles in individual pulse of duration } T_1 \tag{12}$$

gives

$$f_{o_2} T_2 = M \tag{13}$$

That is, the simulation scheme must have the same number of cycles in its pulse as the solar case!

Now, from (10) (noting that $P_1 \sqrt{\eta_1} = 2\sqrt{f_{o_1} T_{d_1} \pi}$) we obtain after squaring both sides,

$$\left(\frac{L_2}{\lambda_{v_c}}\right) = \frac{2(f_{o_1} T_{d_1})(1 - P_2^2)^{3/2}}{P_2} \tag{14}$$

where $\lambda_{v_c} = c/f_c$, with f_c = cutoff frequency of waveguide, $P_2 = f_c/f_{o_2}$. But

$$\beta = \frac{t_{R_1}}{T_1 \sqrt{2}} = \frac{1}{T_1}\sqrt{\frac{T_{d_1}}{f_{o_1}}} \tag{15}$$

therefore,

$$\beta^2 = \frac{(T_{o_1} f_{o_1})}{M^2} \tag{16}$$

Substituting $(T_{d_1} f_{o_1})$ from (16) into (14) gives

$$\left(\frac{L_2}{\lambda_{v_c}}\right) = 2\beta^2 M^2 \frac{(1 - P_2^2)^{3/2}}{P_2} \tag{17}$$

Equations (13) and (17) are then the two conditions which must be satisfied for simulation to hold.

For a specified M and β one uses (17) to determine the length of the guide once P_2 and λ_{v_c} are specified at some convenient values (say X-band). One can deduce T_2 from (13) and the specified value of M and P_2. An example simulation scheme at X-band is given in what follows.

First, it is noted that the bandwidths, Δf_1 and Δf_2, which are the reciprocal of the rise times, t_{R_1} and t_{R_2}, respectively, are related by, via (54) of the text and (16)

$$\frac{\Delta f_1}{f_{o_1}} = \frac{\Delta f_2}{f_{o_2}} = \frac{1}{\sqrt{2}\beta M} = \frac{1}{\sqrt{2 f_{o_1} T_{d_1}}} \tag{18}$$

i.e., the simulation insures that the percentage bandwidths are preserved, and are equal to $\frac{1}{\sqrt{2}\beta M}$.

b. Example of Solar Corona Simulation by Waveguide

Suppose we desire to use X-band waveguide (since X-band components are not too large to be bulky, nor too small to be difficult to fabricate) to simulate the H.F. (70$\rightarrow$80 mHz) experiment. Here $M \approx 2000$ ($f_{o_1} = 75$ mHz, $T_1 = 25.6$ μsec), and $0 \lesssim \beta \lesssim 2$. For standard X-band waveguide, $\lambda_{v_c} = 4.57$ cm, hence from (17), L_2 and P_2 must be chosen to satisfy:

$$\frac{L_2}{\beta^2} \approx 1.20 \cdot 10^6 \frac{(1 - P_2^2)^{3/2}}{P_2} \quad \text{feet} \tag{19}$$

A plot of L_2/β^2 is shown in Fig. XV-1. It is seen that to realize simulation with practical waveguide runs, $P = P_2$ must be chosen close to unity. Unfortunately, as P approaches unity the wall loss attenuation, α, which is governed by [32]

$$\alpha = \frac{R_s}{b\eta\sqrt{1 - P^2}} \left[1 + 2\left(\frac{b}{a}\right)P^2\right], \quad P \neq 1 \tag{20}$$

(where $R_s = \sqrt{\frac{\pi f \mu}{\sigma}}$, a = internal width of waveguide, and b = internal height of waveguide) increases rapidly. A value of $P \approx 0.80$ gives the low attenuations at X-band of approximately 0.10 Db./foot, for silver plated RG-52U guide (a = 0.900", b = 0.400").

Thus, a compromise must be made between a value of P close to unity and yet one giving realistic attenuation.

As an example, to simulate the solar path having $\beta = 0.04$, a run of RG-52/U waveguide of $L \approx 500$ feet operating at $P \approx 0.80$ (i.e., $f_{o_2} = 8.20$ ghz.) which would introduce a loss of 50 Db. could be practically implemented. (The choice of P = .80 or higher is desirable since then no problem with the dispersion of the various waveguide components or connectors, etc., used will be experienced since these components are designed to be flat over the X-band region of

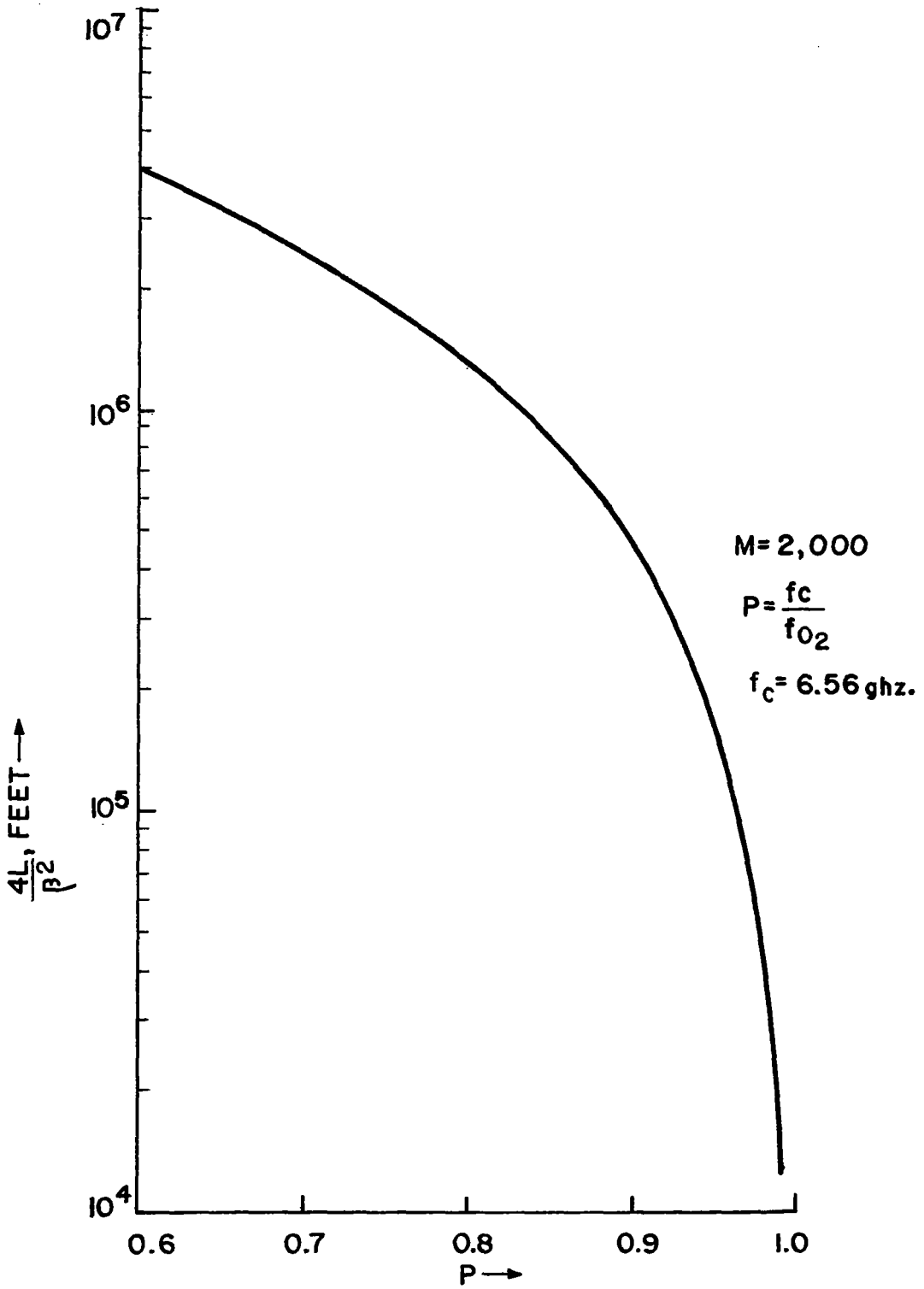

FIG. XV-1. X-BAND WAVEGUIDE LENGTH REQUIRED TO SIMULATE V.H.F SOLAR EXPERIMENT.

$8.2 \lesssim f \lesssim 12.4$ ghz*). A standard X-band source having watts of output would be reduced to tens of microwatts which is more than sufficient to operate the contemplated correlation receiver. Once P is determined, T_2 is then obtained from $T_2 = \frac{M}{f_{o_2}} = \left(\frac{M}{f_c}\right)P$, therefore, here $T_2 = 0.244$ μsec.

Of course, if higher values of β are to be simulated, the waveguide length required becomes unfeasibly long. (This could be prevented by reducing the number of pulses, M, in the basic bit and this factor then should be considered in the design of the solar experiment.)

The preceding is merely an example of a suggested simulation for a specific experiment, and a more detailed look should be undertaken in connection with a given solar experiment with the objective of determining a waveguide simulator of fixed feasible length and yet capable of simulating the entire β range of the solar experiment.

* This bandwidth of $\pm 20\%$ is more than adequate to insure that the various waveguide components will not distort the rise time to be propagated which, as seen from Table XII-2 requires a much smaller bandwidth.

APPENDIX XVI

COMMUNICATION BANDWIDTH AT S BAND

If communication between the solar probe satellite and the earth is desired (at say a higher carrier frequency in the S-band range), then the usable bandwidth, Δf, will be restricted due to the dispersion of the solar path. Now, this bandwidth (by definition) is the inverse of the rise time, hence

$$\Delta f = \frac{1}{t_R} \tag{1}$$

But, from (54) (since $\overline{P^2} \ll 1$)

$$t_R = \sqrt{\frac{t_o \overline{P^2}}{f_o}} \tag{2}$$

Therefore,

$$\Delta f = \frac{f_o^{3/2}}{\overline{f_p} \sqrt{t_o}} \tag{3}$$

Hence, since $\overline{f_p}$ and t_o are fixed for a given satellite location, the bandwidth is seen to be proportional to the 3/2 power of the carrier frequency. Now, we can write

$$\frac{\Delta f}{\Delta f_{H.F.}} = \left(\frac{f_o}{f_{o_{H.F.}}}\right)^{3/2} \tag{4}$$

or, i.e., from (1)

$$\Delta f = \left(\frac{f_o}{f_{o_{H.F.}}}\right)^{3/2} \frac{1}{t_{R_{H.F.}}(\theta)} \tag{5}$$

Taking $f_o = 1$ ghz , and using the plot of $t_{R_{H.F.}}(\theta)$ of Fig. 11 of the text, ($f_{o_{H.F.}} = 75$ mHz) a plot of Δf versus θ can then be obtained as shown in Fig. XVI-1. and also tabulated in Table II of the text. (We recall that Fig. 11 of the text is based on the $n(r) = 10^{12}/r^2$ assumption.)

It is seen that the usable bandwidth varies from about 24 mHz maximum to about 2 mHz minimum for the trajectory considered, which is sufficient for quality T.V. signal transmission.

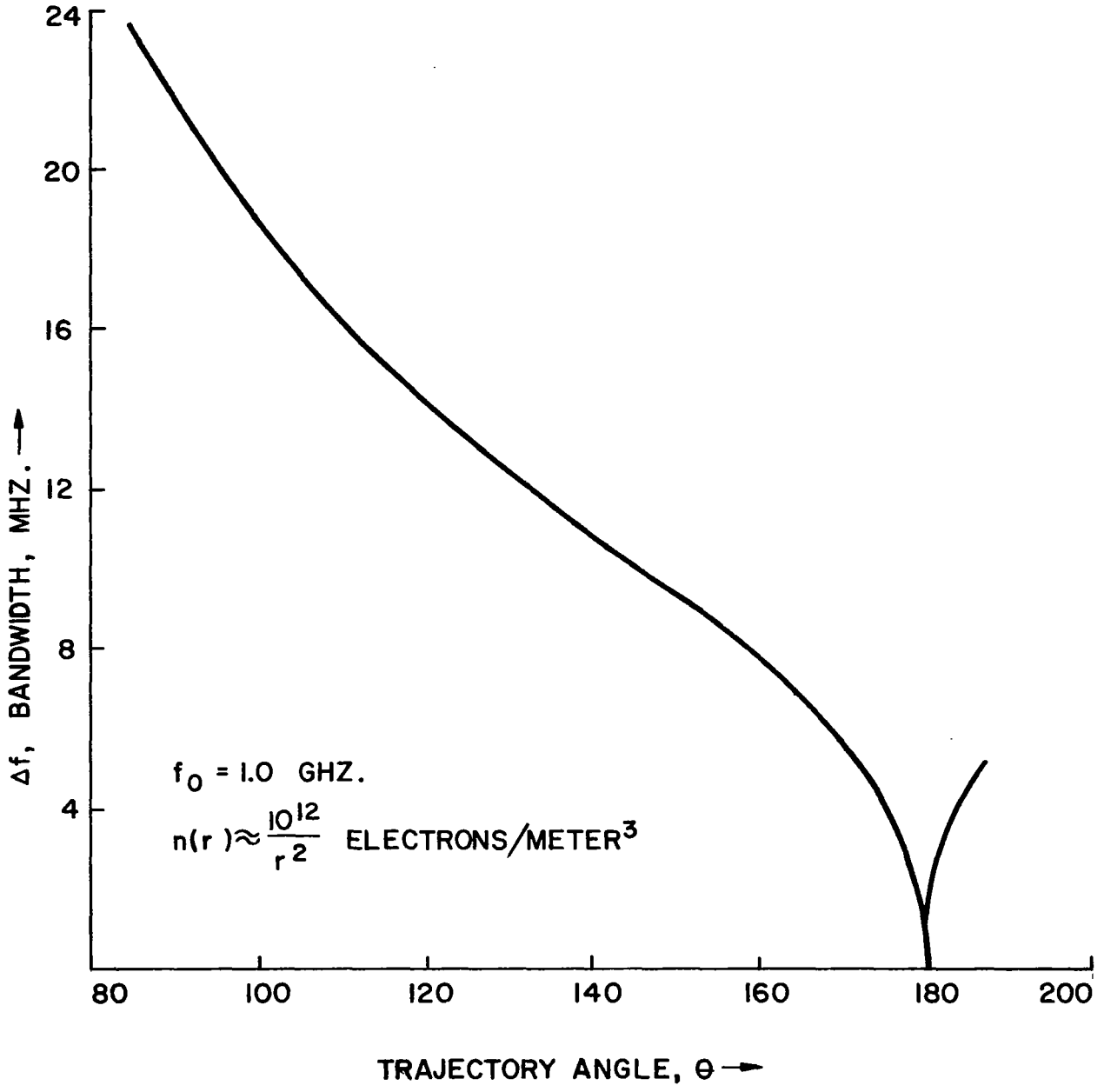

FIG. XVI-1 USABLE BANDWIDTH THROUGH SOLAR CORONA AT S-BAND CARRIER

APPENDIX XVII

DUAL FREQUENCY EXPERIMENT AT S AND X BAND

Due to the fact that a single antenna (parabolic dish with dual frequency feed) is currently being developed for use at both S and X band, it is desirable to take a look at the S.S.P. experiment using these two frequencies.

First, we note from (108) and (109) of the text that we can write

$$\frac{\overline{(\Delta \bar{n})^2}}{(\bar{n})^2}\left(\frac{S_o}{N_o}\right)_{out} = \frac{2\overline{(\Delta \tau_1)^2}\left(\frac{S_o}{N_o}\right)_{out}}{\left[\beta_1^2 f_{o_1} T\left(1 - \frac{f_{o_1}^2}{f_{o_3}^2}\right)\right]^2} \qquad (1)$$

Now, let the S-X band (i.e. $f_{o_1} \simeq 1{,}000$ mHz, $f_{o_3} = 10{,}000$ mHz) case be denoted by primes, and the V.H.F. case (i.e. $f_{o_1} = 70$ mHz, $f_{o_3} = 80$ mHz) by no primes, taking the respective ratios of (1) for these two cases gives

$$\frac{\left[\frac{\overline{(\Delta \bar{n})^2}}{(\bar{n})^2}\left(\frac{S_o}{N_o}\right)_{out}\right]'}{\left[\frac{(\Delta \bar{n})^2}{(\bar{n})^2}\left(\frac{S_o}{N_o}\right)_{out}\right]} = \frac{(Tf_{o_1})^2\left(1 - \frac{f_{o_1}^2}{f_{o_3}^2}\right)^2}{(T'f'_{o_1})^2\left(1 - \frac{f'^2_{o_1}}{f'^2_{o_3}}\right)^2}\left(\frac{\beta_1^2}{\beta_1'^2}\right)^2 \frac{\overline{(\Delta \tau_1')^2}\left(\frac{S_o}{N_o}\right)'_{out}}{\overline{(\Delta \tau_1)^2}\left(\frac{S_o}{N_o}\right)_{out}} \qquad (2)$$

Now, suppose we insist that the output signal to noise levels must both be high (which must be the case for proper operation) and that the same type of correlation output curve dependence on satellite location be maintained at the lower, subscript one, frequencies, i.e.

$$\beta_1 = \beta_1' \tag{3}$$

The former requirement justifies use of the findings of Fig. 15 of the text, while the latter (from this figure) makes $\overline{(\Delta\tau_1)^2}(S_o/N_o)_{out}$ and $\overline{(\Delta\tau_1')^2}(S_o/N_o)'_{out}$ equal. Further, since

$$\left(\frac{S_o}{N_o}\right)_{out_{max}} = 2\left(\frac{E_{IN}}{N_{IN}}\right) \tag{4}$$

suppose we insist that

$$\left(\frac{E_{IN}}{N_{IN}}\right) = \left(\frac{E_{IN}}{N_{IN}}\right)' \tag{5}$$

and assume this makes $(S_o/N_o)_{out} = (S_o/N_o)'_{out}$. Thus (2) gives

$$\frac{\left[\frac{\overline{(\Delta\bar{n})^2}}{(\bar{n})^2}\left(\frac{S_o}{N_o}\right)_{out}\right]'}{\left[\frac{(\Delta\bar{n})^2}{(\bar{n})^2}\left(\frac{S_o}{N_o}\right)_{out}\right]} = \left\{\frac{Tf_{o_1}\left(1-\frac{f_{o_1}^2}{f_{o_3}^2}\right)}{T'f'_{o_1}\left(1-\frac{f_{o_1}'^2}{f_{o_3}'^2}\right)}\right\}^2 \tag{6}$$

Now, (3) implies that the bit length, T', is related to the bit length T by (since $\beta = t_R/(\sqrt{2}\,T)$)

$$\frac{T'}{T} = \frac{t_R'}{t_R} \tag{7}$$

but

$$t_R = \sqrt{\frac{2T_d}{f_o}} \quad , \quad T_d = \tfrac{1}{2}\, t_o \overline{P^2} \tag{8}$$

i.e.

$$t_R = \frac{9}{\sqrt{c}\, f_o^{3/2}} \sqrt{\bar{n}} \tag{9}$$

Hence

$$\frac{t_R'}{t_R} = \frac{f_{o_1}^{3/2}}{f_{o_1}'^{3/2}} = \left(\frac{f_{o_1}}{f_{o_1}'}\right)^{3/2} \tag{10}$$

Therefore,

$$\frac{T'}{T} = \left(\frac{f_{o_1}}{f_{o_1}'}\right)^{3/2} \tag{11}$$

Hence, (6) becomes

$$\frac{\left[\frac{(\Delta\bar{n})^2}{(\bar{n})^2}\right]'}{\left[\frac{(\Delta\bar{n})^2}{(\bar{n})^2}\right]} = \left(\frac{f_{o_1}'}{f_{o_1}}\right) \frac{\left(1 - \frac{f_{o_1}^2}{f_{o_3}^2}\right)^2}{\left(1 - \frac{f_{o_1}'^2}{f_{o_3}'^2}\right)^2} \approx .80 \tag{12}$$

Hence, the percent error in the S-X Band experiment is somewhat smaller than for the V.H.F. experiment.

We note that since $T = 25.6\ \mu$sec., $T' = 0.474\ \mu$sec. in this duration about 474 cycles of the $f'_{o_1} \approx 1{,}000$ mHz frequency will exist so that this is not impractical.

Now, to have (5) hold, we note

$$\frac{E_{IN}}{N_{IN}} = \frac{P_T(NT)G_TG_R\lambda^2}{(4\pi R)^2 K T_I} \tag{13}$$

Suppose we take the ratio of $(E_{IN}/N_{IN})'$ to (E_{IN}/N_{IN}) and hold G_T and G_R constant at the lower, subscript 1, frequencies, then

$$\frac{\left(\frac{E_{IN}}{N_{IN}}\right)'}{\left(\frac{E_{IN}}{N_{IN}}\right)} = \left(\frac{P'_T}{P_T}\right)\left(\frac{f_{o_1}}{f_{o_1}'}\right)^2\left(\frac{T_I}{T'_I}\right)\left(\frac{N'}{N}\right)\left(\frac{T'}{T}\right) \tag{14}$$

Now we note from Figs. 16, 17, and 18 of the text that at S or X band the noise temperatures are much smaller than at V.H.F. For example, at 1 ghz, $T_A \approx 20^\circ$, $T_e \approx 8^\circ$, hence $T_I = 28^\circ$, therefore, $T'_I/T_I \approx 28/2650 \approx 1/100$, hence, for S-band, to have equal signal to noise energy ratios, i.e. (14) equal to unity, we require that

$$\left(\frac{P'_T}{P_T}\right)\left(\frac{N'}{N}\right) = \left(\frac{f_{o_1}'}{f_{o_1}}\right)^2\left(\frac{T'_I}{T_I}\right)\left(\frac{T}{T'}\right) \tag{15}$$

but, from (11), this becomes

$$\left(\frac{P_T'N'}{P_TN}\right)_{S\ BAND} \left(\frac{f_{o_1}'}{f_{o_1}}\right)^{\frac{7}{2}} \left(\frac{T_I'}{T_I}\right) \doteq \left(\frac{1000}{70}\right)^{\frac{7}{2}} \left(\frac{1}{100}\right) \doteq 110 \qquad (16)$$

Thus if the same peak power can be realized at both S and V.H.F. ($P_T' = P_T$) then $N' = 110\ N \approx 13{,}974$. This means the number of bits required is increased by a factor of about 100. This probably can be done, but the associated circuitry is more involved. Alternatively, at S-band P_T' can be made larger than 2 kw and N' correspondingly reduced.

From (13) we note that the signal/noise energy ratio at X-band to that at S-band is (holding P_T, N, T, and G_T constant at the values they have at S-band)

$$\frac{\left(\frac{E_{IN}}{N_{IN}}\right)_X}{\left(\frac{E_{IN}}{N_{IN}}\right)_S} = \frac{\lambda_X^2\ G_{R_X}\ T_{I_S}}{\lambda_S^2\ G_{R_S}\ T_{I_X}} \approx \frac{T_{I_S}}{T_{I_X}} \qquad (17)$$

since gain is inversely proportional to wavelength. Using the curves of Figs. 16, 17, and 18 we note that $T_{I_X} \approx 10^{\circ}K$, hence $T_{I_S}/T_{I_X} \doteq 2.8$, thus the signal/noise energy ratio at X-band is at least equal to that at S-band.

From (89) of the text the difference in differential time between peaks for the S-X band experiment, $\Delta T_{13}'$, is related to that for the V.H.F. experiment by

$$\frac{\Delta T_{13}'}{\Delta T_{13}} = \frac{(\beta_1'^2\, T'^2\, f_{o_1}') \left[1 - \frac{f_{o_1}'}{f_{o_3}'}\right]^2}{(\beta_1^2\, T^2\, f_{o_1}) \left[1 - \frac{f_{o_1}}{f_{o_3}}\right]^2} \tag{18}$$

but $\beta_1' = \beta_1$, and from (11) $T'/T = (f_{o_1}/f_{o_1}')^{3/2}$, hence

$$\frac{\Delta T_{13}'}{\Delta T_{13}} = \left(\frac{f_{o_1}}{f_{o_1}'}\right)^2 \frac{\left[1 - \left(\frac{f_{o_1}'}{f_{o_3}'}\right)^2\right]}{\left[1 - \left(\frac{f_{o_1}}{f_{o_3}}\right)^2\right]} = .02069 \tag{19}$$

Thus, from already computed values of ΔT_{13} (Table II of the text) we get the results of Table XVII-1. This time ΔT varies from about 1 to 130 μsec. over the trajectory considered.

In closing, we note that the input signal to noise <u>power</u> ratios are related by

$$\frac{\left(\frac{S_o}{N_o}\right)_{in}'}{\left(\frac{S_o}{N_o}\right)_{in}} = \frac{\frac{P_T'\, G_T'\, G_R'\, \lambda'^2}{(4\pi R)^2\, K\, T_I'\, B'}}{\frac{P_T\, G_T\, G_R\, \lambda^2}{(4\pi R)^2\, K\, T_I B}} \tag{20}$$

TABLE XVII-1.

ΔT FOR S-X BAND EXPERIMENT

θ	ρ	$\Delta T_{V.H.F.}$ (MILLISECS.)	$\Delta T_{S\ \&X}$ (μ SECS.)
85.0	154.2	.0424	0.8773
97.5	120.1	.0633	1.3097
113.0	91.93	.09735	2.0142
134.0	63.77	.1661	3.437
153.0	40.03	.2986	6.178
164.0	25.21	.5088	10.527
173.5	11.86	1.1424	23.657
178.0	4.45	3.131	64.780
179.0	2.22	6.319	130.74
180.0	0	∞	∞
181.0	2.22	3.0415	62.93
184.0	8.90	1.543	31.92
187.0	14.83	.9102	18.83

which, if we take $B = 1/t_R$ and $B' = 1/t_R'$ and use (10), and take $P_T' = P_T$, $G_T' = G_T$, $G_R' = G_R$, gives

$$\frac{\left(\frac{S_o}{N_o}\right)'_{in}}{\left(\frac{S_o}{N_o}\right)_{in}} = \left(\frac{f_o}{f_o'}\right)^{7/2}\left(\frac{T_I}{T_I'}\right) \tag{21}$$

which we have seen (namely from (16)) is approximately 1/110 . Thus the input signal to noise power ratio is about two orders of magnitude smaller at S-band that at V.H.F.

The signal to noise power ratio at X-band compared to S-band is (holding P_T, G_T, and the product $G_R \lambda^2$ constant)

$$\frac{\left(\frac{S_o}{N_o}\right)_{IN_{X\text{-Band}}}}{\left(\frac{S_o}{N_o}\right)_{IN_{S\text{-Band}}}} = \frac{(T_I B)_{S\text{-Band}}}{(T_I B)_{X\text{-Band}}} \approx \frac{(2.8)}{(10)^{3/2}} \approx \frac{1}{10} \tag{22}$$

and hence is about three orders of magnitude noise than at V.H.F.

Thus the advantages of performing the experiment at S and X-band, i.e. that of using an available antenna, and resulting in higher accuracy measurement (i.e. (12)), have to be weighed against the disadvantages of working with smaller differential displacement times (i.e. (19)), as well as lower signal to noise power ratios (assuming the same power and gains as at V.H.F.) and hence with the associated longer correlation times (i.e. (16)), and more involved correlation receivers.

APPENDIX XVIII

PLASMA DIAGNOSTICS VIA A.M. OR N.B.F.M.

a. Amplitude Modulation (A.M.)

Consider an amplitude modulated carrier wave at the plane $z = 0$ in an infinite homogeneous plasma,

$$e_i(t) = (1 + m_A \sin \omega_m t) \sin \omega_o t \tag{1}$$

where:

m_A = modulation (amplitude) index

ω_m = angular modulation frequency

ω_o = angular carrier frequency

Use of trigonometric identities allows one to write (1) as

$$e_i(t) = \sin \omega_o t + \frac{m_A}{2} \cos \left[(\omega_o - \omega_m)t\right] - \frac{m_A}{2} \cos \left[(\omega_o + \omega_m)t\right] \tag{2}$$

Each frequency component (i.e. the carrier, ω_o, the lower side band $\omega_o - \omega_m$, and the upper side band, $\omega_o + \omega_m$) of this input propagates down the plasma with the phase factor $\beta(\omega)$ correspondingly evaluated at ω_o, $\omega_o - \omega_m$, and $\omega_o + \omega_m$, i.e.

$$e_i(t,z) = e_o(t) = \sin\left[\omega_o t - \beta(\omega_o)z\right]$$

$$+ \frac{m_A}{2}\cos\left[(\omega_o - \omega_m)t - \beta(\omega_o - \omega_m)z\right]$$

$$- \frac{m_A}{2}\cos\left[(\omega_o + \omega_m)t - \beta(\omega_o + \omega_m)z\right] \quad (3)$$

where

$$\beta(\omega) = \frac{1}{c}\sqrt{\omega^2 - \omega_p^2} \quad (4)$$

Now, if

$$\frac{\omega_m}{\omega_o} << 1 \quad (5)$$

we can write

$$\beta(\omega_o + \omega_m) \equiv \beta_+ \approx \beta_o + \beta'(\omega_o)\omega_m + \frac{\beta''(\omega_o)\omega_m^2}{2} \quad (6)$$

$$\beta(\omega_o - \omega_m) \equiv \beta_- \approx \beta_o - \beta'(\omega_o)\omega_m + \frac{\beta''(\omega_o)\omega_m^2}{2} \quad (7)$$

(where $\beta_o = \beta(\omega_o)$). Inserting (6) and (7) into (3) gives

$$e_o(t) = A\sin\omega_o\left(t - \frac{z}{v_{p_o}}\right) + B\cos\omega_o\left(t - \frac{z}{v_{p_o}}\right) \quad (8)$$

where

$$A = 1 + m_A \cos K \sin \omega_m \left(t - \frac{z}{v_{g_o}}\right) \tag{9}$$

$$B = - m_A \sin K \sin \omega_m \left(t - \frac{z}{v_{g_o}}\right) \tag{10}$$

where

$$K = \frac{\beta_o''(\omega_o)\omega_m^2 z}{2} = \text{distortion parameter} \tag{11}$$

$$v_{p_o} = \frac{\omega_o}{\beta_o} \equiv \text{phase velocity at carrier frequency } \omega_o \tag{12}$$

$$v_{g_o} = \frac{1}{\beta'(\omega_o)} \equiv \text{group velocity at carrier frequency } \omega_o \tag{13}$$

Now, using

$$A \sin \theta + B \cos \theta = \sqrt{A^2 + B^2} \sin \left[\theta + \arctan \left(\frac{B}{A}\right)\right] \tag{14}$$

(8) becomes

$$e_o(t) = \sqrt{1 + m_A^2 \sin^2 \omega_m \left(t - \frac{z}{v_{g_o}}\right) + 2m_A \cos K \sin \omega_m \left(t - \frac{z}{v_{g_o}}\right)}$$

$$\cdot \sin \left[\omega_o \left(t - \frac{z}{v_{p_o}}\right) + \phi\right] \tag{15}$$

where

$$\phi = \arctan\left[\frac{-m_A \sin K \sin \omega_m\left(t - \frac{z}{v_{g_o}}\right)}{1 + m_A \cos K \sin \omega_m\left(t - \frac{z}{v_{g_o}}\right)}\right] \tag{16}$$

Thus the output amplitude modulation, i.e., the square root term in (15), has a ratio maximum to minimum of

$$\frac{\left|e_o(t)\right|_{max}}{\left|e_o(t)\right|_{min}} = \sqrt{1 + m_A^2 + 2m_A \cos K} \tag{17}$$

the maximum and minimum occurring for values of time such that $\omega_m\left(t - \frac{z}{v_{g_o}}\right) = \frac{\pi}{2}(2n + 1)$, and πn, respectively. Hence by detecting this signal in the usual A.M. (i.e., envelope detector) fashion, one can measure this ratio

$$\frac{\left|e_o(t)\right|_{max}}{\left|e_o(t)\right|_{min}}$$

and hence determine K (since m_A is known). From (11) one can then determine ω_p, assuming z is known.

b. Special Case of Low Modulation Index

We note for the special case of small index of modulation $m_A << 1$ that (15) becomes

$$e_o(t) = \left[1 + m_A \cos K \sin \omega_m\left(t - \frac{z}{v_{g_o}}\right)\right]$$

$$\cdot \sin\left[\omega_o\left(t - \frac{z}{v_{p_o}}\right) + \phi\right] \tag{18}$$

where

$$\phi \approx - m_A \sin K \sin \omega_m \left(t - \frac{z}{v_{g_o}}\right) \tag{19}$$

Thus for this case the effective index of modulation is changed from m_A to $m_A \cos K$ and the output instantaneous frequency, $\omega_{I_o}(t)$, defined by

$$\omega_{I_o}(t) \equiv \partial_t \left[\omega_o \left(t - \frac{z}{v_{p_o}}\right) + \phi\right] \tag{20}$$

is

$$\omega_{I_o}(t) = \omega_o - m_A \omega_m \sin K \cos \omega_m \left(t - \frac{z}{v_{g_o}}\right) \tag{21}$$

i.e. there is a slight frequency modulation of maximum deviation $\pm m_A \omega_m \sin K$ about the carrier.

c. <u>Narrow Band Frequency Modulation (N.B.F.M.)</u>

Next, suppose we consider the F.M. input of

$$e_i(t) = \sin\left[\omega_o t + m_F \cos \omega_m t\right] \tag{22}$$

where we consider only narrow band F.M. (N.B.F.M.), i.e., restrict m_F so that

$$m_F << 1 \tag{23}$$

Then

$$e_i(t) = \sin \omega_o t \cos (m_F \cos \omega_m t) + \cos \omega_o t \sin (m_F \cos \omega_m t) \tag{24}$$

But due to (23)

$$\cos (m_F \cos \omega_m t) \approx 1 \tag{25}$$

$$\sin (m_F \cos \omega_m t) \approx m_F \cos \omega_m t \tag{26}$$

hence

$$e_i(t) = \sin \omega_o t + m_F \cos \omega_m t \cos \omega_o t \tag{27}$$

i.e.

$$e_i(t) = \sin \omega_o t + \frac{m_F}{2} \cos (\omega_o - \omega_m)t + \frac{m_F}{2} \cos \left[(\omega_o + \omega_m)t\right] \tag{28}$$

Comparing (28) with (2) we see that the N.B.F.M. signal is identical to the A.M. signal except for a sign change (i.e., a phase shift of π) in the upper side band. Hence, if we go through the same operation as before we get (8),

but now

$$A = 1 + m_F \sin K \cos \omega_m \left(t - \frac{z}{v_{g_o}}\right) \tag{29}$$

$$B = + m_F \cos K \cos \omega_m \left(t - \frac{z}{v_{g_o}}\right) \tag{30}$$

where again we must restrict ω_m such that

$$\frac{\omega_m}{\omega_o} << 1 \tag{31}$$

so that (6) and (7) hold.

Hence using (14), we get

$$e_o(t) = \sqrt{1 + m_F^2 \cos^2 \omega_m\left(t - \frac{z}{v_{g_o}}\right) + 2m_F \sin K \cos \omega_m\left(t - \frac{z}{v_{g_o}}\right)}$$

$$\cdot \sin\left[\omega_o \left(t - \frac{z}{v_{p_o}}\right) + \phi\right] \tag{32}$$

where

$$\phi = \arctan\left[\frac{m_F \cos K \cos \omega_m \left(t - \frac{z}{v_{g_o}}\right)}{1 + m_F \sin K \cos \omega_m \left(t - \frac{z}{v_{g_o}}\right)}\right] \tag{33}$$

But since $m_F << 1$ this reduces to

$$e_o(t) \approx \left[1 + m_F \sin K \cos \omega_m\left(t - \frac{z}{v_{g_o}}\right)\right] \sin\left[\omega_o\left(t - \frac{z}{v_{p_o}}\right) + \phi\right] \tag{34}$$

$$\phi \approx m_F \cos K \cos \omega_m \left(t - \frac{z}{v_{g_o}}\right) \tag{35}$$

We note that if there is no dispersion ($K = 0$) (34) reduces to (22) for $z = 0$ as it should.

Thus, the N.B.F.M. signal ends up being amplitude modulated by $m_F \sin K$, and also frequency modulated, its instantaneous frequency being

$$\omega_{I_o}(t) = \omega_o - m_F \omega_m \cos K \sin \omega_m \left(t - \frac{z}{v_{g_o}}\right) \tag{36}$$

i.e. $\omega_{I_o}(t)$ has a maximum deviation of $m_F \omega_m \cos K$ about the carrier. This deviation can be readily measured by an F.M. discriminator circuit and hence K can be determined from which ω_p can be obtained.

d. Conclusion

The pertinent findings of this appendix are summarized in Table XVIII-1. In either the A.M. (with small modulation index) or the N.B.F.M. case both amplitude and frequency modulation exist at the output due to dispersion, however, the frequency modulation is small (being proportional to $\sin K$ via (21)) in the A.M. case, and the amplitude modulation is

small (also being proportional to $\sin K$ via (34)) for the N.B.F.M. case.

For these special cases of small deviations, it is seen that the modulation is propagated at the carrier group velocity, v_{g_o}, while the carrier propagates at the carrier phase velocity, v_{p_o}.

TABLE XVIII-1. SUMMARY OF PLASMA DIAGNOSTICS VIA A.M. OR N.B.F.M.

$$e(t) = A(t) \sin \Phi(t)$$

INPUT SIGNAL	LOCATION	A(t)	$\Phi(t)$	$\omega_{I_o}(t) = \partial_t \Phi$
A.M.	$z = 0$	$1 + m_A \sin \omega_m t$	$\omega_o t$	ω_o
$\frac{\omega_m}{\omega_o} << 1$ $m_A << 1$	$z = L$	$1 + m_A \cos K \cdot \sin \omega_m \left(t - \frac{L}{v_{g_o}}\right)$	$\omega_o \left(t - \frac{L}{v_{p_o}}\right) - m_A \sin K \cdot \sin \omega_m \left(t - \frac{L}{v_{g_o}}\right)$	$\omega_o - m_A \omega_m \sin K \cdot \cos \omega_m \left(t - \frac{L}{v_{g_o}}\right)$
N.B.F.M.	$z = 0$	1	$\omega_o t + m_F \cos \omega_m t$	$\omega_o - m_F \omega_m \sin \omega_m t$
$\frac{\omega_m}{\omega_o} << 1$ $m_F << 1$	$z = L$	$1 + m_F \sin K \cdot \cos \omega_m \left(t - \frac{L}{v_{g_o}}\right)$	$\omega_o \left(t - \frac{L}{v_{p_o}}\right) + m_F \cos K \cdot \cos \omega_m \left(t - \frac{L}{v_{g_o}}\right)$	$\omega_o - m_F \omega_m \cos K \cdot \sin \omega_m \left(t - \frac{L}{v_{g_o}}\right)$

WHERE $K = \beta''(\omega_o)\frac{\omega_m^2 L}{2}$, $v_{p_o} = \frac{c}{\sqrt{1 - \omega_p^2/\omega_o^2}}$, $v_{g_o} = c\sqrt{1 - \omega_p^2/\omega_o^2}$

FOR A TENUOUS PLASMA $\left(\omega_p^2/\omega_o^2 << 1 \text{ , } K \approx -\tfrac{1}{2}(\omega_p^2/\omega_o)^2(\omega_m/\omega_o)^2\left(2\pi \frac{L}{\lambda_{v_o}}\right) \text{ , } \lambda_{v_o} = \frac{c}{f_o}\right)$

LIST OF MAJOR SYMBOLS

c = speed of light in vacuum = $3 \cdot 10^{10}$ meters/sec.

Db. = decibel

f = frequency, cycles/sec.

f_o = carrier frequency, cycles/sec.

f_p = plasma frequency, cycles/sec.; $f_p^2 \approx 81\ n$

L = path length from satellite to earth

t = time, secs.

t_o = L/c = transit vacuum time for path length L

t_g = L/v_g = group velocity time

t_R = envelope rise time = $\sqrt{(2T_d)/f_o}$

t_c = correlation time

T_d = $t_g - t_o$ = delay time

T = bit length

τ = normalized correlation time = $(t_c + t_g)/T$

$n(\xi)$ = electron number density at the point ξ on path from satellite to earth, electrons/meter^3

$\bar{n}(\rho) = \bar{n} = \int_0^L n(\xi)d\xi$ = integrated columnar electron density, electrons/meter^2

$n(r)$ = electron number density at normalized distance r from center of sun, electrons/meter^3

R = distance from center of sun to arbitrary point in corona

R_s = distance from center of sun to center of satellite

LIST OF MAJOR SYMBOLS (CONTINUED)

R_E = distance from center of sun to center of earth

$R_\perp$ = perpendicular offset distance from center of sun to ray path

R_o = radius of sun = $6.960 \cdot 10^8$ meters

r, r_s, r_E, ρ = $\frac{R}{R_o}$, $\frac{R_s}{R_o}$, $\frac{R_E}{R_o}$, $\frac{R_\perp}{R_o}$, respectively, normalized radial distances from center of sun

$y(\tau)$ = normalized output correlation function

mHz = megahertz = megacycle

$\left(\frac{S_o}{N_o}\right)_{in}$ = input (at antenna terminals) peak signal to average noise power ratio

$\left(\frac{S_o}{N_o}\right)_{out}$ = output (output of correlator) peak signal to average noise power ratio

$\frac{E_{IN}}{N_{IN}}$ = input (at antenna terminals) peak energy to average noise power per cycle of bandwidth

$\overline{p^2}$ = $\overline{f_p^2}/f_o^2$ = ratio of square of averaged plasma frequency to square of carrier frequency

$\overline{f_p^2}$ = $\frac{1}{L}\int_0^L f_p^2(\xi)d\xi$ = averaged plasma frequency for path L

ΔT = $T_{d_1} - T_{d_2}$ = differential time delay between T_d of carrier frequency 1 and 2, respectively

LIST OF MAJOR SYMBOLS (CONTINUED)

T_p $= \Delta T$

T_s = time between two successive coded groups ($T_s = 1$ sec. for V.H.F. experiment)

v_g $= \dfrac{1}{\beta_p'(\omega_o)} \doteq \dfrac{c}{\left(1 + \dfrac{\overline{p^2}}{2}\right)}$ = group velocity evaluated at carrier frequency

β $= \dfrac{t_R}{\sqrt{2}\,T}$ = solar distortion parameter

ω = angular frequency, radians/sec.

All other symbols are defined as they are introduced.

REFERENCES

[1] MIT Center for Space Research, "The Conceptual Design of a Small Solar Probe," MIT CSR-TR-69-1, (Contract No. NASr-249), January, 1969.

[2] R. S. Pindyck, "Reception of Dispersed Barker Codes," MIT Center for Space Research, CSR-T-67-1, May, 1967.

[3] J. V. Harrington, "Study of a Small Solar Probe," Part I, Radio Propagation Experiment, MIT Center for Space Research, PR-5255-5 (NASA Grant NASr-249), July 1, 1965.

[4] Hruby, Somes, Dimeff, and Tashjran, "Tabulated Communication Characteristics of a Steady State Model of Interplanetary Space," NASA Report, NASA SP-3042, 1967.

[5] J. V. Evans and T. Hagfors, Radar Astronomy, McGraw Hill Book Company, p. 333, 1968.

[6] C. P. Kuiper, The Sun, University of Chicago Press, Chicago, Illinois, p. 470, 1953.

[7] D. E. Billings, A Guide to the Solar Corona, Academic Press, pp. 221-223, 1966.

[8] V. L. Ginzburg, The Propagation of Electromagnetic Waves in Plasmas, Addison-Wesley, Chapter VII, 1964.

[9] C. M. Knop and G. I. Cohn, "Comments on Pulse Waveform Degradation due to Dispersion in Waveguide," IEEE Trans., MTT, Vol. MTT-11, 5, pp. 445-447, September, 1963.

[10] J. C. Hancock, An Introduction to the Principles of Communication Theory, McGraw Hill Book Company, New York, p. 126, 1961.

[11] M. Abramowitz and I. A. Stegun, "Handbook of Mathematical Functions," National Bureau of Standards, Applied Mathematics Series 55, June, 1964.

[12] R. E. Haskell and C. T. Case, "Transient Signal Propagation in Lossless Isotropic Plasmas," IEEE Trans. Antennas and Propagation, Vol. AP-15, 3, pp. 458-464, May, 1967.

REFERENCES (CONTINUED)

[13] H. Hodara, Private Communication.

[14] C. M. Knop, "On the Bandwidth of a Waveguide," Proc. IEEE, Letters, Vol. 56, 9, pp. 1621-1622, September, 1968.

[15] M. I. Skolnik, Introduction to Radar Systems, McGraw Hill Book Company, New York, p. 464, 1962.

[16] B. P. Lathi, Communication Systems, J. Wiley, pp. 394-400, 1968.

[17] E. C. Jordan and K. G. Balmain, Electromagnetic Waves and Radiating Systems, 2nd Edition, Prentice Hall, 1968.

[18] Microwave Journal International, Microwave Engineers Technical and Buyers Guide Edition, Horizon House, February, 1969.

[19] F. B. Hildebrand, Advanced Calculus for Engineers, Prentice Hall, pp. 196-197, 1950.

[20] A. Rubinowicz, "Propagation of a Cut-Off Train of De Broglie Waves," Acta Physica Polonica (Poland), Vol. 10, pp. 79-86, 1950.

[21] R. Gajewski, "On Transients in Waveguides," Bull. de L'Academie Polonaise Des Sciences, Vol. 3, pp. 29-34, 1955.

[22] C. M. Knop, "Pulsed Electromagnetic Wave Propagation in Dispersive Media," IEEE Trans. on Antennas and Propagation, Vol. AP-12, pp. 494-496, July, 1964.

[23] Lord Kelvin, "On the Waves Produced by a Single Impulse in Water of Any Depth, or in a Dispersive Medium," Proc. Roy. Soc. XLII, p. 80, 1887.

[24] G. Toraldo Di Francia, Electromagnetic Waves, Interscience Publishers, New York, pp. 35-36, 1955.

[25] Magnus and Oberhettinger, Functions of Mathematical Physics, Chelsea Publishing Company, New York, p. 131, 1954.

REFERENCES (CONTINUED)

[26] Boersma, J., "Computation of Fresnel Integrals," Math. Comp., Vol. 14, p. 380, 1960.

[27] L. S. Bosanquet, "On Abel's Integral Equations and Fractional Integrals," Proc. of the London Mathematical Society, pp. 134-143, June, 1930.

[28] E. C. Titchmarsh, Introduction to the Theory of Fourier Integrals, Oxford University Press, pp. 331, 1948.

[29] J. Irving and N. Mullineux, Mathematics in Physics and Engineering, Academic Press, New York, pp. 628, 1959.

[30] R. E. Matick, Transmission Lines for Digital and Communication Networks, McGraw Hill Book Company, p. 191, 1969.

[31] M. Born and E. Wolf, Principles of Optics-Electromagnetic Theory of Propagation, Interference and Diffraction of Light, The Macmillan Company, New York, pp. 122, 1959.

[32] S. Ramo, J. R. Whinnery, T. Van Duzer, Fields and Waves in Communication Electronics, J. Wiley, p. 423, 1965.